CHARACTERISTICS OF GASEOUS TURBULENT DIFFUSION FLAMES IN CYLINDRICAL CHAMBERS

by

Said Elsayed Elghobashi

Thesis submitted for the degree of

Doctor of Philosophy

in the Faculty of Engineering

University of London

and

for the Diploma of Membership

of Imperial College

Mechanical Engineering Department
Imperial College,
London SW7.

November, 1974

Abstract

A study is reported of the axi-symmetric, gaseous, turbulent, diffusion flames confined in cylindrical chambers in situations where recirculation is present but radiation and swirl are absent.

Solutions are obtained by a numerical procedure employing three mathematical models to simulate: the physics of turbulence, the chemical reaction and the fluctuations of concentration. The equations solved are the six simultaneous elliptic, partial differential equations for: stream function, vorticity, turbulence kinetic energy, the rate of dissipation of turbulent energy, the mixture fraction and the mean-squared fluctuations of the mixture fraction.

Effects of both the concentration and temperature fluctuations are accounted via the use of a clipped-Gaussian probability density function for the instantaneous mixture fraction.

The predictions are compared with measurements where possible.

A method is proposed for calculating the local probability of chemical reaction based on the use of the probability density function for the mixture fraction together with a "reaction range" defining a suitable band of the instantaneous mixture fraction values where reaction may occur.

Results are also presented of the measurements made by an ionization probe of the probability of chemical reaction at many locations inside a small cylindrical furnace.

Reasonably good agreement is obtained between these data and predictions.

Acknowledgements

I would like to express my gratitude to my supervisor, Dr. W.M. Pun for his guidance, suggestions and encouragement during the course of the work described in this thesis. Thanks are also due to various other members of staff and research students of the heat transfer section at Imperial College: in particular, Dr. F.C. Lockwood and Professor D.B. Spalding, for being members of my thesis committee; Dr. A. Odidi and Mr. A.S. Naguib for many helpful discussions; Mr. S. Pope for making available his contour-plotting routine.

The financial support of the Science Research Council under grant number B/RG/861 is gratefully acknowledged.

Finally, I would like to thank the Combustion, Heat and Mass Transfer Ltd. for providing the basic computer program.

CONTENTS

		Page
	Abstract	2
	Acknowledgements	3
	CONTENTS	4
1.	INTRODUCTION	8
1.1	The problem considered	8
1.2	Practical importance	9
1.3	Objectives of the investigation	10
1.4	Previous work	10
	1.4.1 Experimental	11
	1.4.2 Theoretical	13
1.5	The present contributions	14
1.6	Outline of the thesis	17
2.	EXPERIMENTAL INVESTIGATION	19
2.1	Introduction	19
2.2	Review of chemi-ionization and chemi-luminescence measurements in turbulent flames	20
2.3	Selection of the probe for the present investigation	23
2.4	Principles of operation of the ionization method	24
	2.4.1 Basic principles	24
	2.4.2 Dominant positive ion concentration in hydrocarbon flames	25
	2.4.3 Relation between the probability of reaction P and the measured positive ion current	26
	2.4.4 The effect of the comparator discrimination level on P.	29

		Page
2.5	The ionization probe	31
	2.5.1 Details of construction	31
	2.5.2 Electronic circuit	31
2.6	Experiments	35
	2.6.1 General arrangement	35
	2.6.2 Experimental procedure	36
	2.6.3 Measurements taken	36
2.7	Summary of main points	38
3.	MATHEMATICAL ANALYSIS	40
3.1	Introduction	40
3.2	Equations and models for turbulent reacting flows	41
	3.2.1 The time-mean motion	41
	3.2.2 The turbulence model	42
	3.2.3 The time-mean density	47
	3.2.4 The chemical-reaction model	48
	3.2.5 Thermodynamic considerations	53
	3.2.6 Concentration-fluctuations model	54
	3.2.7 Evaluation of the time-mean properties	61
3.3	Solution of the equations	68
	3.3.1 The finite-difference procedure	68
	3.3.2 Special considerations near a wall	70
4.	COMPUTATIONS FOR CONCENTRATION FLUCTUATIONS IN ISOTHERMAL TURBULENT CONFINED COAXIAL JETS	74
4.1	Introduction	74
4.2	The particular problem considered	74
	4.2.1 The flow	74
	4.2.2 The equations	76
	4.2.3 Boundary conditions	76

Page

4.3 Results and discussions 78

4.3.1 Some details of the computations 78

4.3.2 Results and comparison with measurements 79

4.4 Conclusions 92

5. COMPUTATIONS FOR TURBULENT DIFFUSION FLAMES IN CYLINDRICAL CHAMBERS 93

5.1 Introduction 93

5.2 The problem specification 93

5.2.1 The geometry of the flow domain 94

5.2.2 The equations 94

5.2.3 Boundary conditions 94

5.3 Details of the computations 98

5.3.1 The solution procedure 98

5.3.2 A method for predicting the local probability of chemical reaction, P 99

5.3.3 Accuracy and convergence criteria 106

5.3.4 Computer time 112

5.4 Results and discussions 112

5.4.1 Discussion of the computations 112

5.4.2 Probability of chemical reaction, P 143

5.4.3 Typical variation of λ 155

5.5 Conclusions 155

6. CLOSURE 161

6.1 Concluding remarks 161

6.1.1 Theoretical 161

6.1.2 Experimental 162

	Page
6.2 Recommendations for future research	162
6.2.1 Theoretical	162
6.2.2 Experimental	163
REFERENCES	164
NOMENCLATURE	171
APPENDIX A	175
APPENDIX B	183

CHAPTER 1

INTRODUCTION

1.1 The problem considered

The present investigation is concerned with time-steady, gaseous, turbulent, diffusion flames confined in cylindrical chambers. In these flames, fuel and oxidant are separately admitted into the combustion chamber, and since the chemical reaction time-scale is often several orders of magnitude smaller than the time-scale of turbulent mixing, the mixing imposes a limit on the reaction rate, thus controlling the combustion process. Nevertheless, chemical reaction takes place at the molecular level; molecular diffusion between fuel and oxidant must therefore take place before any reaction is possible.

Currently available experimental evidence (Hawthorne et al, 1949; Pompei and Heywood, 1972; Bilger and Kent, 1972) suggests that the instantaneous concentration of a species at a point in a turbulent flame experiences large random fluctuations. Because of these concentration fluctuations even a high reaction-rate, which ensures that instantaneously either fuel or oxidant only can exist at a given point, cannot prevent the time-mean mass fractions of both reactant from being non-zero at the same location. This "unmixedness" is responsible for the appearance of the brush-like, thick reaction zones of turbulent diffusion flames.

Thus, a complete characterisation of these flames must involve specification in the flow field of both the time-mean values and the variation with time, of properties such as concentrations, temperature, density and velocity. An adequate experimental study of turbulent

flames requires a probe of high degree of resolution in both space and time; to predict these flames accurately the procedure used should take into account some, if not all, of the effects of these fluctuations on the time-mean values of the flow properties. These considerations were the motives for research work presented in this thesis.

1.2 Practical importance

Turbulent diffusion flames are common in propulsive systems and industrial furnaces. Gas-turbine combustors, power station boilers and glass-making furnaces are some practical examples. These combustion systems employ turbulent diffusion flames because they allow a more sensitive control of the performance and eliminate the detonation hazards of premixed flames.

Recent awareness of the limitations of energy resources has provided a new incentive for studying these flames. In order to achieve higher combustion efficiencies, detailed studies of the factors that enhance the rate of turbulent mixing of fuel and oxidant are needed. Present and future fuel shortages may even force many existing combustion equipment to run with fuels other than those specified for high-output and low pollutant emission. This pressing situation poses the problem of designing new, or modifying the existing, combustion chambers to satisfy both performance and emission-control requirements. The consideration of these important and difficult problems renders urgent the need for a fundamental understanding of turbulent diffusion flames in practical combustion systems.

1.3 Objectives of the investigation

The present investigation forms part of a larger research program at Imperial College for the developing and validating of numerical procedures to predict turbulent reacting flows in practical combustion systems.

The incorporation of the calculation of concentration fluctuations into a numerical procedure for free turbulent diffusion flames was first demonstrated by Spalding (1970). One of the objectives of the present investigation was to apply and refine wherever necessary Spalding's model to a computational procedure for a practical furnace. The second objective was to obtain detailed and reliable measurements of the extent of the brush-like reaction zone in a small experimental furnace to allow for an assessment of the prediction procedure.

1.4 Previous work

For nearly three decades, many research workers have been engaged intensively in the investigation of turbulent diffusion flames, and numerous experimental and theoretical studies have been performed to attempt to elucidate the very complex nature of these flames.

The state of the current knowledge on these flames can be summarised in the following brief review on the experimental and theoretical works pertinent to non-swirling turbulent diffusion flames for both free and confined situations.

1.4.1 Experimental

Table 1.4.a shows a classified survey of previous experimental work. A more detailed survey can be found in Appendix A.

From the above review of available measurements of other workers in the field of turbulent diffusion flames, the following conclusions can be drawn:

(a) Some data for the time-mean concentrations for confined situations exist in the literature. However sampling errors associated with these data are often uncertain.

(b) No direct measurements for the concentration fluctuations of stable species have been made. The deduction of the values of concentration fluctuations from the quenched-sample analysis by Hawthorne et al (1949) and Bilger and Kent (1972) is an indirect approach and is based on unrealistic assumptions of the probability-density functions of the concentration fluctuations.

(c) Reliable data are available for the time-mean temperature for unconfined flames.

(d) Data for temperature fluctuations for unconfined situations are available, but their accuracy is not high.

(e) The only data for the time-mean values and the fluctuations of velocity in turbulent diffusion flames were obtained by Baker et al (1973) for a free-jet situation using the laser doppler

Table 1.4.a Survery of experimental work

Property measured	Measurement technique	Reference	Findings and Remarks
Time-mean concentration	Quenched-sample probe	Hawthorne et al (1949) Vranos et al (1969) Kent and Bilger (1972)	- time-mean concentrations of both fuel and oxidant overlap. - large sampling-errors arise from the intermittent nature of the flow. - recirculation zone in confined flames increases the flame length.
	Oxygen-enriched sample	El-Mahallawy et al (1973)	- Flame length increases with increasing inlet F/A ratio. - Reynolds number has little effect on flame length.
Time-mean and R.M.S. of temperature	Thermocouple	Kunugi and Jinno (1959) Smith et al (1969) Kent and Bilger (1972) Odidi (1974)	- Errors in the time-mean temperature measurements are of the order of 5%. - Errors in the R.M.S. of temperature fluctuations are about 35%.
Time-mean and R.M.S. of velocity	Pitot-tube	Kent and Bilger (1972)	- Errors up to 25% in time-mean velocity result from 1% error in concentration measurements.
	Condenser-microphone probe	Ebrahimi (1967)	- Density fluctuations have been ignored in obtaining the velocity fluctuations from the measured pressure fluctuations.
	Laser-doppler anemometer	Durst et al (1972) Baker et al (1973)	- High degree accuracy
Positive ion current	Ionization probe	Karlovitz et al (1953) Vlasov (1959) Odidi (1974)	- rapid response of the probe could be used in studying the instantaneous structure of the reaction zone.
Chemi-luminescence	Optical probe	Günther and Simon (1969) Chomiak (1972) Kuhnert and Gunther (1973)	- Probe response is one order of magnitude faster than that of the ionization-probe but spatial resolution is less accurate.

anemometer.

(f) No data are found for chemi-ionization or chemi-luminescence for the confined siutations.

It is obvious from the above conclusions that detailed and reliable measurements of the time-mean values and the fluctuations of scalar quantities in continuous-flow combustion chambers are still lacking.

1.4.2 Theoretical

In the theoretical study of turbulent diffusion flames, one encounters two main problems; one is mathematical, and the other is physical. The mathematical problem, which is common to all turbulent flows, reacting and non-reacting, arises because the rigourous equations governing the instantaneous structure of the flow are coupled, non linear, partial differential equations (for example, Favre 1965, Bray 1973-a). In flames, the magnitude of the problem increases because the number of the dependent variables is larger than that fór a non-reacting flow (density, enthalpy, concentration, reaction rates), and hence the number of equations is greater. Although numerical procedures exist for solving these equations, the computational mesh required to cover the smallest eddy sizes is too fine to be handled by the present-day computers. The usual way of surmounting this difficulty is by expanding the terms of the instantaneous equations into their time-mean and fluctuating parts, resulting in a set of equations (Bray 1973-a) with more unknowns than equations; this is a closure problem. In order to close the set of equations, turbulence models are often used to approximate the fluctuating correlations in terms of known time-mean quantities.

The introduction of turbulence models requires the understanding of the complex nature of turbulent reacting flows. The physical problem arises from our inadequate knowledge of the laws that govern both the turbulence and the chemistry of reaction. This lack of knowledge makes it difficult to construct satisfactory and universally applicable turbulence and reaction models.

Table 1.4.b below, shows a summary of previous studies on turbulent diffusion flames. A more detailed study is given in appendix A.

From the above survey of the theoretical studies currently available, it can be concluded that:

(a) Numerical procedures which incorporate the effects of turbulent concentration fluctuations on the rates of chemical reaction appear to be the only reliable approach for predicting turbulent flames (Spalding 1970, Kent and Bilger 1972).

(b) The effects of combustion on the flow through the spatial variation of the time-mean density should take into account the influence of concentration and temperature fluctuations on the density (Kent and Bilger 1972).

(c) As far as it is known, no published work to date has incorporated both the effects mentioned in (a), (b) above in a procedure for predicting turbulent diffusion flames.

1.5 Present contributions

(a) Concentration fluctuations in isothermal confined turbulent flows

Before one can predict the major role of concentration

Table 1.4.b Survey of theoretical work

Reference	Turbulence model	Combustion model	Nature of flow	Comments
Pun and Spalding (1967) El-Mahallawy et al (1973)	ad hoc viscosity model	equilibrium reaction	elliptic	- concentration fluctuations neglected. - turbulence viscosity depended on on local density, geometry and inlet velocity.
Spalding (1970)	k-w-g model*	equilibrium reaction	parabolic	- simple model of concentration fluctuations. - no quantitative assessment made.
Kent and Bilger (1972)	k-w-g model	equilibrium reaction	parabolic	- unrealistic probability density distribution for concentration fluctuations.
Chung (1972)	Maxwellian distribution for the fluctuations of all dependent variables under all conditions	equilibrium and non-equilibrium reactions	parabolic	- incompressible treatment of the reacting flow.
Bush and Fendell (1973)	k-kl model	equilibrium reaction	parabolic	- model has not been employed in numerical solutions.
Sala and Spalding (1973)	k-w-g model	equilibrium reaction	parabolic	- effect of fluctuations in concentration and temperature on density neglected.

*Symbols are defined on p. 171

fluctuations in turbulent diffusion flames, it is essential that one should be able to predict successfully the distributions of the time-mean values as well as some fluctuating properties of concentration in an isothermal, inhomogeneous, turbulent flow. The first part of the theoretical study is therefore concerned with the predictions of these quantities; the results are compared with the available experimental data.

(b) The turbulent diffusion flame

Another part of the theoretical investigation is devoted to the prediction of the time-mean quantities for a turbulent diffusion flame, due account being taken of the effects of concentration fluctuations on these properties. Validation of the prediction procedure is provided by comparing the predictions with the available measurements of the time-mean mixture fraction, El-Mahallawy et al (1973).

The predictions are concerned only with non-swirling confined gaseous flames. Thermal radiation effects are neglected. Heat transfer to the furnace walls is not accounted for due to reasons which will be mentioned later. Buoyancy effects on the mean motion due to the density gradients and on the turbulence motion due to the density fluctuations are neglected. This is because the predictions are compared with experimental data for a horizontal furnace, while the prediction procedure is based on axisymmetric flow conditions.

(c) Experimental investigation

The present experiment is carried out to provide further validation for the prediction procedure, as suitable data for flucutating scalar quantities in turbulent diffusion flames

could not be found in the published literature (see the remarks on the survey of the experimental studies in Sec. 1.4a). The main objective of this experiment is to map the extent of the flame by measuring the fraction of time that the reaction zone spends, i.e. the probability of reaction, at discrete points in the flow field. This is accomplished by using a Langmuir type probe to measure the instantaneous positive ion concentrations at these points. The experiment provided a mapping of the contours of the probability of reaction, P, throughout the furnace.

(d) The prediction of the probability of chemical reaction P

The final task of the present investigation is to predict the spatial distribution of the probability of chemical reaction in the flow field. As was mentioned in (c) above, the experimental values of P were deduced from measurements of the positive ion concentration at discrete points in the field. Since in the present prediction procedure local ion concentrations are not computed, certain assumptions are introduced to provide a link between the local ion concentrations and predicted dependent variables. The formulation of P in the prediction procedure requires the evaluation of certain constants from comparison with experimental data.

1.6 Outline of thesis

The thesis consists of six chapters. The next chapter, Chapter 2, contains the details of the experimental investigation; results of measurements are presented later in Chapter 5.

Chapter 3 is concerned with the mathematical analysis; there details are given of the turbulence model, the combustion model and the probability density function for the concentration fluctuations. The finite difference procedure is also, briefly discussed in that chapter.

The predictions of concentration fluctuations in confined, turbulent, isothermal flows are discussed in Chapter 4.

Chapter 5 presents the computations of the turbulent diffusion flame, together with the prediction of the probability of chemical reaction.

The last chapter, Chapter 6, summarises the main conclusions of the thesis and makes some suggestions for future research.

CHAPTER 2

EXPERIMENTAL INVESTIGATION

2.1 Introduction

Designers of combustion equipment, such as gas-turbine combustors, industrial furnaces, etc., have much need of a prediction procedure that computes correctly the time-mean quantities, at least in the combustion-chamber. In order to allow a procedure to be assessed, suitable measurements of high accuracy are required. Such data are scarce in the literature, as shown in the review in Sec. 1.4. The present experimental investigation was therefore designed to provide some measurements for the confined, turbulent diffusion flames which are not available in the published literature. Specifically, the object was to probe the extent of the "flame brush" in a cylindrical furnace by measuring the fraction of time that the reaction zone spends at different points in the flow field, i.e. to map the probability of chemical reaction in the furnace space.

To detect instantaneously the local occurrence of chemical reaction in turbulent hydrocarbon-air flames, attention was focused on the phenomena of chemi-ionization and chemi-luminescence. Chemi-ionization refers to the existence, in the reaction zone of hydrocarbon flames, of large numbers (typically about $10^6/mm^3$ at atmospheric pressure) of free electrons and positive ions due to the lack of chemical equilibrium. Chemi-luminescence is the emitted radiation of radicals such as CH^*, C_2^*, and CH^*, which is considerably stronger than thermal radiation and is associated with the occurrence of chemical reaction.

Due to their rapid response, chemi-ionization or chemi-luminescence probes can be used to study the structure of turbulent flames

(Günther and Simon, 1969; Kuhnert and Günther, 1973). The fast response can be explained as follows. The life times of the electronically excited species are about 10^{-8} to 10^{-6} sec (Bulewicz 1967), and the recombination times of ions are of the order of 10^{-7} to 10^{-5} sec (Chomiak 1972). These time-scales are at least one order of magnitude shorter than the turbulence time-scale in flames which is about 10^{-4} sec (Günther and Simon 1969). Before describing the technique selected to achieve the goal of the experimental investigation, a review of the application of both chemi-ionization and chemi-luminescence methods is given below.

2.2 Review of chemi-ionization and chemi-luminescence measurements in turbulent flames

The following summarises the two probe techniques of chemi-ionization and chemi-luminescence.

(a) Chemi-ionization (or Langmuir) probe technique

The Langmuir probe consists essentially of a thin wire with a certain bias voltage applied to it. The wire is electrically insulated from its holder except for a small length which is used as the ion collector. This probe, though known since 1923 (Mott-Smith and Langmuir, 1926), was first used in 1953 by Karlovitz et al to measure positive-ion concentration in turbulent flames. They processed the probe signal of fluctuating local positive-ion current in a turbulent premixed flame to deduce the frequency with which the instantaneous reaction zone comes into contact with the probe wire. Denniston et al (1957) mapped the most probable position of the reaction zone of a turbulent premixed flame using the technique

of Karlovitz et al. They varied the probe wires from 0.5mm to 0.8mm dia. and the collector length from a few mm to 30mm. The probe-holder size was relatively large compared to that of the flame; this caused their measured local ion current to be dependent on the direction of the probe approach. Matton (1957) used a water-cooled Langmuir probe (wire dia. 0.6mm) to study qualitatively the structure of the reaction zone of a free turbulent premixed air-kerosene flame stabilized by an obstacle. Vlasov (1959) employed an ionization probe to measure the frequency of occurrence of the reaction and to estimate the turbulence length-scale in the reaction zone of a free turbulent premixed air gasoline flame. He did not, however, indicate the criterion he used for detecting the occurrence of reaction, i.e. the local ion concentration level which corresponds to the incidence of reaction. Odidi (1974) measured both the time-mean value and R.M.S. of positive ion concentration in turbulent diffusion and premixed free jet flames. He also obtained the local probability density of the fluctuating ion concentrations and the probability of chemical reaction.

(b) Chemi-luminescence (or optical) probe techniques

The optical probe records instantaneously the radiation emitted by the excited molecules in the reaction zone. This probe consists mainly of a lens system and a photomultiplier. The photomultiplier converts the radiation signal into an electric signal.

Measurements of the local fluctuations of emission, within certain wave length range, in the reaction zone can provide valuable information about the structure of this zone. Günther and Simon (1969) used this method to measure the instantaneous chemi-luminescence, within a wave length range 3000 to 18000 A^{o}, in a free turbulent diffusion flame. From these data, together with the values of the time-mean velocity, they mapped the length scale of the emitting turbulent eddies. The

optical probes used by Günther and Simon consisted mainly of a water-cooled hollow cone, of base dia. 68 mm and angle 12°, through which the radiation penetrated to a system of lens and a photomultiplier. The viewing range of this optical probe was 5 mm.

Chomiak (1972) measured the total chemi-luminescence within a wave length range of 3000 A° to 6000 A° in a small confined turbulent premixed flame, using an optical probe with a 40 mm viewing distance and 3 mm depth of focus. His measurements suggest that the smallest highly-luminous eddies inside the reaction zone have a size which corresponds approximately to the local Kolmogorov's microscale, which is about 1.5 mm.

Recently, Kuhnert and Günther (1973) measured the turbulence macroscale of OH* - radiation (wave length 3067 A°) in the reaction zone of a free-jet diffusion flame. In order to separate the local chemi-luminescence signal from the emissions of the neighbouring points, they used a crossed-beam correlation technique. The experimental device consisted mainly of two optical probes whose axes enclosed a 90° angle. This arrangement ensured that only the radiation from a small region of about 5 mm dia. was measured, since the only correlated signals from the two detectors originated from the range of the crossing point. From the measurements of the macroscale at different axial locations, the authors were able to examine the mixing pattern of the air and fuel vortices.

2.3 Selection of probe for the present investigation

In the light of the above review, the chemi-ionization probe technique was chosen, in preference to the optical one, for mapping the extent of the flame in the furnace. This choice was based on the following two considerations:-

(1) The spatial resolution of the ionization probe is superior to that of the optical probe. A probe wire of 0.5 mm dia. and 1.5 mm length provides a spatial resolution of 0.66 $[mm]^3$; this is based on the fact that the sheath diameter is about 1.5 times the wire diameter (Clements and Smy, 1969). The measurement control volume of the optical probe used by Günther and Simon was about 5 mm, and that in Chomiak's experiment was 3 mm; the size of the crossed-beam measurement region of Kuhnert and Günther was about 5 mm.

(2) The ionization probe, when used in furnaces, requires a simpler mechanical arrangement than either the optical-probe or crossed-beam technique. The holes in the furnace wall required for inserting the ionization probe are about 10 mm dia., whereas the viewing windows for the optical probes should be at least 6 times bigger, and the number of windows required is doubled for the crossed-beam technique.

On the other hand, the drawback of both the ionization and the optical probes is the physical presence of the probe in the flow field. This may give rise to quenching effects in the reaction zone and may induce local recirculation behind the probe.

How the ionization probe can be used to measure the reaction probability is explained in the sections following.

2.4 Principles of operation of the ionization method

2.4.1 Basic principles

As a substantial amount has been written on the principles of operation of ionization probes [Mott-Smith and Langmuir (1926), Travers and Williams (1965), Clements and Smy (1969) and Odidi (1974)], only a brief description will be presented here.

Consider a small cylindrical wire in an ionized gas; the wire potential V is made negative with respect to the region around it. If the absolute value of V is greater than the potential barrier which stops even the most energetic electrons from crossing, then the wire will repel negative ions and electrons but attract positive ions. This potential barrier is equal to KT_e/e (Clements and Smy 1969) where K is the Boltzmann's constant, T_e is the electron temperature and e is the electron charge. In other words, in order for the probe wire to collect only positive ions, it has to be negatively biased to a voltage V such that $V \gg \frac{KT_e}{e}$. When this condition is satisfied, the wire will be surrounded by a cylindrical positive "sheath" or region of positive space charge. This sheath is of such dimensions that its total positive charge equals the negative charge on the wire; the field of the wire does not extend beyond the edge of the sheath.

It is important to note that the probe wire collects all the positive ions without preference to their atomic structure. It is

thus impossible to formulate a quantitative relationship between the time-mean rate of reaction and the positive-ion concentrations in the reaction zone without making certain assumptions about the identity of the individual ions which exist in the reaction zone of hydrocarbon flames. This is the subject of discussion in the following section.

2.4.2 Dominant positive-ion concentration in hydrocarbon flames

Green and Sugden (1963) employed the mass spectrometric technique to study the mechanism of chemi-ionization in flames containing hydrocarbons. They demonstrated that the positive ions in the reaction zones of these flames consist mainly of H_3O^+, although other ions exist in small concentrations. The ratio of the concentration of the dominant positive ion H_3O^+ (mass 19) to that of the primary produced ion CHO^+ (mass 29) was found to be 4×10^5. These findings accorded with those of Calcote (1962, 1963).

The mechanism of chemi-ionization in hydrocarbon flames has been the subject of intensive research by many combustion chemists. Using different techniques, Calcote (1962, 1963) and Green and Sugden (1963) have come to the conclusion that this mechanism can be satisfactorily represented by the following three steps:

(i) Chemi-ionization

$$CH + O \xrightarrow{K_i} CHO^+ + e^-, \quad \Delta H \approx 0 \ \text{KJ/mol} \qquad (2.4\text{-}1)$$

(ii) Charge exchange

$$CHO^+ + H_2O \xrightarrow{K_e} H_3O^+ + CO, \quad \Delta H = -34 \times 4.187 \ \text{KJ/mol} \qquad (2.4\text{-}2)$$

(iii) Ion recombination

$$H_3O^+ + e^- \xrightarrow{K_r} H_2O + H, \quad \Delta H = -145 \times 4.187 \ \text{KJ/mol} \qquad (2.4\text{-}3)$$

where K_i, K_e and K_r are the reaction rate constants for the three steps respectively and ΔH is the heat of reaction of each step.

In the following section, the above steps will be used to deduce the probability of reaction P from the measured positive-ion current.

2.4.3 Relation between the probability of reaction P and the measured positive ion current

The probability of chemical reaction at a given point was defined in section 2.1 as the fraction of time that the reaction zone spends at that point. In the present experimental investigation, the occurrence of reaction was detected by the probe when the square of the instantaneous positive-ion current was greater than a finite value(Odidi, 1974). The squaring of the positive-ion current signal is performed because of the following consideration .

Available experimental evidence(Karlovitz et al, 1953 and calcote, 1962) indicates that the concentration of positive ions is several times higher in the immediate vicinity of the instantaneous reaction zone than in the hot combustion-products region. The rate of recombination of the positive ions is here taken as a measure of the overall reaction process. This rate is calculated from eq.(2.4-3) as:

$$d\, n_{H_3O^+} / dt = k_r\, n_{H_3O^+}\, n_e = \left(d\, n_{H_2O} / dt\right)_i \qquad (2.4\text{-}4)$$

where n is the instantaneous concentration of the subscripted species and $\left(d\, n_{H_2O} / dt\right)_i$ is the rate of H_2O production from the ion recombination reaction (2.4-3). Equation(2.4-4), together with the charge balance:

$$n_{H_3O^+} = n_{e^-} = n_+ \quad , \qquad (2.4\text{-}5)$$

gives

$$- d\, n_+ / dt = k_r\, n_+^2 = \left(d\, n_{H_2O} / dt\right)_i \qquad (2.4\text{-}6)$$

i.e. the rate of recombination of H_3O^+ is proportional to the square of the positive-ion concentration*.

---

* It is emphasized here that the rate of H_2O production from the ion-recombination reaction is only a small fraction of the total H_2O production rate.

The probability of reaction P at a point in the flow field can be evaluated according to the three steps shown in figs. 2.4.a to c. These steps are:

(a) The ionization-probe current I_i is converted into vol[illegible] through a converting resistor R_c. Figure 2.4.a [illegible] variation of V_i with time.

(b) The volta[illegible] (fig. 2.4.b). This squaring ar[illegible] one relationship between the rate of reaction [illegible]sitive ion concentration (eq. 2.4-6). The approximation here comes from the experimental evidence (Clements and Smy 1969) which shows that V_i is proportional to $(n_+)^{0.8\pm.1}$ and not to (n_+).

(c) The voltage V_i^2 is passed through a comparator which produces a pulse of constant amplitude V_H (fig. 2.4.c) when V_i^2 is greater than a pre-set value V_c.

The value of P is then obtained from:

$$P = \Sigma_i \tau_i / \tau_t$$

$$= [\Sigma_i \tau_i (V_H - V_L)/\tau_t]/(V_H - V_L) \qquad (2.4\text{-}7)$$

where:

V_H is the high voltage output of the comparator (equals 10 volts) and corresponds to the values of $V_i^2 > V_c$;

V_L is the low voltage output of the comparator (equals 0.026 volts) and corresponds to the values of $V_i^2 < V_c$;

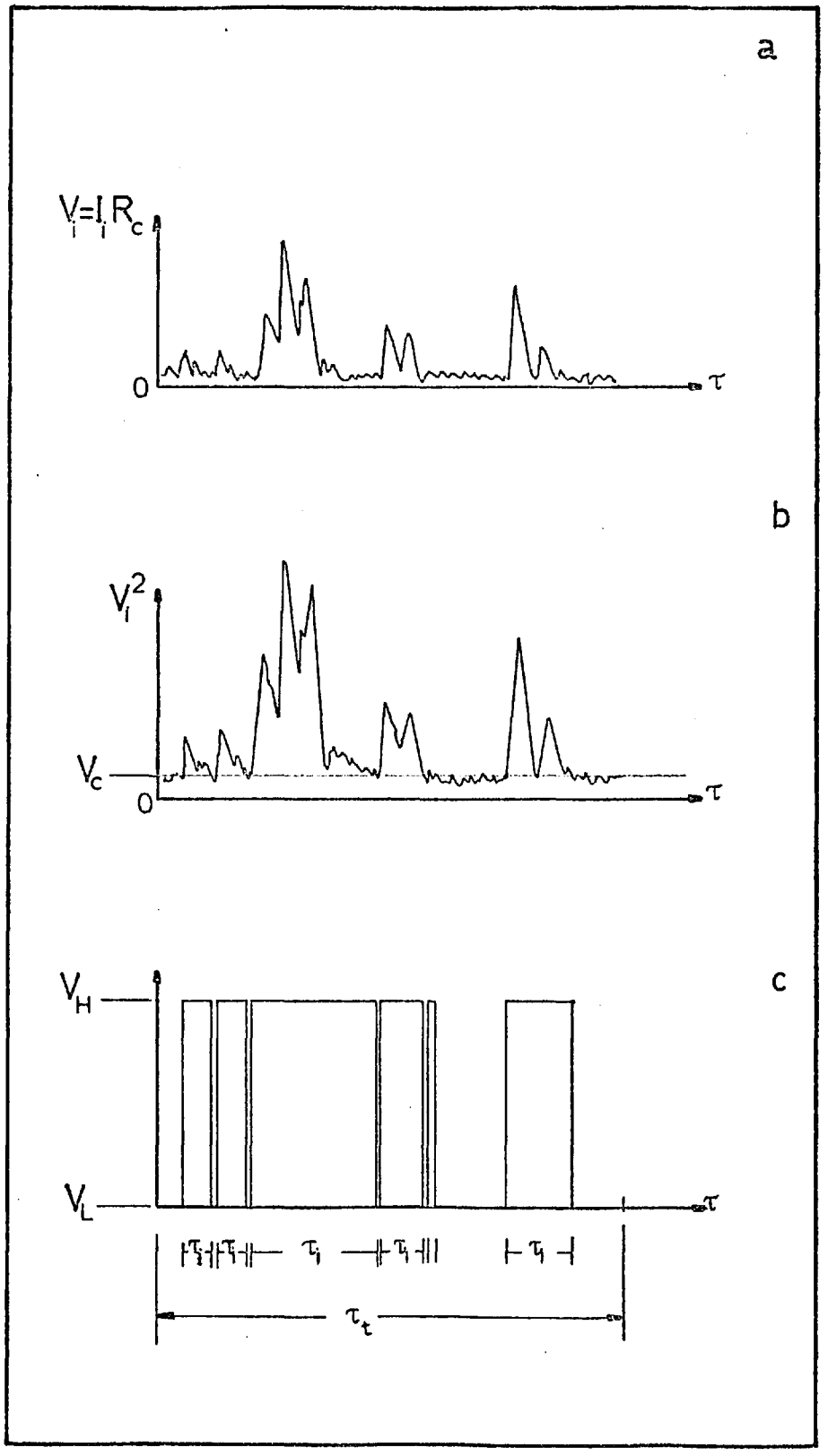

Fig. 2.4.a, b, c.

τ_i is the fractional time that $V_i^2 > V_c$,
and τ_t is the total time. The term inside the square bracket represents the time-average of the pulse signal in fig. 2.4.c.

The determination of V_c value and the effect of its variation on the measured P is discussed below.

2.4.4 The effect of the comparator discrimination level on P

The comparator discrimination level, V_c, is arbitrarily chosen to counteract the effect of electronic noise on the probe signal. Ideally, the value of V_c should be zero, which means that the comparator triggers a pulse whenever $V_i^2 > 0$. Unfortunately, this could not be achieved due to the background electronic noise. Consequently, an optimum value for V_c had to be determined so that the comparator would not be falsely triggered by the noise. Figure 2.3.2 shows a typical plot of P versus V_c for a point in flame I at an axial distance of z/D = 1.73 and at a radial location of r/R = 0.66. The graph demonstrates the monotonic increase of P with the decrease of V_c. The value of V_c was found to equal 0.0045 volts and was kept constant throughout the entire experimental investigation. The dashed line on fig. 2.4.d is an extrapolation of the curve through the measurements not influenced by noise triggering. If we compare the two values of P corresponding to the chosen V_c and to the ideal V_c (zero volts), namely 0.195 and 0.22 respectively, it can be readily seen that the error in the measured P is about 11%.

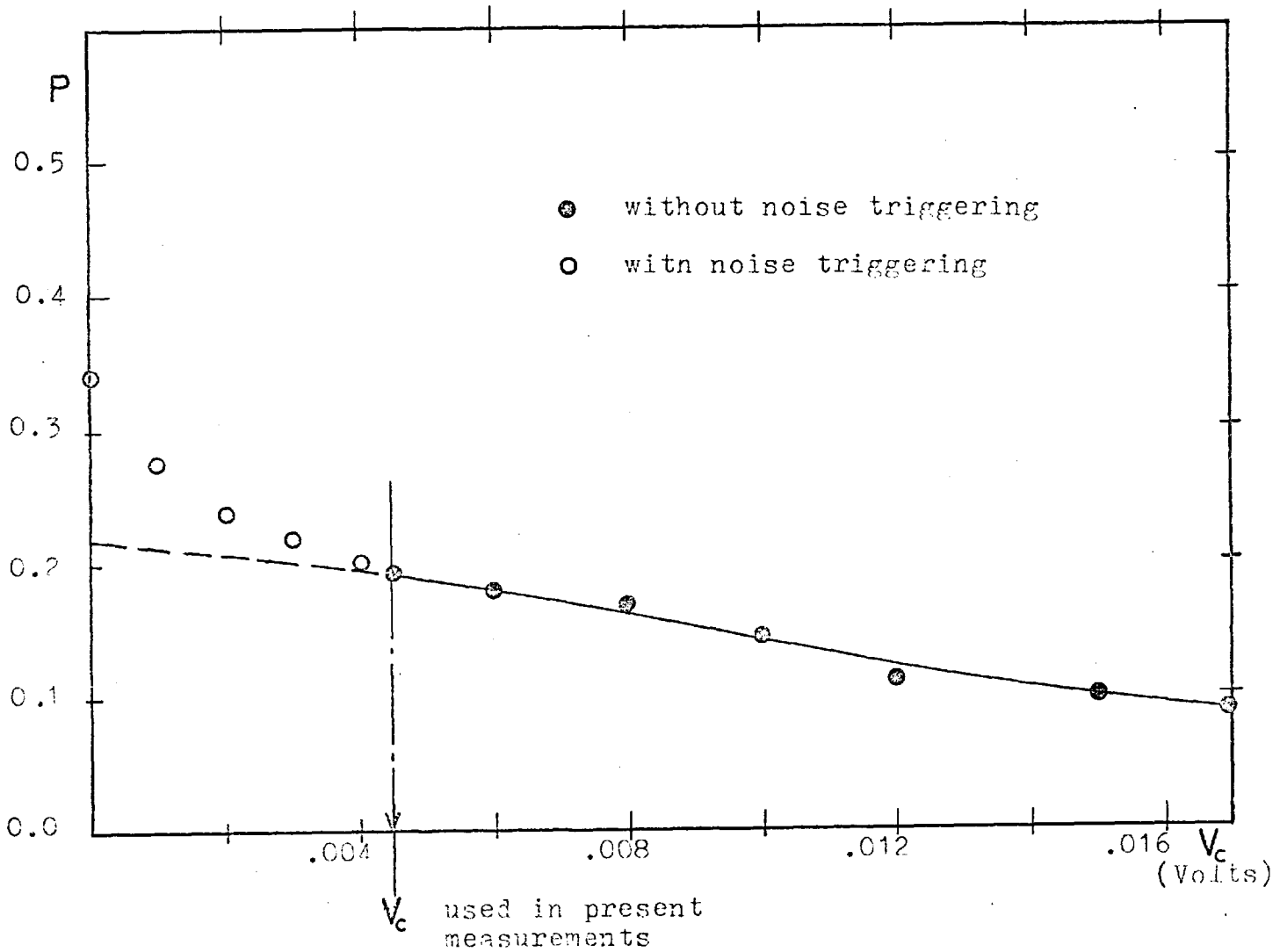
P
0.5
0.4
0.3
0.2
0.1
0.0
without noise triggering
witn noise triggering
.004
.008
.012
.016
V_c
(Volts)
V_c used in present measurements

Fig. 2.4.d

2.5 The ionization probe

2.5.1 Details of construction

The probe, fig.2.5.a,consists mainly of a wire , an insulating tube and a water-cooled holder. The wire is 0.3 m long, 20% Rh/Pt, and 0.5 mm dia. An alumina tube, 2 mm dia. and 0.3 m long, is fitted over the wire to provide electrical insulation at flame temperatures. A straight length of the wire, 1.5 mm,protruding outside the insulating tube to serve as the ion collector. The wire-insulating tube assembly is then inserted into a water-cooled stainless steel jacket. The jacket's water-cooling is achieved by a set of 6 stainless hypodermic tubes 1 mm o.d., soft-soldered on the jacket. Each tube was bent through 180^{o} at its midpoint forming a "U" shape; i.e. the cooling set has 6 inlets and 6 outlets. Distilled water, as a cooling fluid, is supplied by a pump to the tubes. The probe assembly is carried by an electric traversing mechanism that allows the scanning of the field in the r-z space.

The probe wire is connected to the negative pole of a 22 volts D.C. power supply. The value of 22 volts was chosen to achieve a high bias condition for the probe, i.e. $V/(KT_e/e) \simeq 100$, ($V = 22$, $T_e \simeq 2000^{o}K$). This condition ensures that the ion drift velocities in the sheath are much higher than the local gas velocities (Clements and Smy, 1969), thus rendering the ion-concentration measurement more reliable.

2.5.2 Electronic circuit

The electronic circuit used in the present investigation was

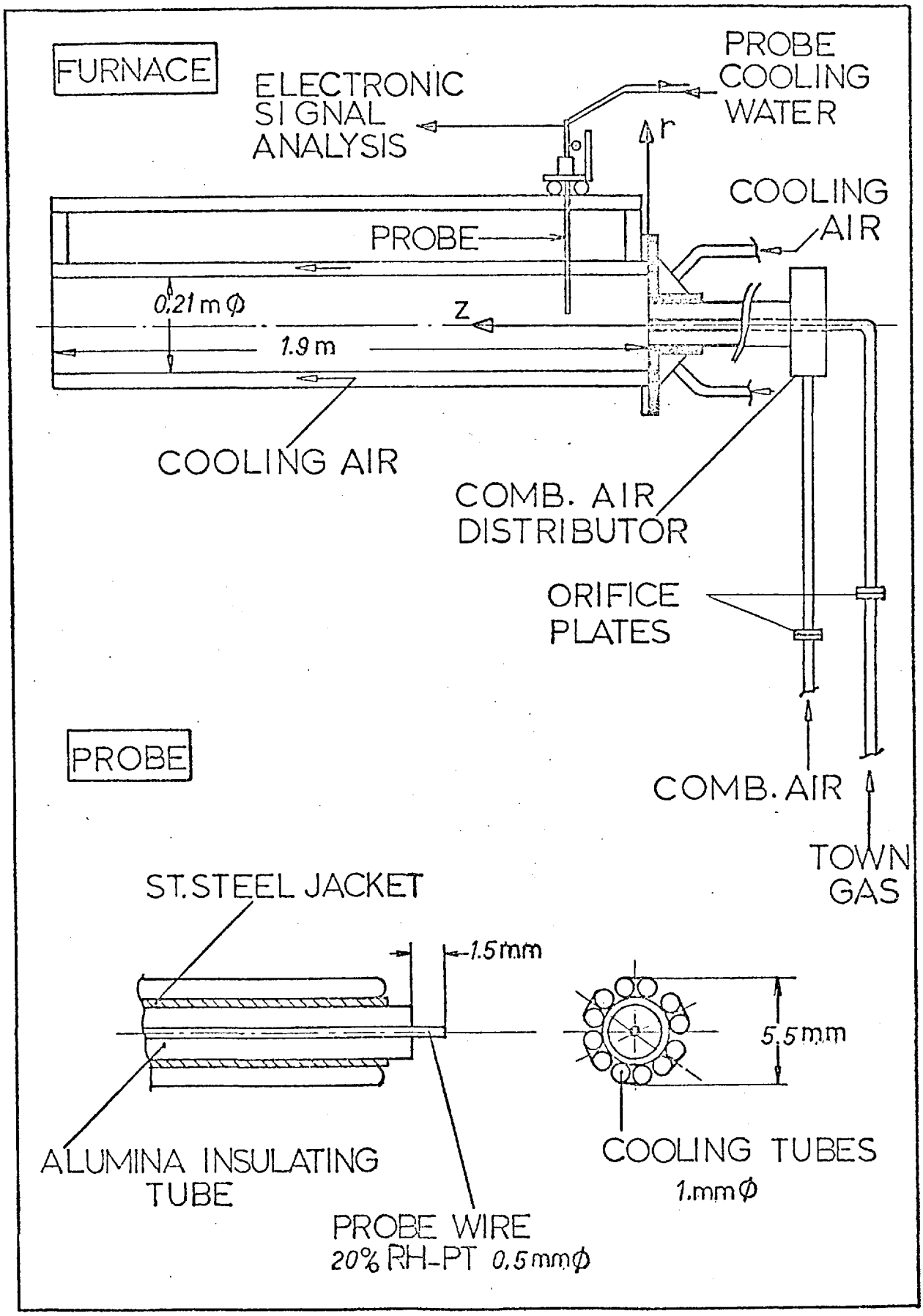
FURNACE
ELECTRONIC SIGNAL ANALYSIS
PROBE COOLING WATER
r
COOLING AIR
PROBE
0.21 m φ
Z
1.9 m
COOLING AIR
COMB. AIR DISTRIBUTOR
ORIFICE PLATES
PROBE
COMB. AIR
TOWN GAS
ST. STEEL JACKET
1.5mm
5.5mm
ALUMINA INSULATING TUBE
PROBE WIRE
20% RH-PT 0.5mmφ
COOLING TUBES
1.mmφ

Fig. 2.5.a

designed by Odidi (1974); as full details of the circuit components have been given there, only a brief exposition is given here.

The circuit, fig. 2.5.b, consists mainly of two parts; the first is concerned with the amplification of the signal, and the second pertains to the evaluation of the probability of reaction P (section 2.4.4).

The positive-ion current, 10^{-9}A to 10^{-6}A, is converted to voltage by passing it through a resistor R_c (1 KΩ). The resulting voltage (10^{-6} to 10^{-3} volts) is amplified on two stages to the value of 10 volts. The first amplification is accomplished by a differential amplifier (Analog Device, model AD 41K) with an amplification of 100. The differential amplifier permits the probe cooling-jacket to float at the plasma potential, i.e. to draw no current. The second stage amplification is achieved by an inverting amplifier (model AD 45K) with an amplification of 100. The output signal from this amplifier is fed to an R.M.S. meter (model Solarton T.D.A. JM 1860) to measure the time-mean value and R.M.S. of the fluctuating positive-ion current.

To evaluate P, the signal from the second amplifier is passed to a high-accuracy multiplier (model AD 427) for squaring (see section 2.4.4). The squared signal is then fed into a comparator (model AD 351 J) to produce different pulses having a constant amplitude, V_H, when $V_i^2 > V_c$ (see fig. 2.4.c). The integrator (model DISA 52B30) is used to evaluate the square bracket in equation 2.4-7, namely:

$$[\Sigma_i \tau_i (V_H - V_L)/\tau_t].$$

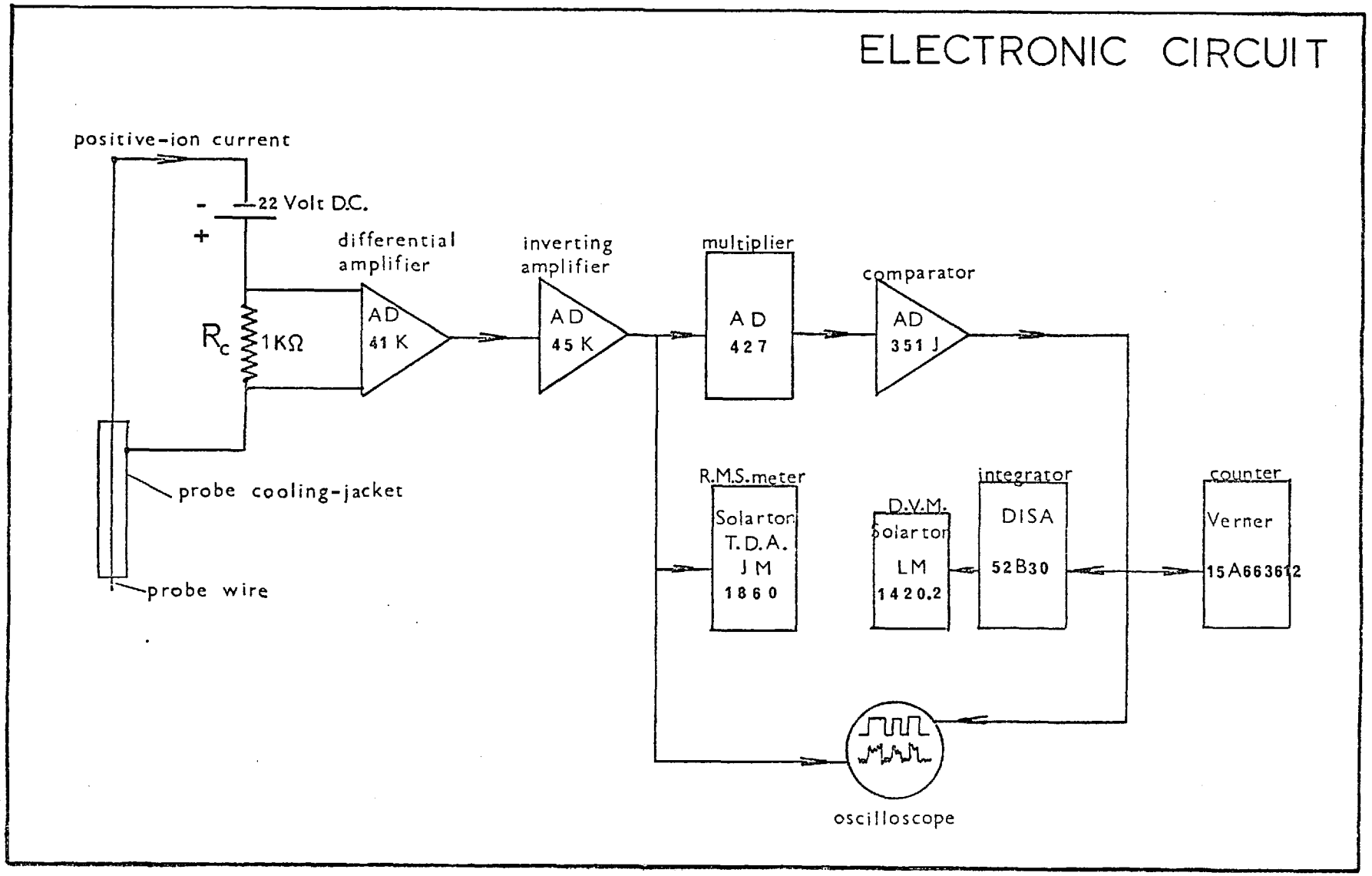
ELECTRONIC CIRCUIT
positive-ion current
-
+
22 Volt D.C.
differential amplifier
inverting amplifier
multiplier
comparator
R_c
1KΩ
AD 41 K
AD 45 K
AD 427
AD 351 J
probe cooling-jacket
probe wire
R.M.S.meter
Solartron T.D.A. J M 1860
D.V.M.
Solartron LM 1420.2
integrator
DISA 52B30
counter
Verner 15A663612
oscilloscope

Fig. 2.5.b

The counter (model VERNER 15A663612) is used to measure the number of times that $V_i^2 > V_c$ at a given point.

2.6 Experiments

2.6.1 General arrangement

The general arrangement of the test facility is shown schematically in fig. 2.5.a. Town-gas fuel is admitted into the furnace at one end through a central pipe, and air is introduced through the annulus. Standard orifice-plates are used to meter the flow rates of both air and fuel. The pressure differences across the orifices are recorded either by mercury or paraffin manometers.

The furnace was originally designed and used by El-Mahallawy et al (1973) to measure the time-mean concentration in a diffusion flame. It consists of an air-cooled stainless steel cylinder of 0.21 m i.d. and 1.9 m long, mounted horizontally. Twenty-five steel bushings are vertically mounted into threaded holes along the top furnace_wall to guide the vertical motion and to serve as locators for the measuring stations. The stations are non-uniformly placed to give more closely spaced measurements near the furnace inlet and less so near the exhaust end.

The probe-traversing mechanism, which allows the probe motion in r and z directions, consists of a four-wheeled carriage guided by two rails which run parallel to the furnace axis. The probe vertical motion is controlled by a D.C. electrical motor.

2.6.2 Experimental procedure

Before each run, the chemical analysis of the town gas was obtained from the supplier. Ambient temperature and pressure as well as air and town gas temperatures were recorded.

The town gas was ignited using a pilot flame through the guiding bushing near the furnace inlet, and then both air and fuel flow rates were adjusted. Steady state conditions were reached when the measured expansion, by a specially designed gauge, of the inner furnace tube showed a constant reading.

The ionization probe was then inserted into the first bushing until the probe wire was 30 mm below the furnace axis. The symmetry axis of the flow was located from measurements below and above the furnace axis. The readings of the true integrator (fig. 2.5.b) through the D.V.M. and of the R.M.S. meter were observed until they reached a steady value which was recorded. The probe was then moved upward to the next location at a distance of 2.5 to 5 mm from the previous one. The procedure was repeated until the furnace top wall was reached. Traverses were made at all stations between the inlet and the end of the flame where the probe detected no measurable ions.

2.6.3 Measurements taken

Mappings of the time-mean, R.M.S. of local positive-ion current, the frequency of reaction and the probability of reaction have been obtained for four different town gas turbulent diffusion flames. The input parameters for each flame are shown in Table 2.6. The choice

TABLE 2.6

Investigator	Present				El-Mahallawy et al (1973)
Parameter	Flame I	II	III	IV	A
Town gas vol. analysis:					
H_2	0.468	0.446	0.468	0.486	0.55
CH_4	0.29	0.323	0.29	0.309	0.27
CO_2	0.102	0.101	0.102	0.111	0.08
N_2	0.073	0.075	0.073	0.049	0.04
CO	0.027	0.023	0.027	0.024	0.04
C_2H_6	0.04	0.032	0.04	0.021	0.02
Stoich. A/F ratio	9.5	9.6	9.5	9.7	10.6
Inlet A/F ratio	22.9	15.4	20.1	16.9	15.75
Lower value of heat of reaction H J/kg of reactants.	5.75×10^7	5.77×10^7	5.75×10^7	5.88×10^7	5.75×10^7
Inlet fuel vel. u_1 (m/s)	6.01	17.18	22.0	23.0	21.57
Inlet air vel. u_0 (m/s)	17.37	12.64	21.0	17.0	13.46
Inlet vel. ratio (u_1/u_0)	.9	1.4	1.05	1.3	1.6
Inlet fuel density ρ_1 (kg/m^3)	0.566	0.572	0.566	0.542	0.474
Inlet air density ρ_0 (kg/m^3)	1.165	1.165	1.165	1.165	1.165
Re based on inlet conditions and furnace diameter	20500	15200	25000	21200	16200
Fuel nozzle i.d. (m)	.020	.020	.020	.020	.020
Fuel nozzle o.d. (m)	.045	.045	.045	.045	.045
Air nozzle i.d. (m)	.078	.078	.078	.078	.078

of the magnitude of each parameter was limited by three factors.

(a) In order to avoid the blow-off situation, the air/fuel ratios were selected within the flame stability limits.

(b) The second factor is the time required for mapping the entire field. A flame that extends to the furnace exit would require more than 12 hours (25 stations x 30 points x 1 minute). Also, the volumetric analysis of town gas is likely to change from day to day. Therefore, the air/fuel ratios were selected in order to have a flame well within the furnace.

(c) The expansion of the furnace tube in the axial direction depends on the input air/fuel ratio and the heat loss to cooling air, and it affects probe location relative to the fuel nozzle exit. The amount of expansion was kept constant throughout the measurements at 6 mm at the end of the furnace tube.

The results of the measurements will be presented and discussed in detail in Chapter 5.

2.7 Summary of main points

The main points discussed in this chapter are:

(a) The ionization-probe technique was described, exposing its advantages and limitations as compared to the optical-probe.

(b) The principle of operation of the ionization probe was summarised and a relation was obtained between the rate of recombination and the concentration of the positive-ion.

(c) The probability of chemical reaction, P, was defined and evaluated from measurement of the instantaneous positive-ion current at a given point. The error, due to the use of the present discrimination level of the comparator, in the measured P is estimated to be of the order of 10%.

(d) Finally, the test facilities and the measurement conditions were described. The limitations of the input parameters to the furnace were also discussed.

CHAPTER 3

MATHEMATICAL ANALYSIS

3.1 Introduction

In this chapter we introduce three mathematical models that are presumed to describe with sufficient accuracy the physics of turbulence, of chemical reaction and of concentration fluctuations in turbulent diffusion flames. The analysis is restricted to time-steady, gaseous phase, axially symmetrical situations where recirculation may occur.

The models, in the form of a set of time-steady partial differential equations, allow the prediction of both the fluid dynamic and thermodynamic properties of the flow.

The chemical reaction is assumed to influence the flow field through only the spatial variation of the time-mean density. In obtaining the density, the effects of the fluctuations of both temperature and concentration are accounted for.

Buoyancy effects on both the mean motion and turbulence are ignored. The data, which are compared with the predictions in Chapter 5, were collected from a furnace whose axis of symmetry is horizontal; consequently the buoyancy forces must give rise to three-dimensional effects which cannot be treated by the present numerical procedure.

Also heat transfer to or from the system is not accounted for; the reason is explained in sec. 3.2.4.

The equations governing the time-mean motion are given in the next section; the proposed mathematical-models are described and discussed in the subsequent sections (from 3.2.2 to 3.2.7), and finally a numerical procedure which was used to solve the equation set is briefly discussed in section 3.3.

3.2 Equations and models for turbulent reacting flows

3.2.1 The time-mean motion

The time-mean motion of a turbulent flow is governed by the laws of mass and momentum conservation. For the present axisymmetric case, these laws can be expressed in terms of a stream function ψ and a vorticity ω (Wolfshtein 1967, Gosman et al 1969). These two variables are defined as follows:

$$\psi \equiv \int [\rho r(udr - vdz)], \qquad (3.2\text{-}1)$$

$$\omega \equiv \frac{\partial v}{\partial z} - \frac{\partial u}{\partial r} \qquad (3.2\text{-}2)$$

where u and v are the time-mean velocity components in the axial and radial directions respectively. The two resulting equations are non-linear, partial differential equations of the elliptic type; they can be cast in the following common form, in cylindrical-polar coordinates:

$$\underbrace{a[\partial(\phi\partial\psi/\partial r)/\partial z - \partial(\phi\partial\psi/\partial z)\partial r]}_{\text{CONVECTION TERMS}} - \underbrace{\partial[br\partial(c\phi)/\partial z]/\partial z - \partial[br\partial(c\phi)/\partial r]/\partial r}_{\text{DIFFUSION TERMS}} + \underbrace{rd}_{\text{SOURCE TERM}} = 0 \qquad (3.2\text{-}3)$$

In the above equation, ϕ stands for either ψ or ω/r, and the meanings of the functions a, b, c and d are given below in table 3.2.1.

Table 3.2.1

ϕ	a	b	c	d
ψ	0	$1/\rho r^2$	1	$-\omega/r$
ω/r	r^2	r^2	μ_{eff}	$r\left[\frac{\partial}{\partial r}\frac{(u^2+v^2)}{2}\frac{\partial\rho}{\partial z} - \frac{\partial}{\partial z}\frac{(u^2+v^2)}{2}\frac{\partial\rho}{\partial r}\right]$

The use of the stream function and vorticity as dependent variables avoids the need to consider directly the pressure and the two component velocities, u, v. However, the velocities can be recovered from the stream function via the definition (3.2-1) and the pressure from the r- and z- direction momentum equations (Gosman et el 1969).

From table 3.2.1, it is clear that in order to solve eqs. (3.2-3) for ψ and ω, it is necessary to provide information about ρ, the time-mean density, and about μ_{eff}, the effective viscosity. First, we shall address ourselves to the task of obtaining μ_{eff} with the help of a turbulence model.

3.2.2 The turbulence model

(a) Background

For all turbulent flows, the exact time-dependent conservation equations of mass, momentum, concentration, etc., cannot be solved analytically or numerically by present-day computers because:

(i) the equations are non-linear, partial differential;

(ii) turbulence is three-dimensional motion, and many of the important processes take place on very small scales. Therefore, numerical techniques which calculate the dependent var..ables at discrete points in space would need approximately 10^6 grid points to cover a volume of one cubic centimetre; this requirement is beyond the capacity of even the largest existing computers.

Fortunately, experience with turbulent flows in pipes, boundary layers on walls and in free jets suggests that the time-dependent character of turbulence can be ignored (Gosman et al 1969 pp.10), and the time-averaged equations provide sufficient information about the flow. Also there is no need for excessively fine grids, since the time-averaged properties vary with position far more gradually than the details of the turbulence structure. In the process of time-averaging, the number of unknowns (correlations) grows faster than the number of equations; thus closure cannot be achieved. One way to close the system of the time-averaged equations is by approximating some or all of the correlations in terms of quantities that can be calculated; this process is often referred to as "turbulence modelling".

There are two approaches of modelling cross-correlations involving fluctuations of vectoral quantities, e.g. $\langle u'v' \rangle$, namely the eddy or turbulent viscosity and the Reynolds' or turbulent-stress concepts. The turbulent-viscosity concept was first introduced by Boussinesq (1877) who suggested that the effective turbulent shear stress, $-\rho \langle u'v' \rangle$, could be replaced by $\mu_t \, \partial u/\partial r$. The task of evaluating μ_t has been the concern of many workers in the field of turbulence.

Since an up-to-date survey of such efforts has been given by Launder and Spalding (1972), only a brief exposition is given here.

The different methods of modelling μ_t may be classified as either algebraic-equation or differential-equation type. The former approach is the one where μ_t is calculated from algebraic formulae involving only a mean velocity and an empirically-defined mixing length (for example, Prandtl's mixing-length hypothesis). In the second, μ_t is obtained by solving the differential equations for one or more properties of the turbulent motion.

The Reynolds'stress concept of modelling the correlations of velocity fluctuations provides differential transport equations for the turbulent correlations themselves (Hanjalic and Launder 1972). For 2-D recirculating flows, as in the present investigation, the Reynolds'stress model requires at least five partial differential equations in addition to the ones for the mean flow. The computer time and storage required for solving these equations become prohibitively large when considering the details of the turbulent reacting flow. The employment of the Reynolds' stress model, however, becomes necessary for highly anisotropic flows, for example, when strong swirl is present in the flow.

For the economic reasons mentioned above, and with the absence of swirl, the turbulent-viscosity approach is adopted in the present investigation. Specifically, μ_{eff} is calculated from:

$$\mu_{eff} = \mu_t + \mu \,, \qquad (3.2\text{-}4)$$

and

$$\mu_t = c_\mu \rho \, k^2/\varepsilon \qquad (3.2\text{-}5)$$

where c_μ is a constant, ρ is the local fluid time-mean density, k is the kinetic energy of turbulence and ε is the time rate of dissipation of k. The turbulence quantities k and ε are obtained from the solution of two differential equations to which we now turn our attention.

(b) The equations for k and ε

The kinetic energy of turbulence k is defined as:

$$k \equiv \langle u_i' u_i' \rangle /2, \qquad (3.2\text{-}6)$$

where u_i''s are the components of velocity fluctuations in the three directions of space, and the summation convention is used (i.e., $a_i b_i = a_1 b_1 + a_2 b_2 + a_3 b_3$). The transport equation for k has been considered by many authors (e.g., Hinze 1959, Bray 1973-a). Gosman et al (1969) introduced a modelled k equation in cylindrical coordinates in the form of eq. (3.2-3). This form of the k-equation is adopted here, and the meaning of the corresponding functions a, b, c and d are given below in table 3.2.2.

Table 3.2.2

ϕ	a	b	c	d
k	1	μ_{eff}/σ_k	1	$\rho\varepsilon - G_k$
ε	1	$\mu_{eff}/\sigma_\varepsilon$	1	$c_2 \rho \varepsilon^2/k - c_1 G_k \varepsilon/k$
The generation expression for k, G_k is given by: $G_k \equiv \mu_{eff} \{ 2[(\partial u/\partial z)^2 + (\partial v/\partial r)^2 + (v/r)^2] + (\partial u/\partial r + \partial v/\partial z)^2 \}$				

It must, however, be pointed out that Bray (1973a,1974) has demonstrated, by order of magnitude analysis, that large number of terms in his rigorously derived time-averaged k equation cannot all be simply neglected. An assessment of the effects of these terms on the predicted results is needed.

The rate of viscous dissipation of turbulent kinetic energy, ε is defined as:

$$\varepsilon \equiv \nu \left\langle \left(\frac{\partial u'_i}{\partial x_j} \right)^2 \right\rangle \qquad (3.2\text{-}7)$$

which is the mean scalar product of the instantaneous viscous stress and the instantaneous rate of strain. In the definition (3.2-7), the x_j's are the distances along the coordinates r,z; ν is the kinematic viscosity, and the summation convention is used. Davydov (1961) and Harlow and Nakayama (1968) have derived the exact transport equation for ε . Hanjalic (1970) has found that the ε equation can be modelled in a form similar to that of the k equation; the source term for ε is modelled by proportionality to that of k, where the proportionality factor is equal to a constant multiplied by ε/k. For recirculating flows with a high Reynolds' number of turbulence, $R_{e_{turb}} \equiv \frac{\rho k^2}{\mu \varepsilon}$, the ε equation in cylindrical coordinates takes the form of equation (3.2-3), with the source term d as presented in table 3.2.2 (Rodi, 1970).

In practical turbulent flows, knowledge of k and ε alone does not readily allow a physical description of the nature of the flow to be built up. It is however possible to deduce from k and ε some definitions for the length and time-scales that can be easily compared with characteristic scales of the flow. A local length scale of turbulence proportional to the size of energy-containing eddies, ℓ ,

can be defined as:

$$\ell \equiv k^{3/2}/\varepsilon \quad ; \qquad (3.2\text{-}8)$$

the corresponding time-scale, t, is obtained from:

$$t = k/\varepsilon \qquad (3.2\text{-}9).$$

Equation (3.2-4) indicates that μ_{eff} can be obtained only if ρ, the time-mean density, is known at every point in the flow field; furthermore, the knowledge of ρ is required to close the equation set (3.2-3), as has been discussed in the preceding section.

3.2.3 The time-mean density

In a turbulent reacting flow, the instantaneous density at a given point exhibits large fluctuations caused by the fluctuations of temperature and concentration (Kent and Bilger 1972, Bray 1973-a). This is demonstrated as follows.

The instantaneous mixture density can be written as:

$$\tilde{\rho} = \frac{\tilde{p}}{\mathcal{R}} / \tilde{T} \Sigma_j \left(\frac{\tilde{m}_j}{M_j}\right), \qquad (3.2\text{-}10)$$

where $\tilde{\rho}$, $\tilde{p}$, $\tilde{T}$ and $\tilde{m}_j$ stand for the instantaneous values of density, absolute pressure, temperature and the j-species mass-fraction respectively; $\mathcal{R}$ is the universal gas constant and M_j is the molecular weight of the j-species. Defining $\tilde{\alpha}$ as $\Sigma_j \left(\frac{\tilde{m}_j}{M_j}\right)$, and writing: $\tilde{\rho} \equiv \rho + \rho'$, $\tilde{T} \equiv T+T'$, $\tilde{p} \equiv p+p'$ and $\tilde{\alpha} \equiv \alpha+\alpha'$, we can express the time-mean density as:

$$\rho = \frac{p}{R\alpha T}\left[1 - \frac{\langle T'\alpha'\rangle}{T\alpha} + \frac{\langle T'\alpha'\rangle^2}{T^2\alpha^2} - \cdots\right] \qquad (3.2\text{-}11).$$

It can be seen that neglecting the first and second order terms in eq. (3.2-11) will over estimate ρ in regions where $\langle T'\alpha'\rangle / T\alpha$ is not much smaller than unity. Thus, to evaluate correctly the time-mean density, it is necessary to include the effects of the fluctuations in both temperature and concentration. Two models are required to achieve this goal. The first is for the chemical reaction whereby the instantaneous values of temperature and concentration are obtained. The second is a model for the fluctuations of concentration which provides a means of evaluating the time-mean properties. Both of these models will be discussed in turn in the following sections.

3.2.4 The chemical-reaction model

The model proposed here is based on the assumption that, whenever fuel and oxidant both exist at a point, chemical reaction will instantaneously proceed to completion in a single step, producing combustion products. In other words, the laminar diffusion flame (Burke and Schumann 1928) holds instantaneously for the turbulent diffusion flame. This assumption of instantaneous chemical equilbrium is not far from reality in turbulent unpremixed flames because the time of recombination of the non-equilbrium radicals in hydrogen-rich flames is of the order of 10^{-6} sec, while the smallest time-scale of turbulence is about 10^{-4} sec (Günther and Simon 1969).

From the above assumptions and from the works of Shvab (1948), Zeldovich (1949), Williams (1965) and Gosman et al (1969), it can be

concluded that a linear combination of the equations describing conservation of two unpremixed-reactants, fuel and oxidant, yields an equation whose form is identical to that describing the convection-diffusion of chemically inert species; that is to say, neither equation has a source term, provided that:

(a) the turbulent transport coefficients for the two reactants are equal at every point in the field, and

(b) one kg of fuel combines always with (i) kg of oxidant to produce (1+i) kg of combustion products.

The dependent variable, the mixture fraction f, of the equation that results from the linear combination of the two conservation equations of fuel and oxidant, is defined as:

$$f \equiv (\gamma - \gamma_0)/(\gamma_1 - \gamma_0) \ , \qquad (3.2\text{-}12)$$

and

$$\gamma \equiv m_{fu} - m_{ox}/i \ , \qquad (3.2\text{-}13)$$

or

$$\gamma \equiv m_{fu} + m_{pr}/(1+i) \ , \qquad (3.2\text{-}14)$$

where i is the mass of oxidant required for the complete combustion of a unit mass of fuel, and the subscripts 1 and 0 denote the initial conditions of the unpremixed fuel and oxidant streams respectively. The conservation equation of f is a partial differential of the elliptic type (Gosman et al 1969) and can be written in the general form of eq. (3.2-3) with Ø standing for f and the meanings of a, b, c and d given below in table 3.2.3.

Table 3.2.3

Ø	a	b	c	d
f	1	μ_{eff}/σ_f	1	0

Since we need the instantaneous values of the mass fractions of the reactants, the definitions (3.2-12) to (3.2-14) can be written in an instantaneous form, using the following relations:

$$\tilde{f} \equiv f + f' \quad , \tag{3.2-15}$$

$$\tilde{\gamma} \equiv \gamma + \gamma' \quad , \tag{3.2-16}$$

$$\tilde{m}_j \equiv m_j + m_j' \quad , \tag{3.2-17}$$

The assumption of chemical equilibrium at the instantaneous level is used to obtain the important relations:

$$0 \leqslant \tilde{f} \leqslant f_{st} : \quad \tilde{m}_{fu} = 0, \quad \tilde{m}_{ox} = m_{ox,0} \, (1-\tilde{f}/f_{st}) \tag{3.2-18}$$

$$f_{st} \leqslant \tilde{f} \leqslant 1 : \quad \tilde{m}_{ox} = 0, \quad \tilde{m}_{fu} = m_{fu,1} \, (\tilde{f}-f_{st})/(1-f_{st}) \tag{3.2-19}$$

where f_{st} is the stoichiometric value of the mixture fraction, being obtained from eqs. (3.2-12), (3.2-13) as:

$$f_{st} = 1/[1 + i(m_{fu,1}/m_{ox,0})] \tag{3.2-20}$$

The mass fraction of the products of combustion is obtained from:

$$\tilde{m}_{pr} = 1 - \tilde{m}_{fu} - \tilde{m}_{ox} \quad , \tag{3.2-21}$$

but the composition of the products, which usually include some inert, is obtained from stoichiometric considerations as will be shown later.

Figure (3.2.a) illustrates the linear relationship between the instantaneous mass fractions of the reactants and $\tilde{f}$ as expressed in eqs. (3.2-18) to (3.2-21). The linear variation of the enthalpy $\tilde{h}$

with $\tilde{f}$ comes from the following considerations.

Zeldovich (1949) and Gosman et al (1969) have indicated that the enthalpy h at a point can be linearly related to f, if the two conditions (a) and (b) above are satisfied together with the following three further conditions:

(c) The boundaries of the combustion system are adiabatic;

(d) the Lewis number (the ratio of thermal diffusivity to the diffusion coefficient of concentration) is unity,

(e) and both the kinetic energy of the mean flow and of turbulence are negligible compared to the heat of reaction H. The relationship between h and f can be written as:

$$f \equiv (h - h_0)/(h_1 - h_0) , \qquad (3.2\text{-}22)$$

where

$$h = \int_0^T c_p dT + H.m_{fu} \qquad (3.2\text{-}23)$$

In eq. (3.2-23), c_p is the specific heat at constant pressure, H is the fuel heat of reaction and the subscripts 0, 1 denote the initial conditions of the unpremixed oxidant and fuel streams respectively.

Gosman et al (1969) have derived a conservation equation for h which is similar in form to eq. (3.2-3) with a zero source term, d; i.e., as in the f equation. The five conditions (a), (b), (c), (d) and (e) above, though advantageous in reducing by two the total number of equations to be solved, do not permit the inclusion of heat transfer to or from the system.

The linear variation of $\tilde{h}$ with $\tilde{f}$ in fig. 3.2.a is obtained from eq. (3.2-22) and by writing $\tilde{h}$ as

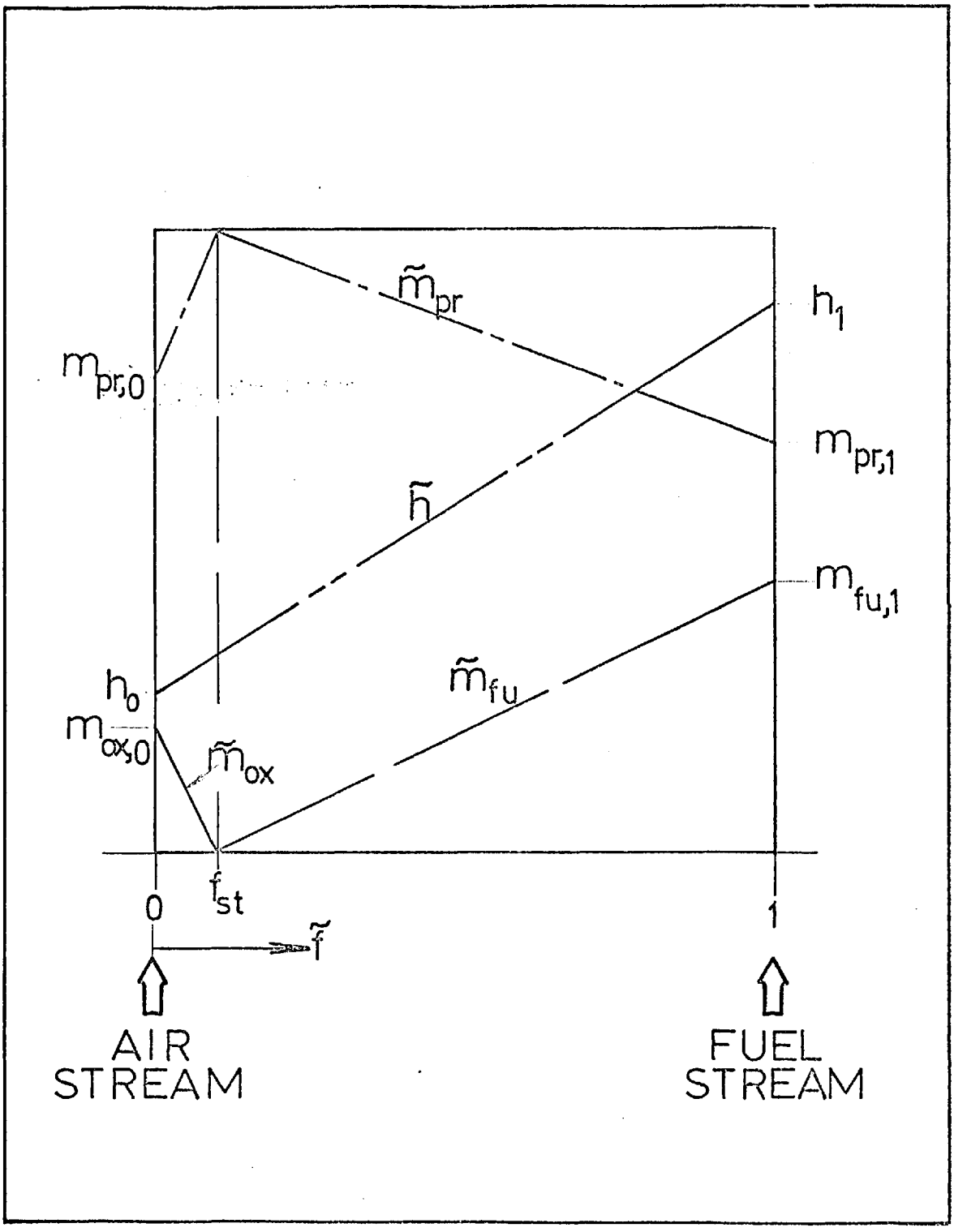
$\tilde{m}_{pr}$
h_1
$m_{pr,0}$
$m_{pr,1}$
$\tilde{h}$
$m_{fu,1}$
h_0
$\tilde{m}_{fu}$
$m_{ox,0}$
$\tilde{m}_{ox}$
0
f_{st}
1
$\tilde{f}$
AIR STREAM
FUEL STREAM

Fig. 3.2.a

$$\tilde{h} \equiv h + h' \; ; \qquad (3.2\text{-}24)$$

$\langle h' \rangle = \langle f' \rangle = 0$ for stationary turbulence.

From the above discussion, and by reference to fig. 3.2.a, we can immediately write the relations:

$$\tilde{h} = h_0 + \tilde{f}\,(h_1 - h_0) \quad , \qquad (3.2\text{-}25)$$

$$\tilde{T} = (\tilde{h} - H.\tilde{m}_{fu}) / \Sigma_j \tilde{m}_j c_{p_j} \quad , \qquad (3.2\text{-}26)$$

where $$h_0 = c_{p_{ox,0}} T_0 + c_{p_{inert,0}} T_0 \qquad (3.2\text{-}27)$$

and $$h_1 = c_{p_{fu,1}} T_1 + c_{p_{inert,1}} T_1 + H\, m_{fu,1} \qquad (3.2\text{-}28)$$

How the instantaneous temperature $\tilde{T}$ can be calculated from eq. (3.2-26) and how the density $\tilde{\rho}$ is evaluated will be discussed in the next section.

3.2.5 Thermodynamic considerations

To evaluate $\tilde{T}$ from eq. (3.2-26), the summation term, $\Sigma_j \tilde{m}_j c_{p_j}$, is calculated from:

$$\Sigma_j \tilde{m}_j c_{p_j} = \tilde{m}_{ox} c_{p_{ox}} + \tilde{m}_{fu} c_{p_{fu}} + \tilde{m}_{pr} c_{p_{pr}} \qquad (3.2\text{-}29)$$

The specific heats, $c_{p_{ox}}$, $c_{p_{fu}}$ and $c_{p_{pr}}$, at a given point in the flow, are taken as functions of the chemical composition of the oxidant, fuel and combustion products respectively. Also it is assumed that the specific heats follow a third order polynomial-type variation with the local time-mean temperature (Glasstone 1946; Tribus and

Desoto 1961). The composition of the combustion products is obtained from the stoichiometric reaction of a hydrocarbon fuel, C_nH_{2n+2}, diluted with inert, and air:

$$C_n H_{2n+2} + \beta_2 CO_2 + \beta_3 CO + \beta_1 N_2 + \alpha_1 O_2 + 3.76\alpha_1 N_2 \longrightarrow$$

$$\alpha_3 H_2O + (3.76\alpha_1 + \beta_1) N_2 + (\alpha_2 + \beta_2) CO_2 \qquad (3.2\text{-}30)$$

where the α_i's and β_i's stand for the species mol-fractions. To solve eq. (3.2-30) for the composition of the products of reaction, three algebraic atom balance equations are written for the carbon, hydrogen and oxygen atoms. The three equations yield the values of the three unknowns α_1, α_2 and α_3.

The knowledge of the instantaneous values of the mass fractions and of the temperature yields directly the value of the instantaneous density $\tilde{\rho}$ via the perfect gas law:

$$\tilde{\rho} = p/\mathcal{R}\tilde{T} \Sigma_j (\tilde{m}_j/M_j). \qquad (3.2\text{-}31)$$

What remains now is the calculation of the time-mean density; this, as mentioned earlier, needs a model for concentration fluctuations.

3.2.6 Concentration-fluctuations model

(a) Background

In order to obtain the time-mean value, θ, of a statistically-steady, randomly fluctuating-quantity $\tilde{\theta}(t)$ which varies with time, t

(as shown in fig. 3.2.b) it is necessary to have information about its

Fig. 32.b

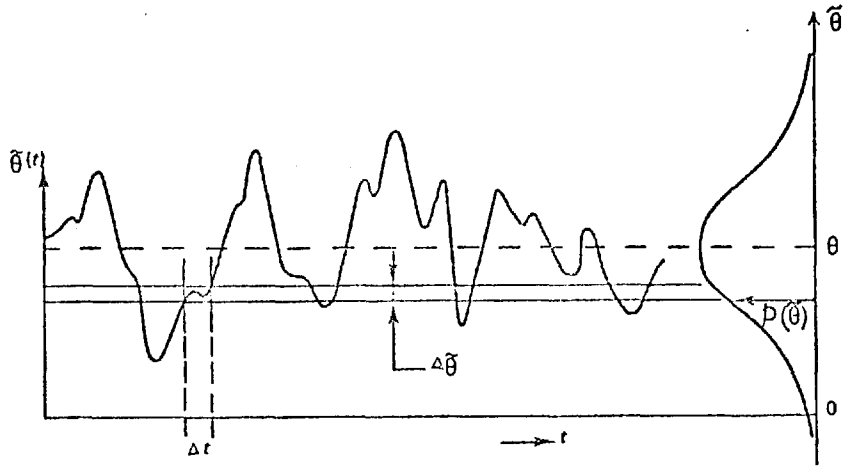

probability density function $p(\tilde{\theta})$ which is defined through:

$$p(\tilde{\theta})\ \Delta\tilde{\theta} \equiv \lim_{t\to\infty} \frac{1}{t}\ \Sigma(\Delta t)\ . \qquad (3.2\text{-}32)$$

The definition (3.2-32) implies that $p(\tilde{\theta})\ \Delta\tilde{\theta}$ is the fraction of time that $\tilde{\theta}(t)$ spends between $\tilde{\theta}$ and $\tilde{\theta} + \Delta\tilde{\theta}$, and that over a long time interval the sum of the values of $p(\tilde{\theta})\ \Delta\theta$ must be equal to one, i.e.

$$\int_{-\infty}^{\infty} p(\tilde{\theta})\ d\tilde{\theta}\ = 1\ . \qquad (3.2\text{-}33)$$

From the knowledge of $p(\tilde{\theta})$, the time-mean value θ can be obtained from the definition:

$$\theta \equiv \lim_{t\to} \frac{1}{t} \int_{to}^{to+t} \tilde{\theta}(t)\ dt\ . \qquad (3.2\text{-}34)$$

From eqs. (3.2-32) and (3.2-34) we get:

$$\theta\ = \int_{-\infty}^{\infty} \tilde{\theta}\ p(\tilde{\theta})\ d(\tilde{\theta}) \quad , \qquad (3.2\text{-}35)$$

which is simply the first moment of $p(\tilde{\theta})$ about the origin, $\tilde{\theta} = 0$.

If we have another time-dependent variable $\tilde{\alpha}(\tilde{\theta})$ which is a

function of $\tilde{\theta}$, its time-mean value α can be obtained from:

$$\alpha = \int_{-\infty}^{\infty} \tilde{\alpha}(\tilde{\theta})\, p(\tilde{\theta})\, d\tilde{\theta} \qquad (3.2\text{-}36)$$

Equation (3.2-36) forms the basis of the time-averaging process used here for all such variables as density, temperature and mass fractions which are dependent on the mixture fraction $\tilde{f}$ only. For example, if it is required to calculate the time-mean mass fraction of fuel, m_{fu}, we have to obtain first $p(\tilde{f})$, the probability density function for $\tilde{f}$; then with the help of the expression for $\tilde{m}_{fu}$, eq. (3.2-19), formula (3.2-36) will lead us to a value of m_{fu}.

Unfortunately, no measurements have been reported, as far as it is aware, which enable us to determine $p(\tilde{f})$ for turbulent diffusion flames. Until such measurements become available, we are left with the alternative of assuming an arbitrary $p(\tilde{f})$. Two parameters are required to specify the probability density function $p(\tilde{f})$. The first is the mean-value f; the other is the mean-square departure from the mean-value or the variance, g, which is defined as:

$$g \equiv [\tilde{f} - f]^2$$

$$\equiv \langle f'^2 \rangle \qquad (3.2\text{-}37)$$

Let us first discuss how g can be calculated; afterwards, a proposal for $p(\tilde{f})$ will be introduced.

(b) The equation for g

The transport equation for the mean-square of concentration fluctuations in isothermal flows has been derived by several authors

e.g., Csanady (1967), Spalding (1971). Bray (1973-a) derived a rigorous time-mean equation for the square of concentration fluctuations for chemically-reacting flows. Independently, Csanady (1967) and Spalding (1970) modelled their isothermal g equation in a form similar to that of the k equation for boundary layer flows modelled by, for example, Rodi and Spalding (1970).

Spalding (1970) used this modelled g equation with the equations of k and w (w being the time-mean square of the vorticity fluctuations) to predict free turbulent diffusion flames. In the present study, we shall use Spalding's model. However, because of the elliptic nature of the flow, we must include in the generation and diffusion terms the gradients of f and g respectively, in both the r- and z- directions. The final equation for g can be written in the same form as eq. (3.2-3); the source term, d, adopted is given in table 3.2.4.

Table 3.2.4

ϕ	a	b	c	d
g	1	μ_{eff}/σ_g	1	$c_{g2}\rho\varepsilon g/k - c_{g1}\mu_{eff}[(\partial f/\partial z)^2 + (\partial f/\partial r)^2]$

It should be pointed out that chemical reaction exerts its influence on g (as also on f, k, ε, ψ and ω) only through the time-mean density ρ in the convection and diffusion terms. It is expected, however, that the fluctuations of the rate of reaction may also influence directly the time decay rate of concentration fluctuations. This analysis will not be pursued here, though an investigation of this problem is required.

Having considered the evaluation of g, we now turn our attention to the problem of ascribing a suitable probability-density function to $\tilde{f}$.

(c) The probability-density function $p(\tilde{f})$

A satisfactory choice of $p(\tilde{f})$ should simulate the physics of concentration fluctuations in turbulent flames; that is, $\tilde{f}$ should vary randomly with time and should be bounded between 0 and 1 (from the definitions 3.2-12 to 3.2-17). Different assumptions have been adopted by various authors; some used random wave forms and others chose deterministic ones.

Hawthorne et al (1949) and Thring and Newby (1953) used a Gaussian distribution extending from $-\infty$ to ∞. Richardson et al (1953) employed a beta-function distribution for values of the mixture fraction between 0 and 1 without taking account of the fraction of time spent by the concentrations at those limits. Bilger and Kent (1972) used a symmetrically truncated Gaussian distribution centred about the time-mean mixture fraction value. The truncation limits were ± 2 which allowed the instantaneous mass fractions to assume values less than 0 or greater than 1. The intermittency level was then used as a weighting factor to ensure non-negative time-mean mass fractions. Spalding (1971) used a probability density function corresponding to a sine wave form of the $\tilde{f}$ variation with time for an isothermal free jet and a battlement-shape wave for free jet turbulent diffusion flame (Spalding 1970). Rhodes and Harsha (1972) employed a triangular probability density function for economical computational considerations, but they stated that a beta-function distribution would be more realistic. Bush and Fendell (1973) suggested a triangular-wave form for $\tilde{f}$, bounded between $f = 0$ and 1. The corresponding probability density is represented by two delta functions at the boundary limits and uniform density in between.

Naguib (1973) used a clipped Gaussian distribution between $\tilde{f} = 0$ and 1 to predict the intermittency in isothermal and reacting free jets. The meanings of truncated and clipped Gaussian distributions are given, for example, by Bendat and Piersol (1971).

In the present study, $p(\tilde{f})$ is taken to be of the clipped Gaussian type, as shown in fig. 3.2.c. In terms of $\tilde{f}$, $p(\tilde{f})$ can be expressed as:

$$p(\tilde{f}) = e^{-(\tilde{f}-F)/2\sigma^2}\,[U(\tilde{f}-0) - U(\tilde{f}-1)]/\sigma\sqrt{2\pi}$$

$$+ 2A_0\,\delta(\tilde{f}-0) + 2A_1\,\delta(\tilde{f}-1)\ . \qquad (3.2\text{-}38)$$

In eq. (3.2-38), $U(\xi)$ is a unit step function defined by $U(\xi) = 0$, $\xi < 0$; $U(\xi) = 1$, $\xi > 0$ and $\delta(\xi)$ denotes the Dirac delta function defined by: $\int_a^b y(\xi)\,\delta(\xi-x)\,d\xi = \frac{1}{2}\,y(x)$, if $x = a$ or $x = b$. A_0 and A_1 are given by:

$$A_0 = \int_{-\infty}^{0} e^{-(\tilde{f}-F)^2/2\sigma^2}\,d\tilde{f}/(\sigma\sqrt{2\pi}) \qquad (3.2\text{-}39)$$

$$A_1 = \int_{1}^{\infty} e^{-(\tilde{f}-F)^2/2\sigma^2}\,d\tilde{f}/(\sigma\sqrt{2\pi}) \qquad (3.2\text{-}40)$$

F and σ are respectively the mean and standard deviation for the complete Gaussian distribution, a portion of which forms part of $p(\tilde{f})$, fig. (3.2.c). The time mean value, f, and the variance, g, of $p(\tilde{f})$ are respectively given by the first moment about $\tilde{f} = 0$ and the second moment about the mean value of the area under $p(\tilde{f})$:

$$f = A_1 + \int_0^1 \tilde{f}\, e^{-(\tilde{f}-F)^2/2\sigma^2}\,d\tilde{f}/(\sigma\sqrt{2\pi}) \qquad (3.2\text{-}41)$$

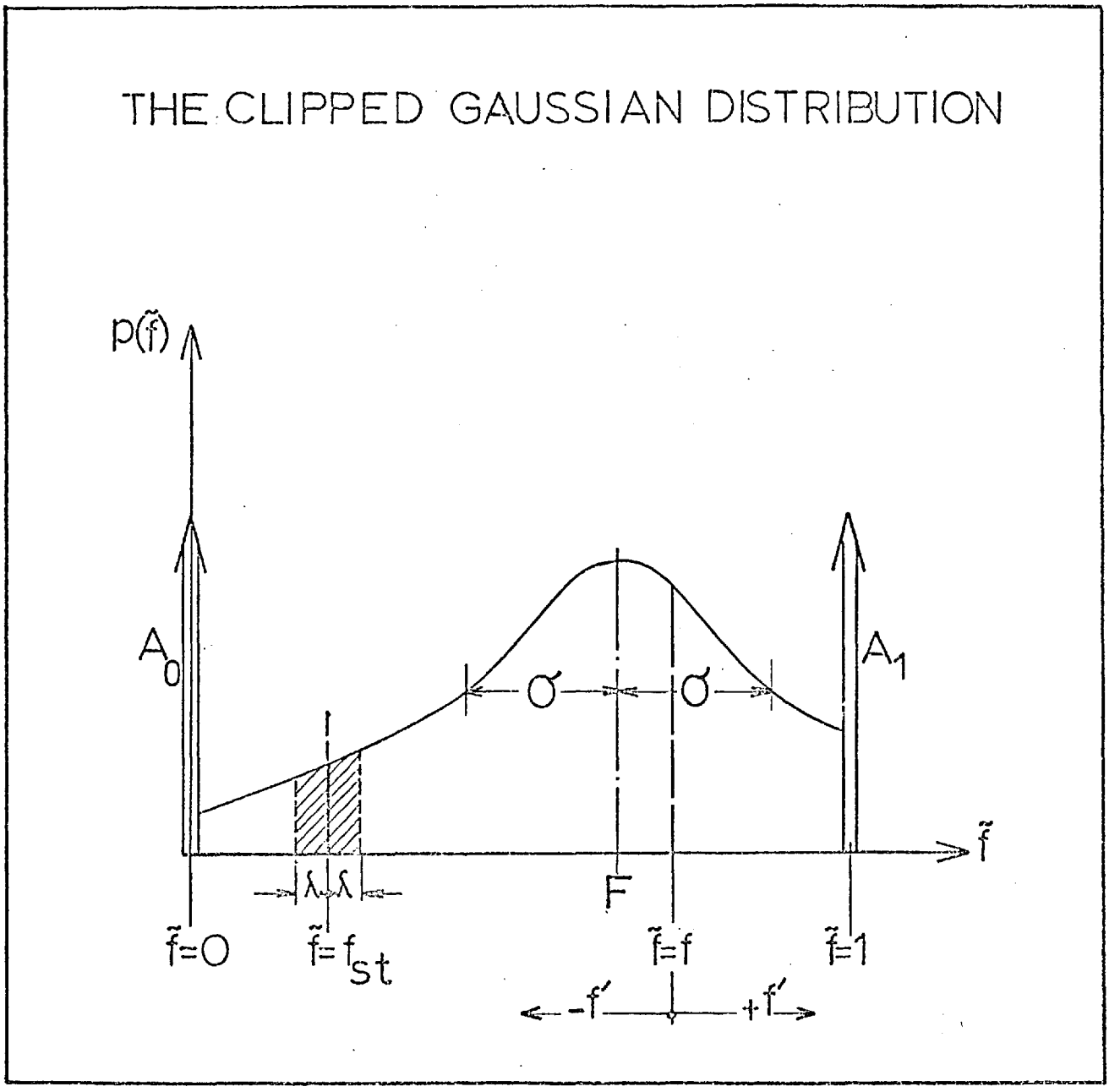
THE CLIPPED GAUSSIAN DISTRIBUTION
p(f̃)
A0
A1
σ
σ
δ
δ
F
f̃
f̃=0
f̃=fst
f̃=f
f̃=1
-f′
+f′

Fig. 3.2.c

$$g = A_1 - f^2 + \int_0^1 \tilde{f}^2 \, e^{-(\tilde{f}-F)^2/2\sigma^2} \, d\tilde{f}/(\sigma\sqrt{2\pi}) \qquad (3.2\text{-}42)$$

Thus, at any given point, when both f and g are known from the solution of the differential eq. set (3.2-3), solution of eqs. (3.2-41) and (3.2-42) will yield the corresponding values for σ and F, and hence $p(\tilde{f})$ via eq. (3.2-38). The solution of eqs. (3.2-41) and (3.2-42) can be speedily accomplished with the aid of a table of values of σ and F against corresponding values of f and g (Appendix B). It is interesting to note that F could assume values less than 0 or greater than 1 while f cannot. Figs. 3.2.d to 3.2.h show $p(\tilde{f})$ for different values of f and g at typical points in the field of a turbulent diffusion flame.

3.2.7 Evaluation of the time-mean properties

The time-mean mass fraction of fuel, m_{fu}, is given by:

$$m_{fu} = m_{fu,1} \; A_1 + \frac{1}{\sigma\sqrt{2\pi}} \int_{f_{st}}^1 [(\tilde{f}-f_{st})/(1-f_{st})] \; e^{-(\tilde{f}-F)^2/2\sigma^2} \; d\tilde{f} \qquad (3.2\text{-}43)$$

time-mean mass fraction of oxidant:

$$m_{ox} = m_{ox,0} \; A_0 + \frac{1}{\sigma\sqrt{2\pi}} \int_0^{f_{st}} [1-\tilde{f}/f_{st}] \; e^{-(\tilde{f}-F)^2/2\sigma^2} \; d\tilde{f} \; . \qquad (3.2\text{-}44)$$

The time-mean mass fraction of combustion products, m_{pr}, is obtained from:

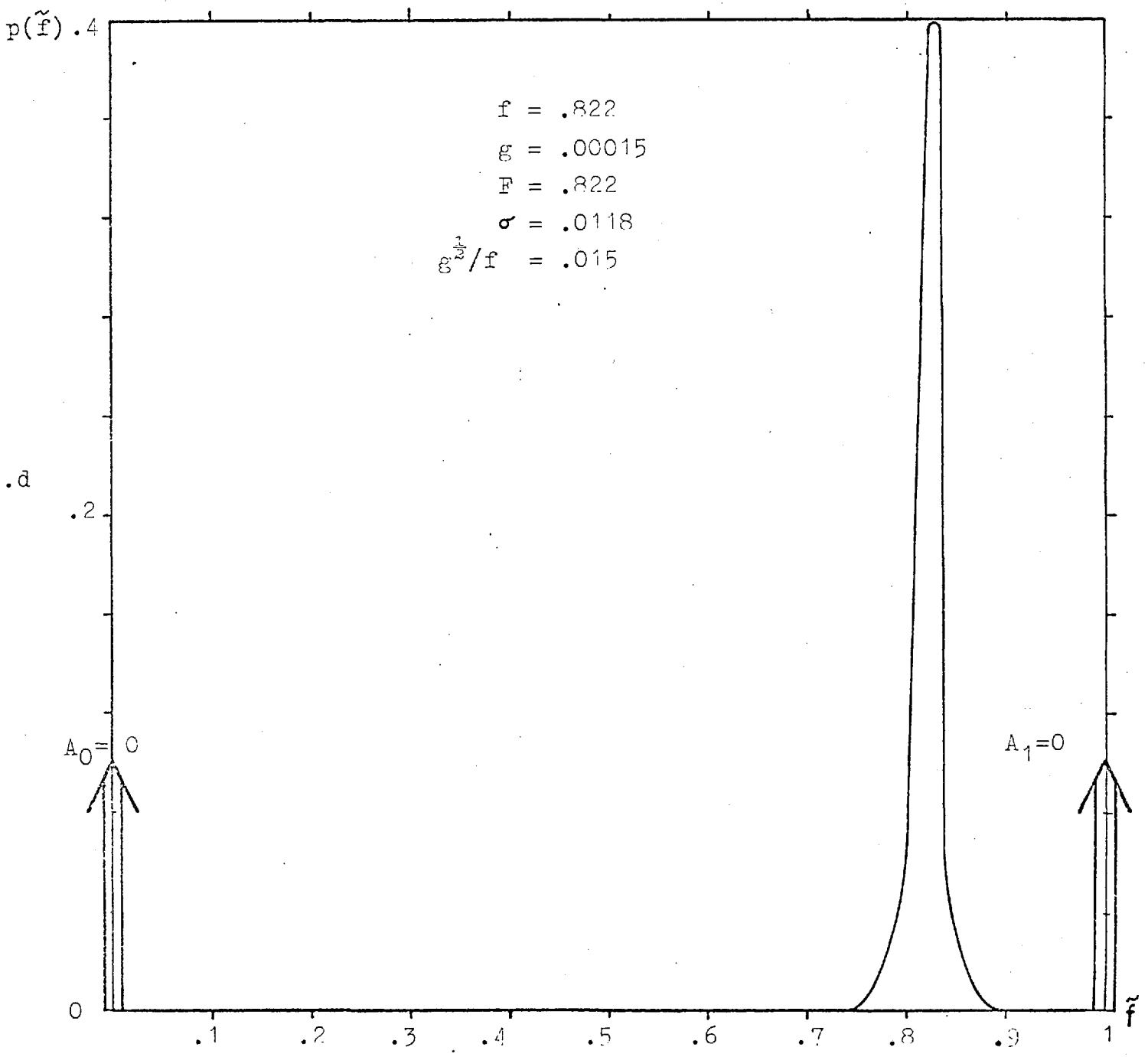

Fig. 3.2.d

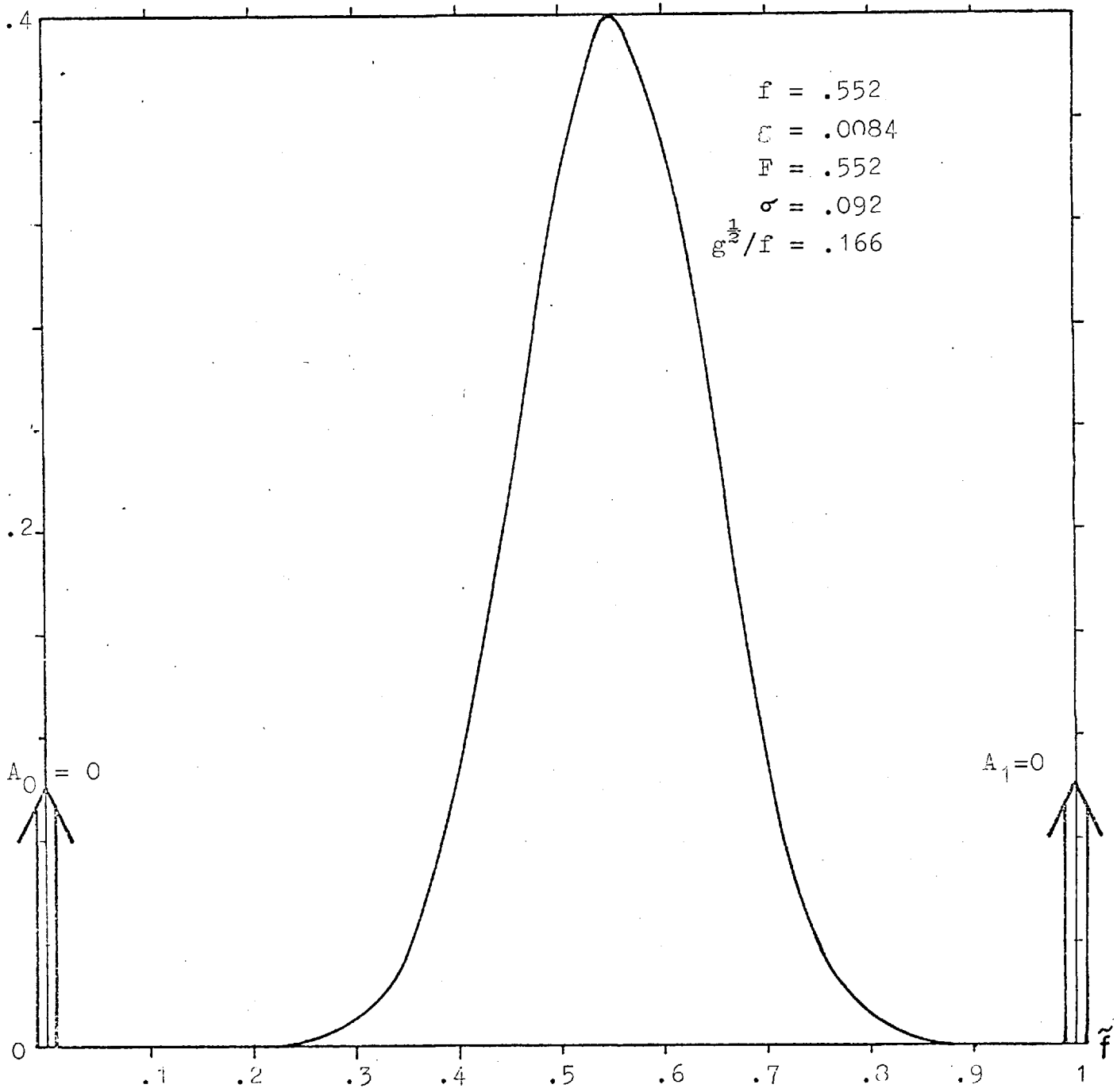

Fig. 3.2.e

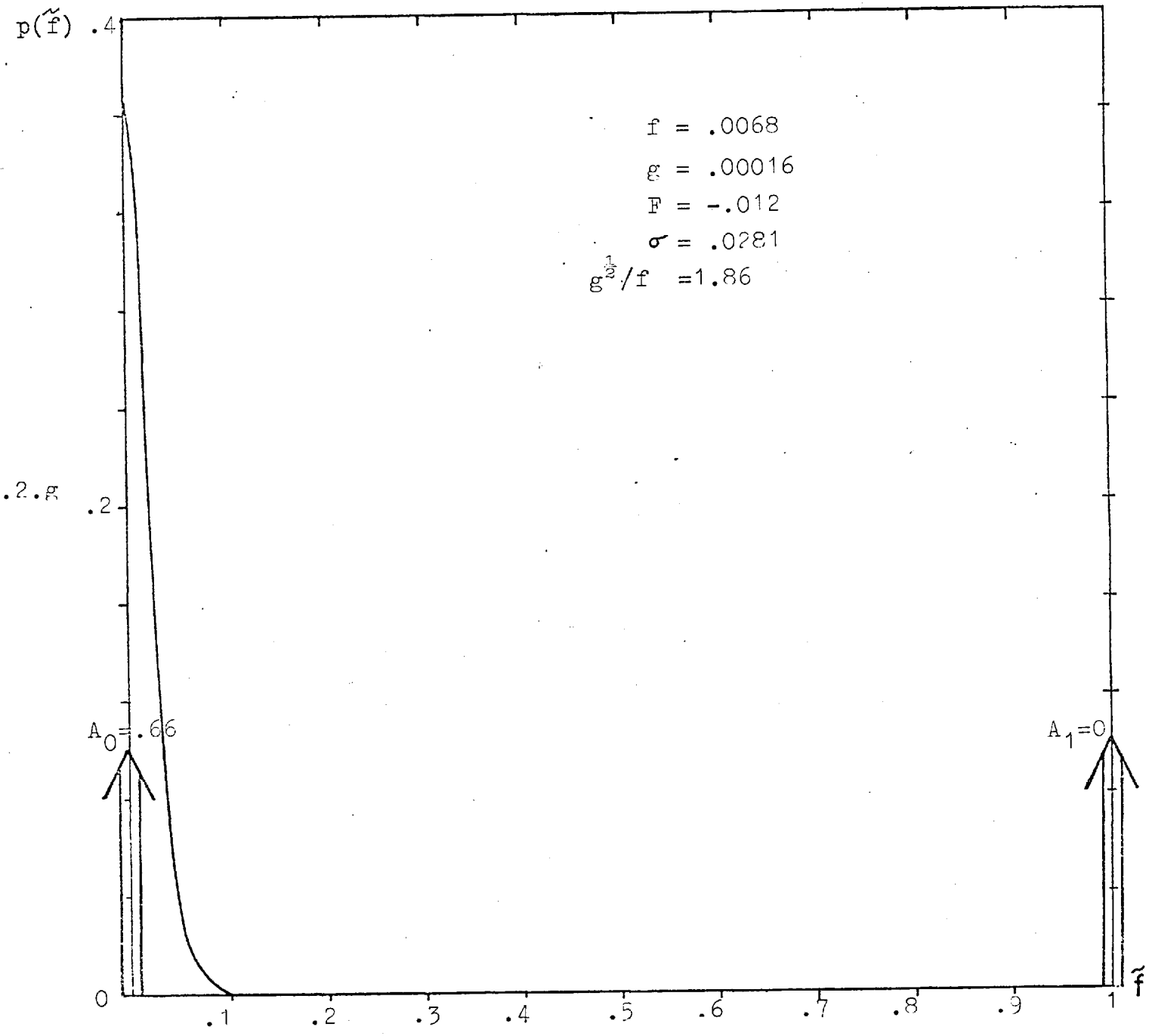

Fig. 3.2.g

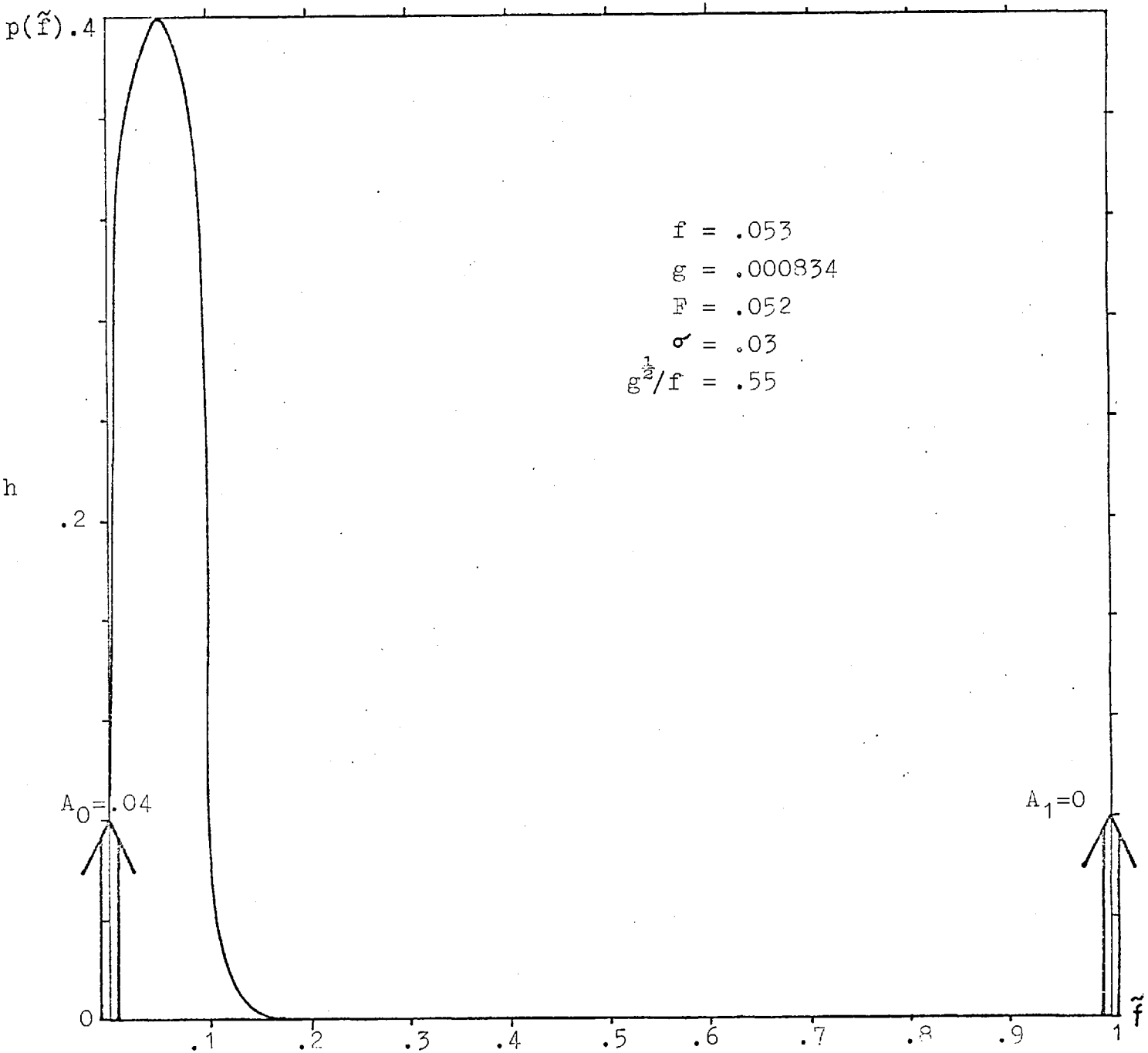

Fig. 3.2.h

$$m_{pr} = 1 - m_{ox} - m_{fu} \tag{3.2-45}$$

The time-mean temperature, T:

$$T = A_0 T_0 + A_1 T_1 + \frac{1}{\sigma\sqrt{2\pi}} \int_0^1 \left[(\tilde{h} - \tilde{m}_{fu} \cdot H) / \Sigma_j \tilde{m}_j c_{p_j} \right] e^{-(\tilde{f}-F)^2/2\sigma^2} \, d\tilde{f} \tag{3.2-46}$$

The time-mean density, ρ:

$$\rho = A_0 \rho_0 + A_1 \rho_1 + \frac{p}{R\sigma\sqrt{2\pi}} \int_0^1 \left[1/\tilde{T} \Sigma_j (\tilde{m}_j / M_j) \right] e^{-(\tilde{f}-F)^2/2\sigma^2} \, d\tilde{f} \tag{3.2-47}$$

In deriving eq. (3.2-47), a simplifying assumption that the joint probability density for temperature and composition fluctuations is the same as $p(\tilde{f})$, has been introduced.

In turbulent flames, a complete picture of the temperature field requires the knowledge of both the time-mean value and the R.M.S. of temperature fluctuations, $\langle T'^2 \rangle^{\frac{1}{2}}$. The latter quantity can be obtained as follows:

$$\langle T'^2 \rangle \equiv \langle [\tilde{T} - T]^2 \rangle \tag{3.2-48}$$

$$\equiv \langle (\tilde{T})^2 \rangle - T^2 \tag{3.2-49}$$

and from

$$\langle T'^2 \rangle = \frac{1}{\sigma\sqrt{2\pi}} \int_0^1 (\tilde{T})^2 \, e^{-(\tilde{f}-F)^2/2\sigma^2} \, d\tilde{f}$$

$$+ A_0 T_0^2 + A_1 T_1^2 - T^2 \qquad (3.2\text{-}50)$$

In the same way, we can obtain the mean-square of the fluctuations of any of the mass fractions (fuel, oxidant or products), i.e. $\langle m'^2_{fu} \rangle$, $\langle m'^2_{ox} \rangle$, etc. In appendix B, the integrals appearing in eqs. (3.2-41) to (3.2-50) are expressed in a suitable form for numerical computation.

The calculation of the time-mean density ρ from eq. (3.2-38) makes it now possible to close the eqs. set (3.2-3) for the six dependent variables, ψ, ω/r, f, k, ε and g. What is required now is a solution procedure.

3.3 Solution of the equations

3.3.1 The finite-difference procedure

The finite-difference procedure, used here to solve the equation set (3.2-3), is basically that of Gosman et al (1969). The fundamentals of the method are discussed in detail in that reference and need not be repeated here. Only the features that have been slightly modified are now described briefly.

(a) The flow domain is divided into a number of rectangular, finite-difference cells, with the flow boundaries coinciding with the appropriate "walls" of the cells along the boundaries. Associated with each cell is a node. The relative positions of the cell walls

and cell nodes are such that the walls are always situated mid-way between two adjacent nodes.

(b) By integrating the differential equations over the area of a cell, finite-difference equations are derived. These equations connect the value of a variable at a node to the values of the variable at the neigbouring nodes. In the derivation of these equations, two conditions are adhered to. Firstly the convectional flux through a cell wall is always equal to the mass flow rate through the wall multiplied by the value of the entity concerned which prevails at the adjacent node upstream of the cell wall; secondly, reciprocity of diffusional fluxes through the common cell wall of two adjacent cells is always ensured. The former is responsible for the high stability property of the numerical procedure at high Reynolds numbers, and the latter helps to ensure the satisfaction of the conservation principle over each cell.

(c) For variables like f, g, k and ε the difference equations for all the touching cells between two boundary lines (for example, between the axis of symmetry and the cylindrical wall of fig.4.1) are solved simultaneously, employing a tri-diagonal matrix algorithm. For ψ and ω , because of their strong inter-linkages effected through the no-slip condition at the wall, the difference equations for both of them are solved simultaneously by a "two-variable algorithm", which extends the tri-diagonal matrix algorithm for "single" variables to include two strongly inter-linked variables.

(d) Starting from one end, all the variables along a line of cells are updated in turn before the next line of cells is swept. The

sweep continues until the whole flow domain is covered. During a sweep all the coefficients in the difference equations are kept unchanged; they are updated before another sweep of the field. The field is repeatedly swept until the solution converges. The adopted convergence-criteria are discussed in chapter 5.

The merits of the above modifications (a, c, d) are two:

(i) The conservation laws are satisfied throughout the whole flow field, thus eliminating the source of error which in the original procedure was caused by neglecting a half-cell space adjacent to the flow boundaries and the axis of symmetry;

(ii) Significant saving of computer-time is realised by using the line-by-line instead of the point-by-point algorithm.

3.3.2 Special considerations near a wall

The k-ε turbulence model which has been discussed in sec. 3.2.2 is valid only for fully turbulent flows. Close to solid walls, there are regions where the viscous effects predominate over the turbulence ones. A method of accounting for these regions is the wall-function method.

The wall-function method, in principle, yields some algebraic relations between the flow-variables in the fully-turbulent region and their fluxes at the wall, without integrating the conservation equations inside the boundary layer. Therefore, when using the wall-function it is necessary to ensure that the grid-node next to the

wall is sufficiently remote so that the viscous effects there are entirely overwhelmed by the turbulent ones.

Now we discuss briefly how the wall-function is derived.

Shear Stress. Near a wall the flow is predominantly parallel to the wall. For this region we shall follow Spalding (1971-b) and assume that the shear stress is constant and that:

$$\frac{\mu_{eff}}{\mu} = \kappa y_{++} \qquad (3.3\text{-}1)$$

where κ is a constant, and y_{++} is defined as $y\rho k_p^{\frac{1}{2}} c\mu^{\frac{1}{4}}/\mu$, y being the distance from the wall and k_p, the value of k at a typical point, for example, at the node of a cell touching the wall.

These assumptions lead us immediately to an equation linking the wall shear stress τ_s to the velocity parallel to the wall:

$$u/(\tau_s/\rho)^{\frac{1}{2}} = \frac{1}{\kappa} \cdot \ln\left[(Ey_{++})\ (\tau_s/\rho)^{\frac{1}{2}}/k_p^{\frac{1}{2}} c_\mu^{\frac{1}{4}}\right] \qquad (3.3\text{-}2)$$

where E is another constant. As u can be evaluated from the stream function distribution, this equation allows τ_s to be computed.

In a situation in which the effects of diffusion and convection of k are negligible, the generation and dissipation of it are in balance, and we have, from the differential equation for k, equality of τ_s/ρ and $k_p c_\mu^{\frac{1}{2}}$. Under these conditions, equation (3.3-2) reduces to the familiar "law of the wall" and κ can be readily identified as

the von Karman's constant and E, the constant expressing the smoothness of the wall. Also, equation (3.3-1) assumes the form:

$$\frac{\mu_{eff}}{\mu} = \kappa \quad y\sqrt{\rho\tau_s} \quad /\mu \qquad (3.3\text{-}3)$$

The reason for employing equation (3.3-1) in the present calculations is now obvious. For in regions of vanishingly small τ_s, for example near a stagnation point, equation (3.3-3) returns a value of μ_{eff} which is too low, whereas equation (3.3-1) will give a much more realistic value.

<u>k, ε, g and ω</u>. Near a wall it is reasonable to assume k to be zero, and this can be used as a boundary condition for k if the finite-difference grid is sufficiently fine to give adequate coverage in the laminar sub-layer. However, for the present turbulence model to be applicable, the first node away from the wall must be situated in the wholly turbulent region. For such a near-wall cell the generation and dissipation of k are far more significant than its diffusion through the bounding wall, and it has been found sufficient to use simply the zero normal-gradient of k as the boundary condition there in the balance of k calculation for the cell. Also, for accuracy the k source-terms for this cell should be evaluated as the mean over the cell. All the above considerations apply equally to the evaluation of g near a wall.

For ε , equations (3.3-1) and (3.2-5) should be used to determine its variation with distance from the wall.

The vorticity variation over a near-wall cell can be evaluated

from τ_s. For accuracy, it has been found desirable to use the space-averaged value of ω in the source term of ψ and to use the point value prevailing at the cell node for the calculation of diffusional and convectional fluxes to other cells.

More details of the solution procedure are given in chapters 4 and 5.

CHAPTER 4

COMPUTATIONS FOR CONCENTRATION FLUCTUATIONS IN ISOTHERMAL TURBULENT CONFINED COAXIAL JETS

4.1 Introduction

The aim of this chapter is to test both the $k-\varepsilon$ turbulence model and the modelled g equation, discussed in chapter 3, in isothermal recirculating flows before employing them in the more complex situation of the turbulent diffusion flame.

Predictions are obtained of the distributions of the time-mean and of the fluctuations of concentration in the turbulent mixing of two steady, coaxial jets of equal density and different concentration which issue into a cylindrical concentric chamber. The range of the jet-velocity ratio considered includes cases in which recirculation occurs. For the case of unity jet-velocity ratio, i.e. the case of a pipe flow, predictions are presented of the time-mean axial velocity, k and ε . Wherever possible, the predictions are compared with available experimental data.

4.2 The particular problem considered

4.2.1 The flow

Figure 4.1. shows a diagramatic sketch of the flow of two co-axial jets. The central jet, with a uniform velocity u_1, issues from a pipe of radius r_j into a cylindrical chamber of radius R. The surrounding jet, with a uniform velocity u_2, covers the annular space between the central jet and the chamber wall. The different flow

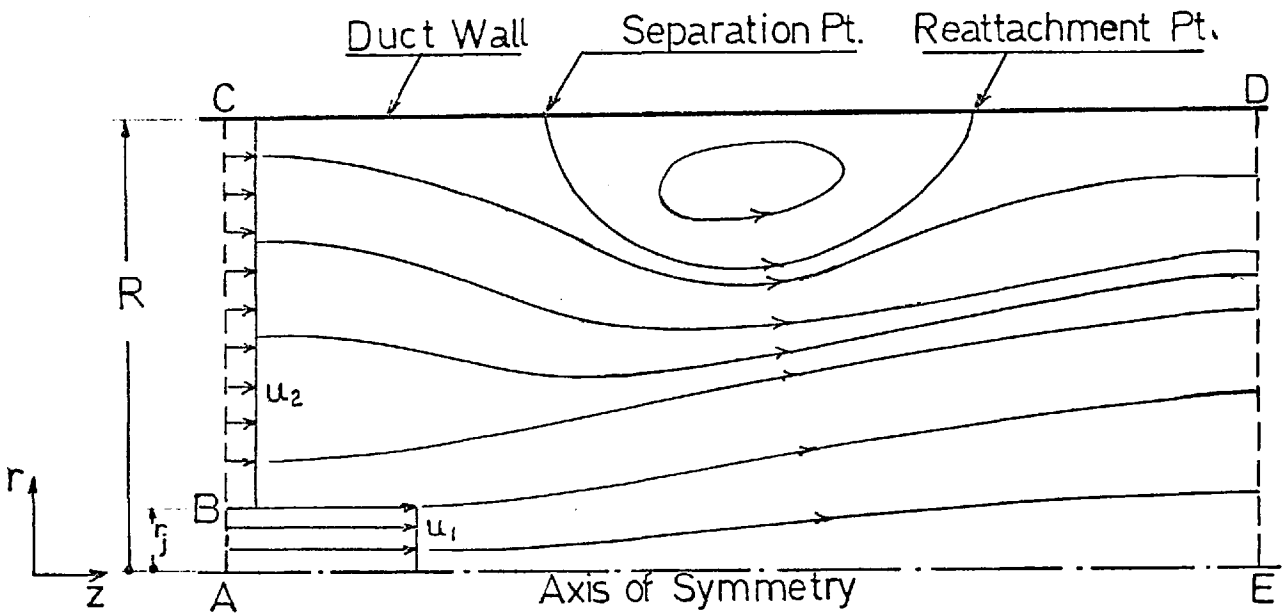

Fig. 4.1 The System Of Coaxial Jets Showing Co-ordinates and Typical Stream Lines

conditions used in the predictions are identical to those reported by Becker et al (1967) and Torrest and Ranz (1970); these are summarised in table 4.2 below. The density is assumed constant throughout the flow field and there is no swirl.

Table 4.2

Investigator		Becker et al (1967)	Torrest and Ranz (1970)
central jet	fluid	oil fog-marked air	salt solution
	r_j (mm)	3.17	1.7
	u_1 (m/s)	130.	2.6
	jet Reynolds no.	54000	9050
surrounding jet	fluid	air	water
	R (mm)	98.5	15.5
	u_2(m/s)	0.45 to 2.6	0.21

4.2.2 The equations

The equation set (3.2-3) for the six dependent variables Ψ, ω/r, f, k, ε and g are solved simultaneously together with the auxiliary algebraic relation for μ_{eff} (eq. 3.2-4).

4.2.3 Boundary conditions

To complete the mathematical formulation of the problem, boundary

conditions must be specified along the boundary of the integration domain, ABCDE of fig. 4.1. Four types of boundaries may be identified. Each of these is discussed in turn below.

Inlet plane ABC. Velocity distributions for the central jet AB and the surrounding jet BC are known, from which the ψ and ω distributions can be deduced; f values are obtained from the definitions (3.2-12) and (3.2-13) as 1 and 0 for AB and BC respectively. The g values are zero for both AB and BC because of the uniformity of f. The values of k are prescribed by assuming a turbulence intensity of 5% in the incoming streams. ε values can be deduced from the k values on the presumption that a constant length-scale exists there. In the computations to be presented later a length scale equal to (0.011 x radius of duct) has been adopted.

Axis of symmetry AE. Along the axis of symmetry the gradients in the radial direction of all the variables are equal to zero. Also ψ is constant.

Exit plane DE. Conditions at the exit are usually difficult to specify. Here we shall adopt the practice of Gosman et al (1969) and assume the axial gradients for all the variables to be zero. This practice is obviously realistic when the duct is of considerable length.

Duct wall CD. Along an impermeable wall ψ is constant; also its gradient normal to the wall is zero, as is that of f. Boundary conditions for k, ω, g and ε are evaluated according to the wall-function practice discussed ealier in section 3.3.2 of the preceding chapter.

4.3 Results and discussions

4.3.1 Some details of the computations

The values of the constants. The constants appearing in tables 3.2.1, 3.2.2, 3.2.3 and 3.2.4 of chapter 3 are given the values displayed in table 4.3.1. These values, except for c_{g1} and c_{g2}, differ slightly from those recommended by Launder and Spalding (1972) after extensive examination of free turbulent flows.

Table 4.3.1

c_1	c_2	c_{g1}	c_{g2}	c_μ	σ_k	σ_ε	σ_f	σ_g
1.45	2.	2.8	2.	.09	1.	1.3	.7	.7

The two constants κ and E used to obtain a relation between the wall shear stress and the local velocity (eq. 3.3-2) have the values of 0.41 and 9. respectively. The values of c_{g1} and c_{g2} have been determined using computer optimisation; in other words, they give the best agreement between the predictions and experiments for the flow studied.

Grid. In order to examine the influence of the grid distribution on the accuracy of computations two different grids have been used. The two were non-uniformly distributed grids of 15 x 15 and 15 x 20 nodes, with the larger number of nodes in the radial direction. In both grids, there were three cells covering the central-jet inlet. The 15 x 20 grid resulted in better agreement between predictions and experiment, with a maximum improvement of about 5%; hence the solution obtained by this grid is considered sufficiently accurate. In all the predictions to be presented, the 15 x 20 grid was employed.

Convergence tests and under-relaxation are discussed in the next chapter.

4.3.2 Results and comparisons with measurements

(a) Distributions of time-mean velocity and concentration and flow patterns

Velocity. When the two jets enter the duct with the same uniform velocity, a pipe-flow situation is obtained. By using a very long pipe, it is not difficult to attain fully-developed conditions. For this situation accurate measurements of the time-mean velocity are available, for example, those of Laufer (1953). Table 4.3.2 presents a comparison between the predicted velocity values and Laufer's measurements at a Reynolds number of 5×10^5. Evidently, very good agreement has been obtained for the velocity distributions .

Table 4.3.2

y/R^*	$u/u_{MAX.}$		$k/(\tau_s/\rho)$		$\varepsilon.R/(\tau_s/\rho)^{1.5}$	
	Predict-ions	Expt. (1953) Laufer	Predict-ions	Expt. (1953) Laufer	Predict-ions	Expt. (1953) Laufer
0.1	.776	.78	3.33	3.70	22.9	22.
0.2	.848	.85	2.87	2.90	12.1	11.5
0.3	.889	.89	2.50	2.50	7.47	7.5
0.4	.924	.92	2.18	2.1	4.99	6.5
0.5	.949	.95	1.90	1.90	3.49	5.
0.6	.968	.97	1.67	1.40	2.53	3.5
0.7	.983	.98	1.49	1.20	1.89	3.
0.8	.992	.99	1.35	1.10	1.51	2.6
0.9	.998	1.0	1.28	0.9	1.29	2.5
1.0	1.00	1.0	1.25	0.9	1.23	2.4

*y is the distance from the wall and R is pipe radius.

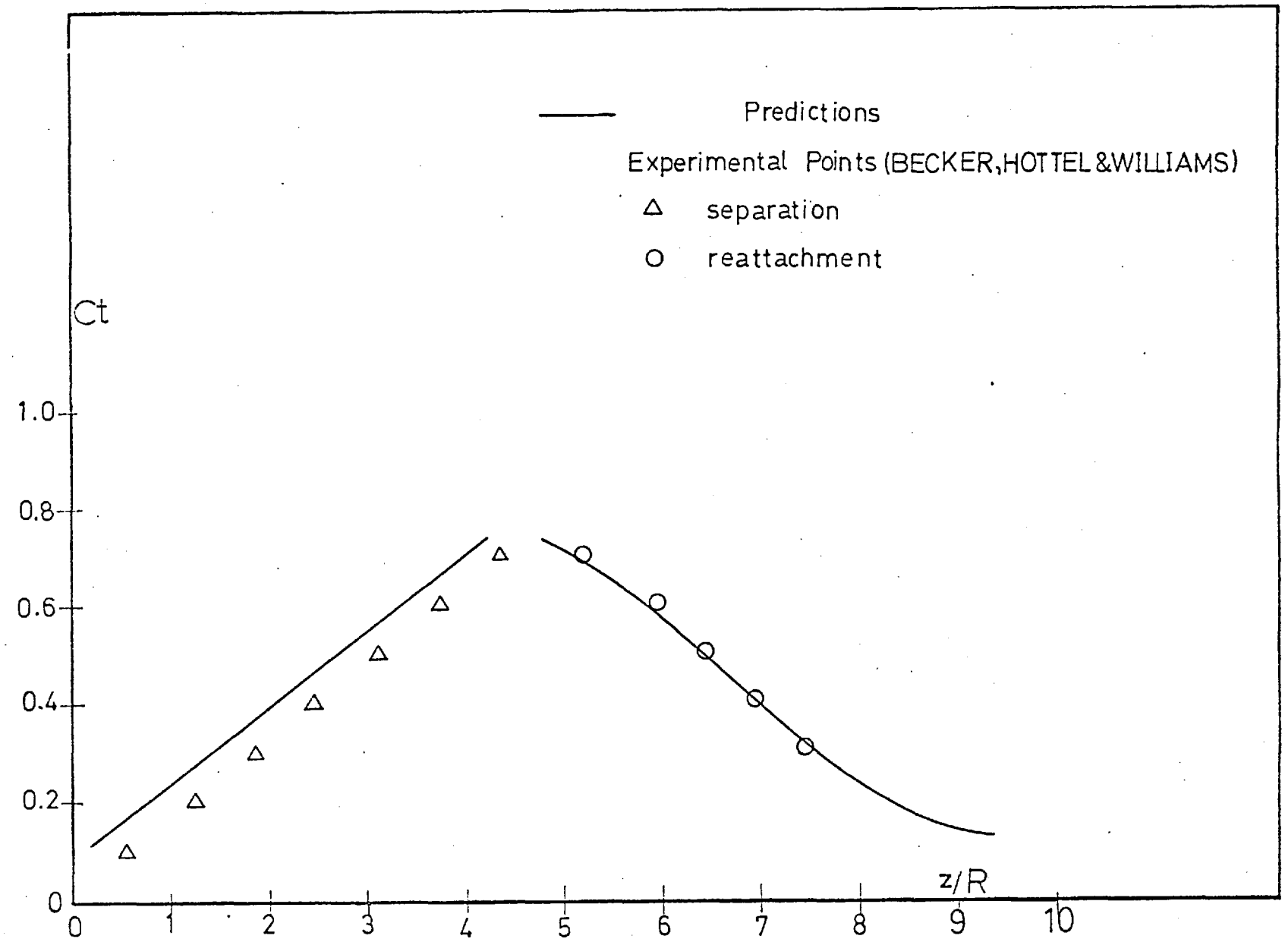
Predictions
Experimental Points (BECKER, HOTTEL & WILLIAMS)
△ separation
○ reattachment
Ct
1.0
0.8
0.6
0.4
0.2
0
0
1
2
3
4
5
6
7
8
9
10
z/R

Fig. 4.2

Flow patterns. For a given geometry, if the ratio of the central-jet velocity to that of the surrounding jet is progressively increased, a point will be reached beyond which the rate of entrainment into the central jet exceeds the supply available from the surrounding fluid. Under these circumstances a region of recirculation will appear downstream of the inlet plane, as illustrated in fig. 4.1. The flow pattern for such a situation can be characterised by the locations of the points of separation and reattachment. Becker et al (1965) measured these positions for a wide range of the Craya-Curtet number Ct, which they defined as:

$$Ct \equiv \frac{u_o}{\left[(u_1^2 - u_2^2).(r_j/R)^2 + 0.5(u_2^2 - u_o^2)\right]^{1/2}} \qquad (4.3\text{-}1)$$

where $u_o = (u_1 - u_2).(r_j/R)^2 + u_1$.

Fig. 4.2. displays the predicted variation of the locations of the separation and reattachment points with Ct for the flow situation of Becker et al (1965); also plotted are their measurements. As can be seen, the agreement is very good for the position of the reattachment point. For the separation points, their locations are somewhat underestimated, but the trend is well predicted. It is encouraging to note that both prediction and measurement seem to indicate the same Ct value at which recirculation disappears, i.e., when the separation point coincides with the reattachment point.

Concentration. The decay of the time-mean concentration of the central-jet fluid along the axis is presented in fig. 4.3 for a Ct value of 0.875. These computations were obtained for the particular

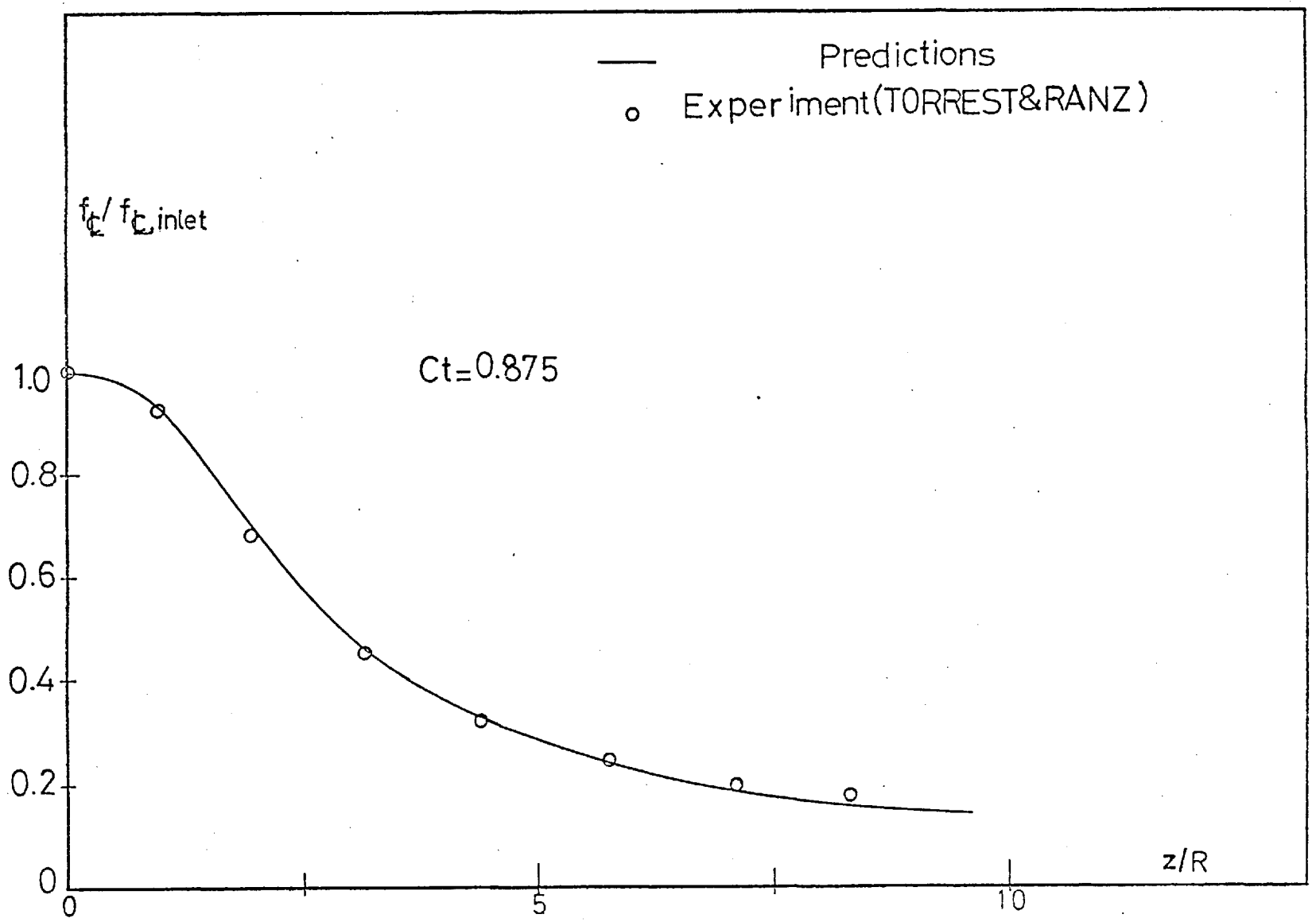
Predictions
Experiment(TORREST&RANZ)
$f_\xi / f_{\xi,inlet}$
Ct=0.875
1.0
0.8
0.6
0.4
0.2
0
0
5
10
z/R

Fig. 4.3

situation reported by Torrest and Ranz (1970); their measurements are also shown on the graph for comparison. Very good agreement is obtained. It should be noted that at this Ct value no recirculation was detected, as is also evident in the measurements of Becker et al, fig. 4.2.

(b) Distributions of turbulence quantities

Fluctuations of concentration. The variations with axial distance of $g^{\frac{1}{2}}$ at the axis are shown in figs 4.4 to 4.7 for different Ct values. In each case $g^{\frac{1}{2}}$ is normalised by the local time-mean concentration of the central jet fluid. The full curves represent predictions and the points are the measurements of Becker et al (1967) and Torrest and Ranz (1970). Overall, fair agreement between predictions and experiments is observed. It is especially encouraging to note that the variation of the axial location of maximum $g^{\frac{1}{2}}$ with Ct is well reproduced by the predictions.

From fig. 4.2 and figs. 4.4 to 4.7, the effects of recirculation on the decay of concentration fluctuations intensity along the jet axis, with increasing distance from the jet exit, can be summarised as follows:

(i) the decay of the intensity begins roughly at the leading edge of the recirculation eddy, or the point of separation;

(ii) the decay rate is faster the larger the eddy size, or the smaller the Ct value.

The above two effects can be explained by the fact that the

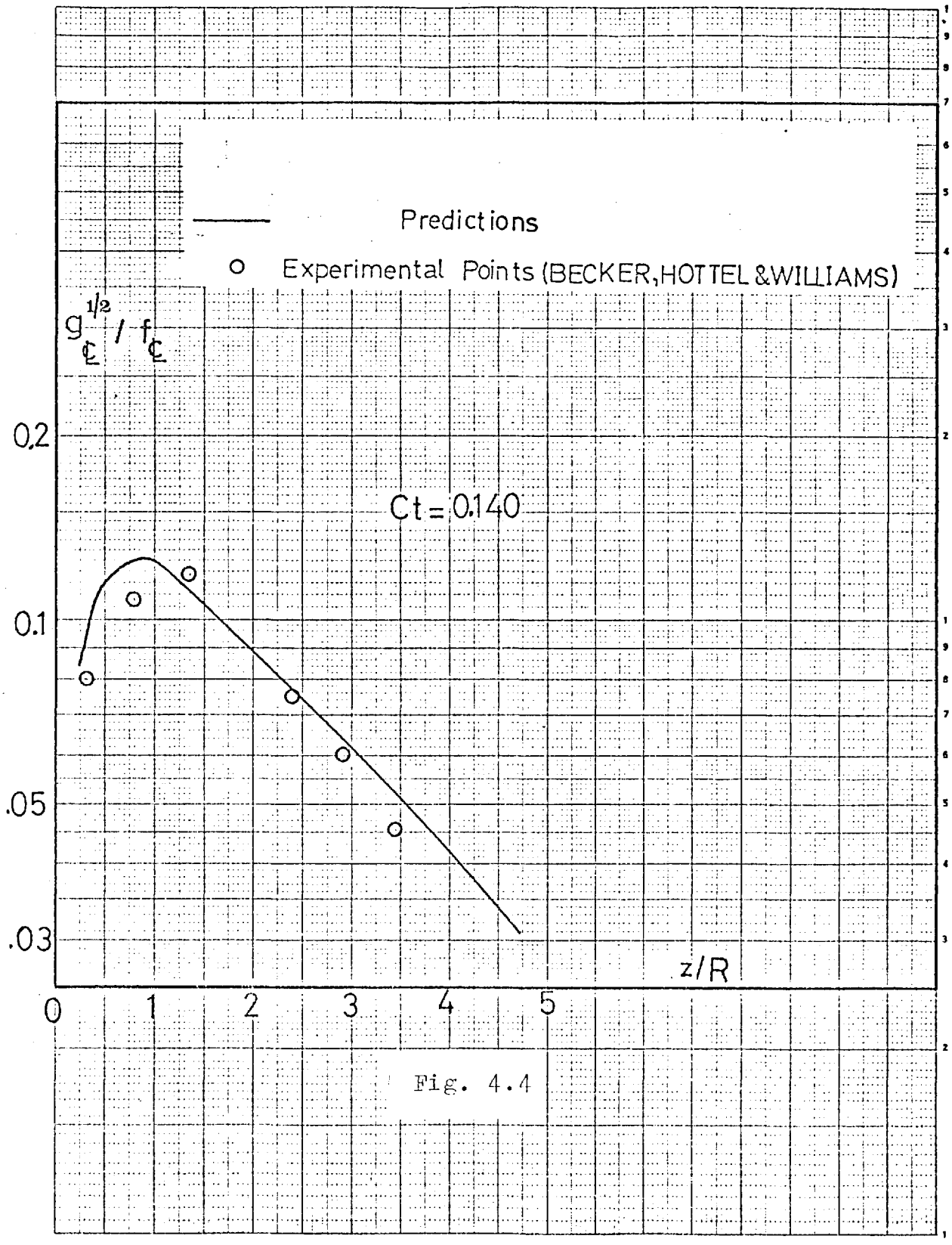
Predictions
Experimental Points (BECKER, HOTTEL & WILLIAMS)
$g_{\ell}^{1/2} / f_{\ell}$
0.2
0.1
.05
.03
Ct = 0.140
z/R
0
1
2
3
4
5

Fig. 4.4

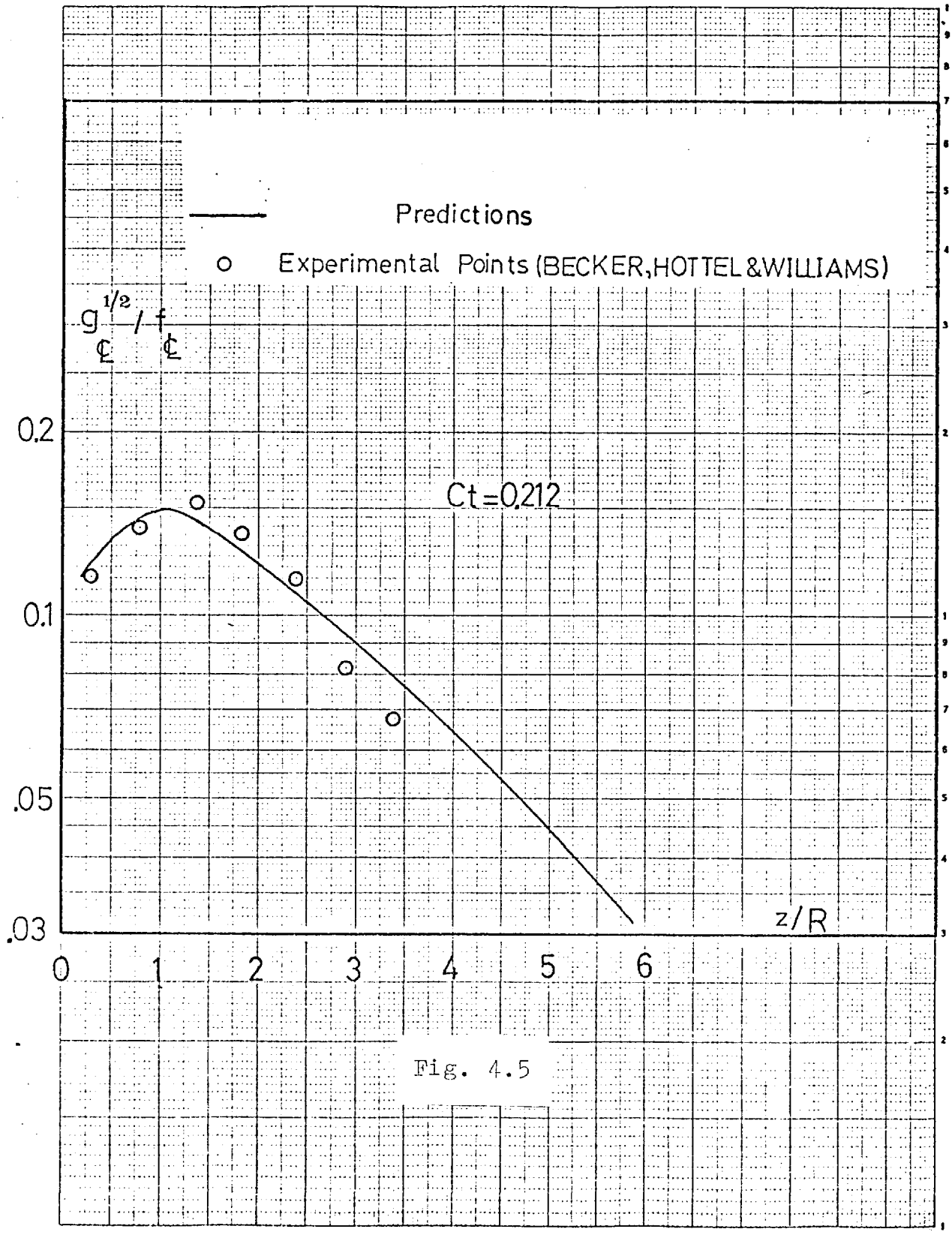
Predictions
Experimental Points (BECKER, HOTTEL & WILLIAMS)
$g_{\mathcal{L}}^{1/2} / f_{\mathcal{L}}$
Ct=0.212
0.2
0.1
.05
.03
0
1
2
3
4
5
6
z/R

Fig. 4.5

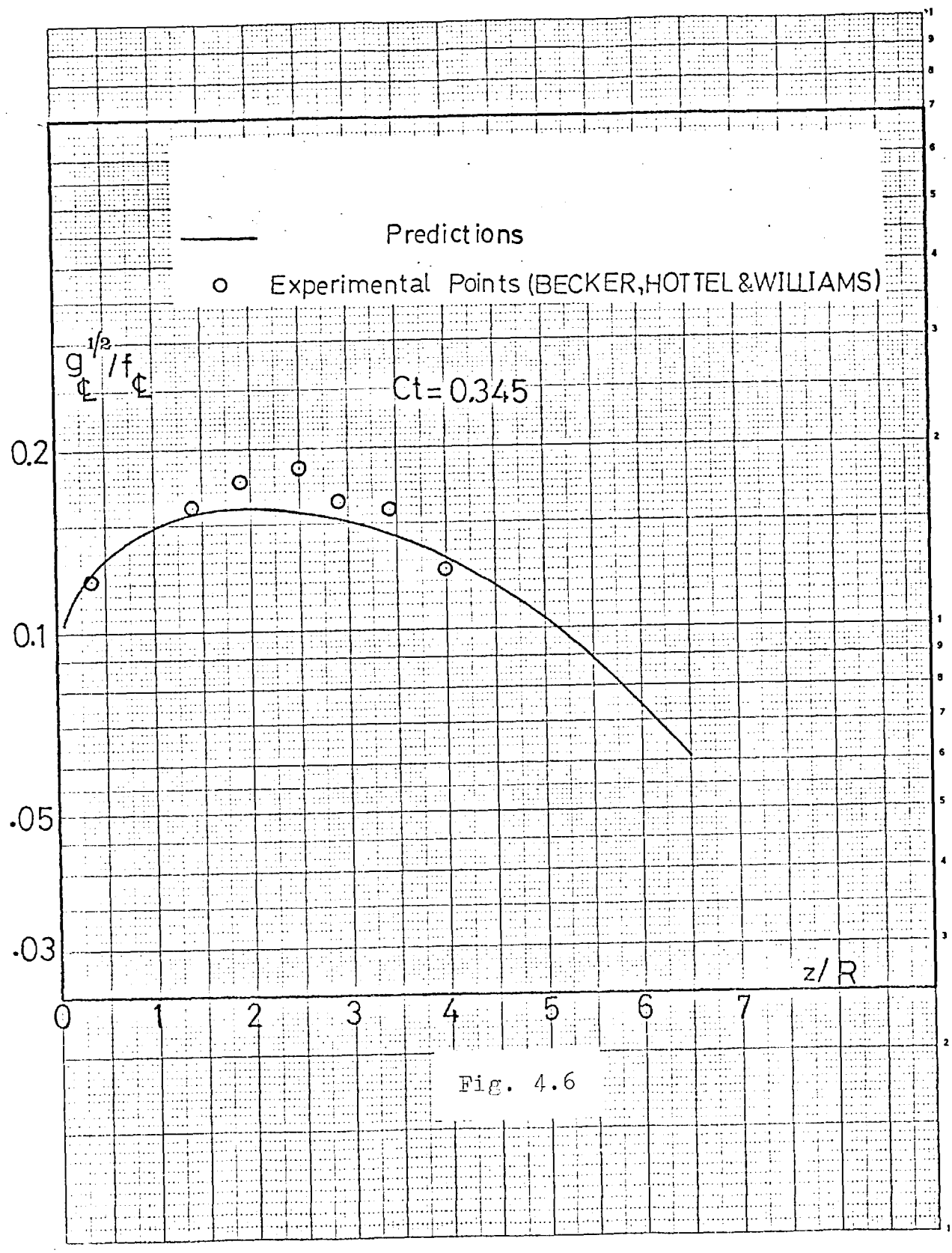
Predictions
Experimental Points (BECKER, HOTTEL & WILLIAMS)
$g_{\mathbb{C}}^{1/2}/f_{\mathbb{C}}$
Ct = 0.345
0.2
0.1
.05
.03
z/R
0
1
2
3
4
5
6
7

Fig. 4.6

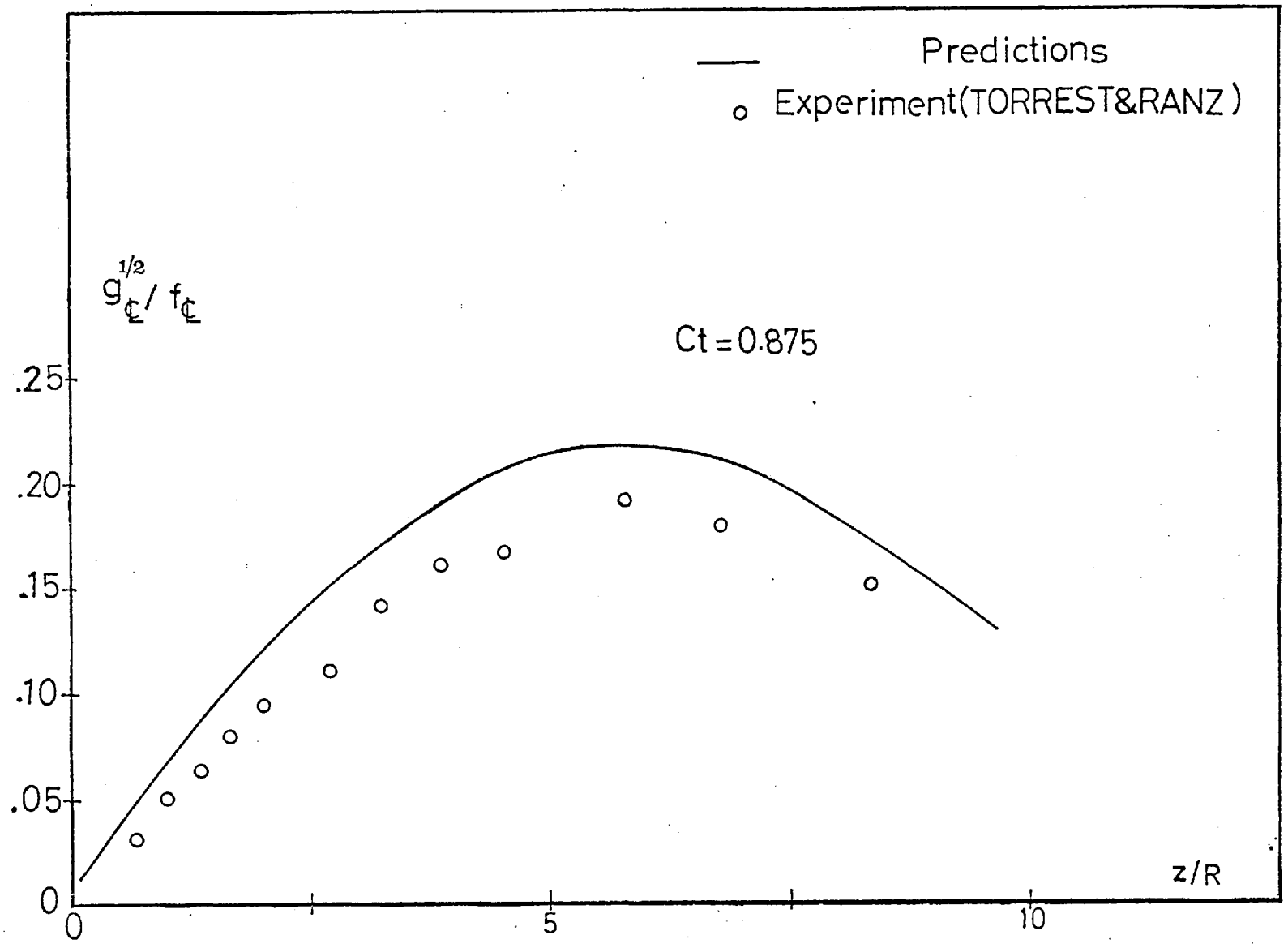
Predictions
Experiment(TORREST&RANZ)
$g_{\text{¢}}^{1/2} / f_{\text{¢}}$
Ct = 0.875
.25
.20
.15
.10
.05
0
0
5
10
z/R

Fig. 4.7

recirculation eddy supplies the expanding central-jet with fluid which originated from the jet itself, hence erasing the gradients of concentration which are the source of fluctuations.

The radial variation of $g^{\frac{1}{2}}$ at three axial locations for a Ct value of 0.673 are shown in figs. 4.8 to 4.10. The full lines are predictions and the points are measurements of Becker et al. The ordinates represent values of $g^{\frac{1}{2}}$ normalised by its value at the axis of symmetry, and the abscissae are radial distances normalised by the radius at which the value of $g^{\frac{1}{2}}$ is equal to half its value at the axis. Fair agreement is seen between predictions and experiments. Although the existence of peaks is predicted, their locations are not very well reproduced. It should however be remarked that at this Ct value recirculation was present, but the recirculation zone (see fig. 4.2) was some distance upstream of the three locations of figs. 4.8 to 4.10.

Although the measurements reported by Becker et al (1967) are very extensive, because of insufficient information for the normalising values used to be deduced, many of their data cannot be utilised in the present comparison.

k and ε . For the case of two jets with equal and uniform velocities, the fully developed profiles of $k/(\tau_s/\rho)$ and $\varepsilon.R/(\tau_s/\rho)^{1.5}$ are presented in Table 4.3.2 for a Reynolds number of 5×10^5. The measured values by Laufer (1953) are also presented; the agreement is seen to be fair.

As far as is aware, no measurements of k or ε have been reported

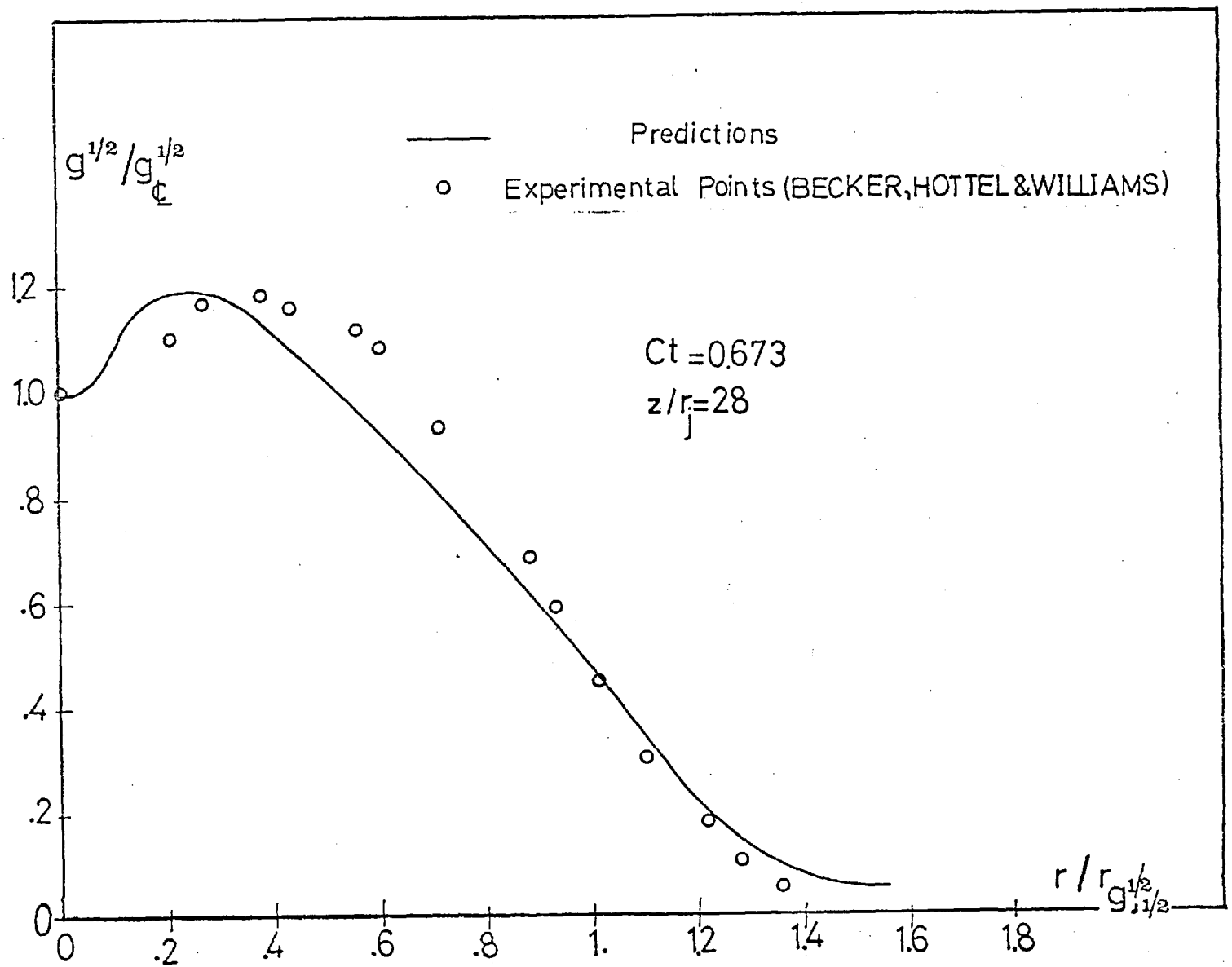
Predictions
Experimental Points (BECKER, HOTTEL & WILLIAMS)
$g^{1/2}/g_{\mathbb{C}}^{1/2}$
Ct = 0.673
z/r_j = 28
$r/r_{g^{1/2}}$
0
.2
.4
.6
.8
1.0
1.2
1.4
1.6
1.8

Fig. 4.8

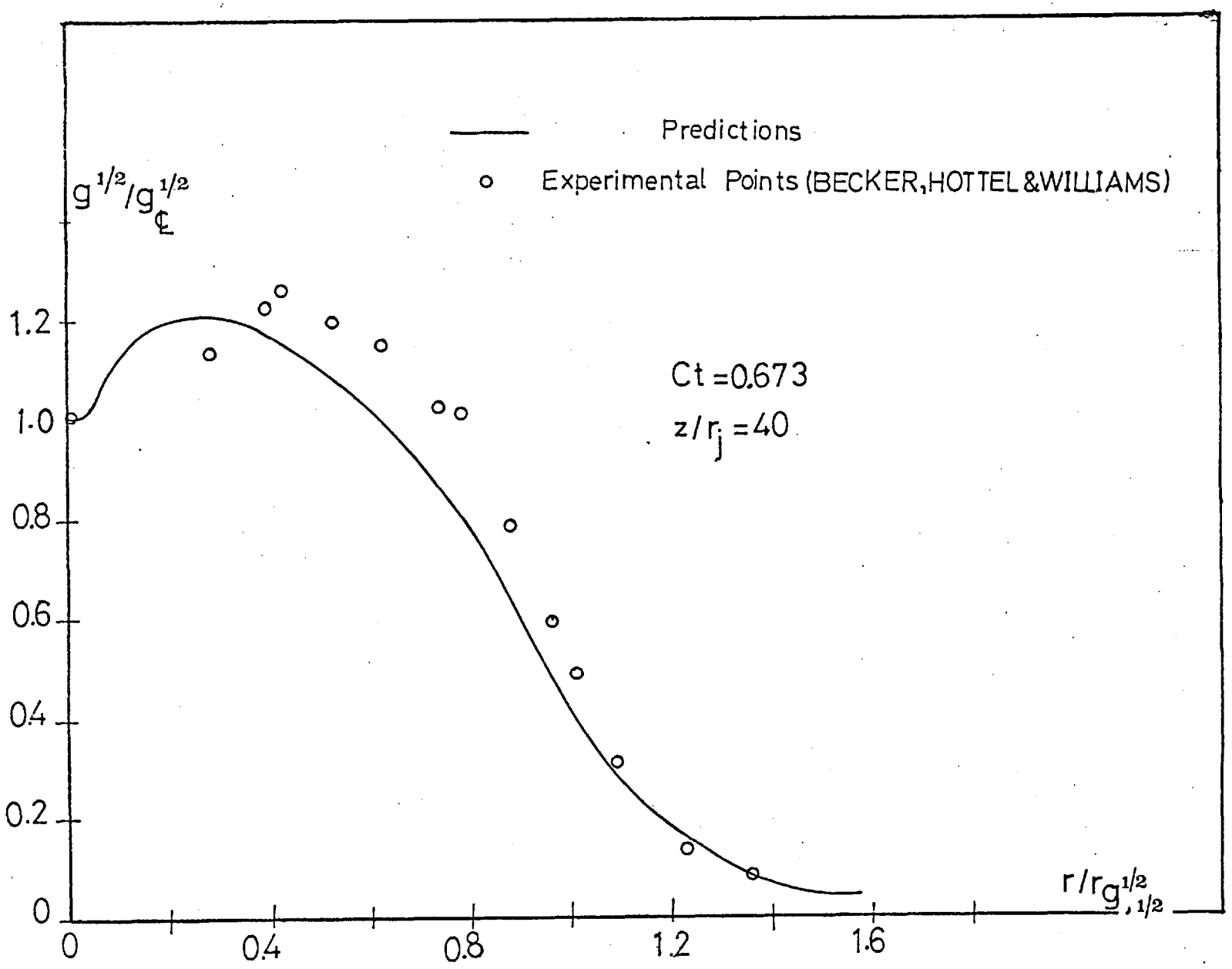
Predictions
Experimental Points (BECKER, HOTTEL & WILLIAMS)
$g^{1/2}/g^{1/2}_{\mathbb{C}}$
Ct = 0.673
$z/r_j = 40$
$r/r_{g^{1/2}, 1/2}$
0
0.2
0.4
0.6
0.8
1.0
1.2
0
0.4
0.8
1.2
1.6

Fig. 4.9

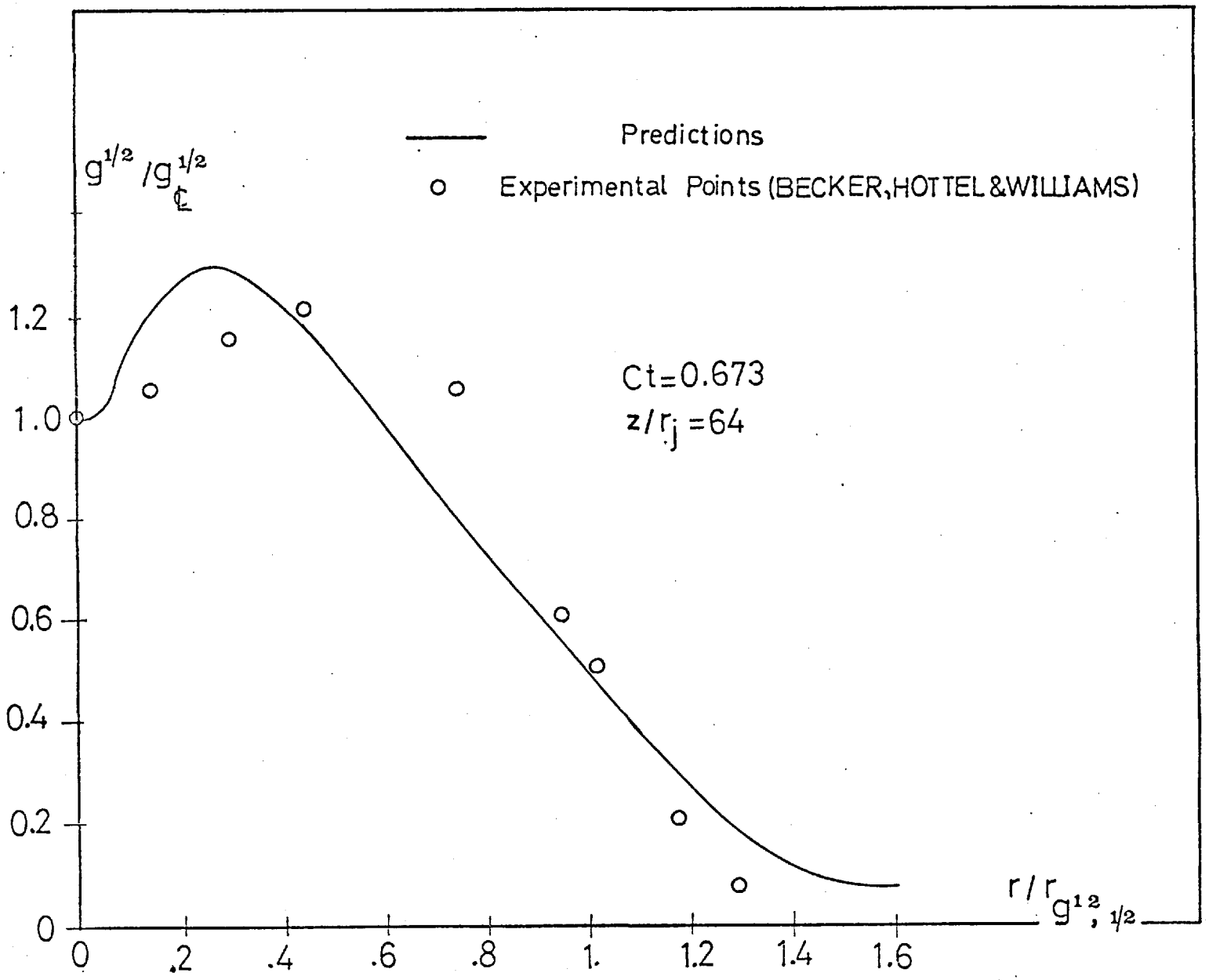
Predictions
Experimental Points (BECKER, HOTTEL & WILLIAMS)
$g^{1/2}/g^{1/2}_{\ell}$
Ct=0.673
z/r_j =64
1.2
1.0
0.8
0.6
0.4
0.2
0
0
.2
.4
.6
.8
1.
1.2
1.4
1.6
$r/r_{g^{1/2},1/2}$

Fig. 4.10

for a coaxial-jet system in which a recirculation region exists.

4.4 Conclusions

The use of the k- ε turbulence model together with the modified form of the law of the wall has been found to give satisfactory predictions to the hydrodynamics of two-dimensional, steady, confined, recirculating flows. The ability to reproduce the correct locations of the separation and reattachment points in a system of coaxial jets is especially gratifying.

Concentration-fluctuation results of the present study have provided further validity of the analysis put forward by Spalding (1971). For the present case, the best values of the two constants in the g-equation, c_{g1} and c_{g2}, are found to be 2.8 and 2.0 respectively. The value of cg_1 is very close to 2.7 as used by Spalding; c_{g2} has the same value as the constant in the dissipation term of the equation for ε . More reliable experimental data are needed for a more extensive validation of the model. However, sufficient confidence has already been generated for us to apply the model to turbulent-diffusion flames.

CHAPTER 5

COMPUTATIONS FOR TURBULENT DIFFUSION FLAMES

5.1 Introduction

In this chapter we present the predictions of the hydrodynamic and thermodynamic properties of the four flames I, II, III, IV of table 2.6, chapter 2. These predictions were obtained with the aid of the three mathematical models discussed in chapter 3. The predicted distributions of velocities, turbulence intensity, temperature, etc., will be discussed qualitatively only since no suitable experimental data were available. The predicted f will be compared with measurements for flame A (table 2.6).

In chapter 2 we introduced a method for mapping the probability of chemical reaction, P, from measurements of the instantaneous positive-ion current in the furnace. The results of these measurements will be presented and compared with the predictions in section 5.4. In order to predict P, some additional assumptions other than the chemical-reaction model are necessary; these will be discussed in section 5.3.

5.2 The problem specification

The flow considered here is the one described in section 2.6. There is no swirl in either the fuel or the air stream. The heat transfer to or from the system is ignored for reasons which have been explained in section 3.2.4

5.2.1 The geometry of the flow domain

Figure 5.2.a shows a sketch of the axisymmetric flow domain ABCDEFG for which the computations have been obtained. The dimensions displayed in the figure are those of the furnace described in section 2.6.

5.2.2 The equations

The equation set (3.2-3) for the six dependent variables ψ, ω/r, f, k, ε and g are solved simultaneously together with the auxiliary relations for μ_{eff}, eq. (3.2-5), and for ρ, eq. (3.2-47).

5.2.3 Boundary conditions

The boundary conditions for each of the six dependent variables are discussed below.

Fuel and air inlets AB and CD. Uniform axial-velocity profiles, u_1 and u_0, are prescribed for the fuel and air streams respectively (see table 2.6.). The radial velocities v_0 and v_1 are both zero. The stream function distribution is determined from the ψ definition (3.2-1). The values of k and ε are prescribed as follows:

$$k_0 = .005\ u_0^2, \quad k_1 = .005\ u_1^2,$$

$$\varepsilon_0 = k_0^{1.5}/\ell_0 \text{ and } \varepsilon_1 = k_1^{1.5}/\ell_1, \text{ where}$$

ℓ_1 and ℓ_0 are the length scales of turbulence in the two streams, taken as .011 times the radius of AB and the annular gap CD respectively.

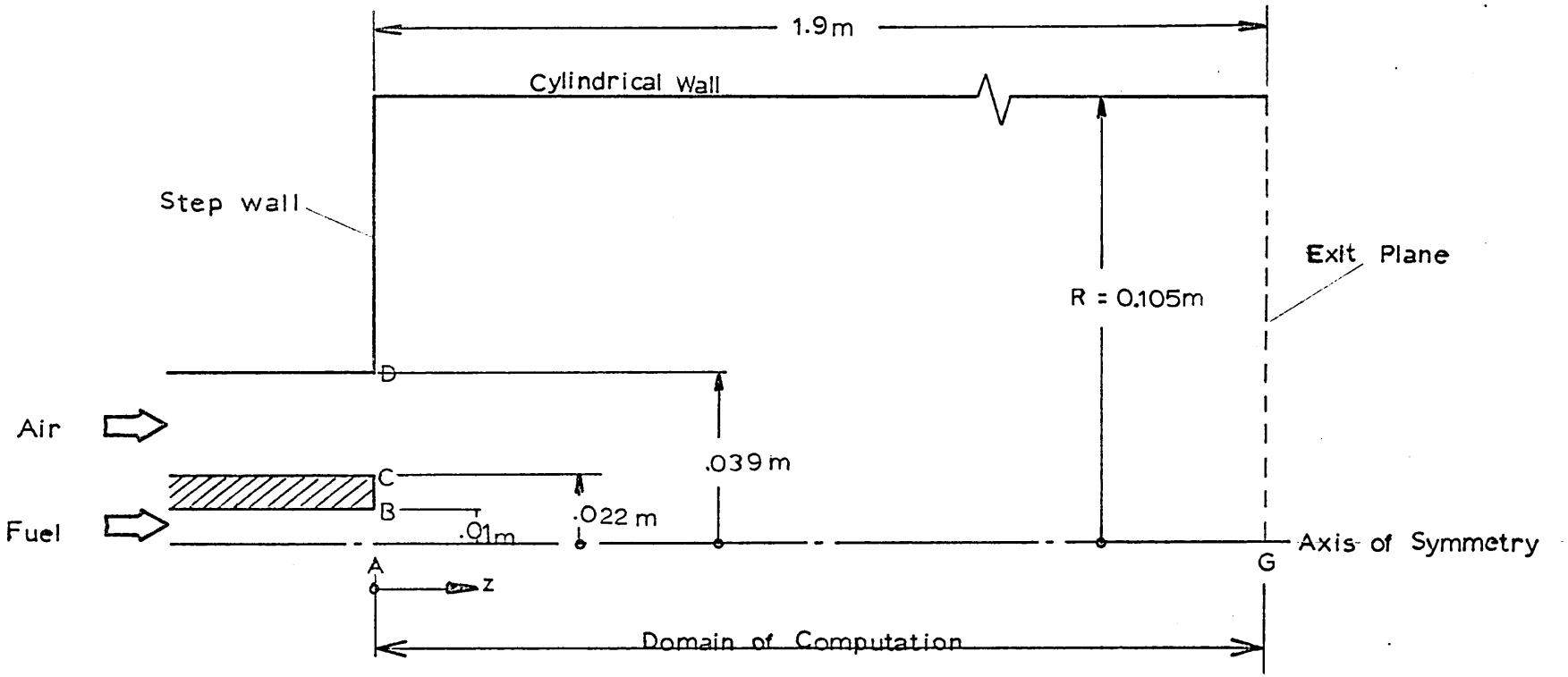
1.9m
Cylindrical Wall
Step wall
Exit Plane
R = 0.105m
D
Air
.039 m
C
B
Fuel
.01m
.022 m
Axis of Symmetry
A
z
G
Domain of Computation

Fig.5.2.a

From the definitions (3.2-12) and (3.2-13), the f values are deduced as 1 and 0 in the fuel and air streams respectively. Because of the uniform distribution of f in each of the streams, the g values are zero on the inlet plane.

The separation lip BC. On the lip BC, ψ is constant and equals ψ_B; also the normal gradient $\partial\psi/\partial z$ is zero, as is that of f and g. Boundary conditions for k, ε and ω/r are evaluated with the aid of the wall function discussed earlier in section 3.3.2.

The step wall DE and the cylindrical wall EF. The treatment of the boundary conditions for all variables along both walls is the same as that described above for BC; here however $\psi_{DE} = \psi_{EF} = \psi_D$.

The exit plane FG. The assumption of zero axial-gradient for all variables at the exit plane is adopted here.

The axis of symmetry AG. $\psi = 0$, and $\partial\phi/\partial r = 0$ where ϕ stands for all the variables.

Vorticity boundary-conditions near the corners B, C and D. For the gemoetry of the flow field ABCDEF, it was found that the predicted velocities, particularly near the inlet plane ABCD, were sensitive to the vorticity boundary-conditions at the inlet cells B', C' and D' which have the solid corners B, C, and D respectively (fig. 5.2.b). It was attempted first to calculate the space average values of $\omega_{B'}$, $\omega_{C'}$ and $\omega_{D'}$

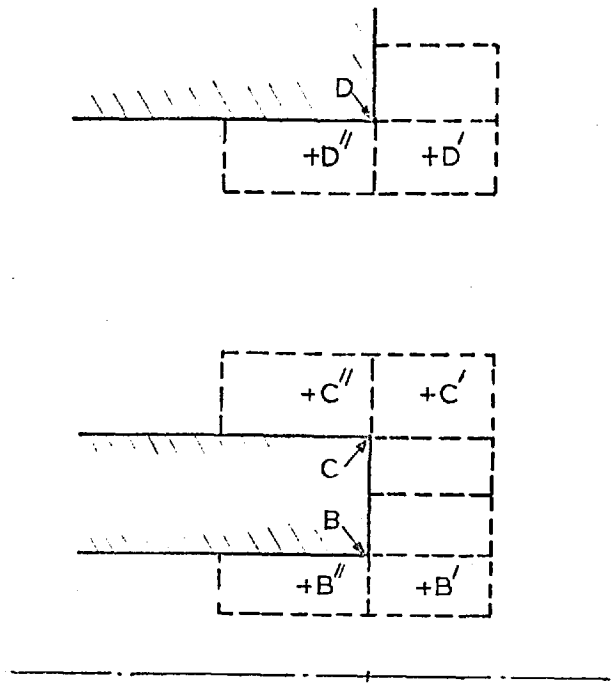

Fig. 5.2.b

from the circulation principle* and assume that they equal the values of the point velocities $\omega_{B'}$, $\omega_{C'}$ and $\omega_{D'}$ respectively. The result was that the predicted axial velocities along the axis in the vicinity of the inlet plane were unrealistically higher than those at AB in both isothermal and reacting flows.

After some investigations it was concluded that lower values of $\omega_{B'}$, $\omega_{C'}$ and $\omega_{D'}$ were needed to improve the predicted hydrodynamics. One way to get round this difficulty is to assume that stream lines passing by the nodes B', C' and D' from left to right run parallel to the z-direction, i.e. $[\partial\psi/\partial z]$ vanishes, provided that these nodes are located at a small distance from the inlet plane. The vorticity values at B', C' and D' can then be obtained by applying the circulation principle at the corresponding cells. This practice, though improving the predicted velocities along the axis, eliminated the recirculation zone downstream the step wall DE.

---

*The circulation principle states that the line integral of fluid velocity round a closed curve is equal to the flux of vorticity across an open surface bounded by the curve. This principle can be written as: $\oint u\,dx = \int \omega\,dA$ where u is the velocity in the x-direction and dA is the elemental area.

The shortcomings of the above two methods suggested that a combination of the two would produce a realistic velocity-distribution. In other words the value of ω_D equals that of the space-average vorticity at D" and the values of ω_B and ω_C are to be calculated from the circulation principle at the cells B' and C' where the stream lines run parallel to the axis. This hybrid method resulted in qualitatively realistic velocity distributions in both reacting and non-reacting flows; all the results to be presented later were obtained by the aid of this method.

5.3 Details of the computations

5.3.1 The solution procedure

The equation set (3.2-3) for the dependent variables ψ, ω/r, f, k , ε and g are solved simultaneously using the finite difference method discussed in section 3.3 and with the boundary conditions specified in section 5.2.3 above.

The values of the constants c_1, c_2, c_{g1}, c_{g2}, c_μ, σ_k and σ_ε are the same as those for the isothermal case discussed in chapter 4, and are given in table 4.3.1. The values of both the Schmidt numbers σ_f and σ_g are reduced from the value of 0.7 used in the isothermal case to a lower value of 0.6. The adjustment of σ_f was necessary to increase the diffusion of f in the radial direction (see eq. 3.2-3 and table 3.2.2) in order to achieve better agreement between the predictions of f and the measurements of El-Mahallawy et al (1973). The σ_g value of 0.6 was found to improve the predictions of the probability of reaction P.

5.3.2 A method for predicting the local probability of chemical reaction, P.

(a) The relation between P and $\tilde{f}$. It was mentioned in section 5.1 that some additional assumptions other than the chemical-reaction model (section 3.2.4) are needed to predict P. These are discussed below.

Consider fig. 3.2.c. At a given point in the flame, the probability that $\tilde{f}$ lies between the two values, $\tilde{f}_a$ and $\tilde{f}_b$ is

$$\int_{\tilde{f}_a}^{\tilde{f}_b} p(\tilde{f})\, d(\tilde{f}) \qquad (5.3\text{-}1)$$

We now postulate that there exists a choice of the limits $\tilde{f}_a$ and $\tilde{f}_b$ which renders the expression (5.3-1) into an expression for the probability of reaction, P. What should we take as these limits? We shall address ourselves to this matter.

Since reaction is possible only when $\tilde{f}$ is close to f_{st}, we shall suppose at the outset that $\tilde{f}_a$ and $\tilde{f}_b$ should be symmetrically situated on either side of f_{st}, subject to the conditions: (i) $\tilde{f}_a \geq 0$ and $\tilde{f}_b \leq 1$, (ii) at either of the above extremes, the delta function there, A_0 or A_1 (fig. 3.2.c) should be excluded from $p(\tilde{f})$. Introducing a "reaction range" λ, we can now write the probability of reaction, P as:

$$P \equiv \int_{f_{st}-\lambda}^{f_{st}+\lambda} e^{-(\tilde{f}-F)^2/2\sigma^2} [U(\tilde{f}-0) - U(\tilde{f}-1)]\, d\tilde{f}/\sigma\sqrt{2\pi} \qquad (5.3\text{-}2)$$

P is represented by the shaded area under the probability density curve of fig. 3.2.c. Thus, once λ is known P can be evaluated.

(b) The evaluation of the "reaction range" λ

Initial choice - a constant λ. At first it was attempted to find an an optimum constant value for λ that would give satisfactory agreement between the predicted and measured values of P. This attempt was guided by the concept of flammability limits of combustible mixtures.

It can be seen from eq. (5.3-2) that for a constant λ, P is a function of f and g only. A consequence of this is that P has the same value at two separate locations in the furnace, if the values of f and g are the same at these points. Measurements, however, indicate that P values can be very different at two separate points having the same predicted values of f and g. This contradiction between predictions and experiment suggested that λ cannot be assumed as constant.

Final choice - λ as a function of some local turbulence quantities. Having decided that λ should be allowed to vary, we were faced with the question: on what should λ depend? In the search for an answer we were guided by the fact that should depend on quantities that were readily available and that the functional relationship between and these quantities should be sufficiently simple to allow it to be used in the prediction procedure without undue difficulty.Because the experimental values of P were deduced from measurements of local ion-concentrations (section 2.4.3), we would expect that consideration of the chemical kinetics of the ionization process would yield some useful information.

Let us rewrite, for convenience, the three chemical reactions describing the chemi-ionization mechanism, (2.4-1) to (2.4-3):

chemi-ionization

$$CH + O \xrightarrow{k_i} CHO^+ + e^-, \Delta H = 0 \text{ KJ/mol} \qquad (2.4\text{-}1)$$

charge exchange

$$CHO^+ + H_2O \xrightarrow{k_e} H_3O^+ + CO, \Delta H = -34 \times 4.187 \text{ KJ/mol} \qquad (2.4\text{-}2)$$

ion recombination

$$H_3O^+ + e^- \xrightarrow{k_r} H_2O + H, \Delta H = -145 \times 4.187 \text{ KJ/mol} \qquad (2.4\text{-}3)$$

where k_i, k_e and k_r are the reaction-rate constants for the three reactions respectively. It has been shown in section (2.4) that the rate of production of H_2O, $\frac{dn_{H_2O}}{dt}$, is approximately proportional to n_+^2 where n_+ is the local instantaneous molar concentration of the positive ion H_3O^+. We shall attempt to seek a connection between n_+^2 and other quantities.

Now, the net rates of production for H_3O^+ and of recombination for CHO^+ can be written as:

$$\frac{d[H_3O^+]}{dt} = k_e [CHO^+] [H_2O] - k_r [H_3O^+][e^-] \qquad (5.3\text{-}3)$$

$$\frac{d[CHO^+]}{dt} = k_i [CH] [O] - k_e [CHO^+] [H_2O] \qquad (5.3\text{-}4)$$

where [j] denotes the instantaneous molar concentration of the species j.

In a steady state, the net rates $\frac{d[H_3O^+]}{dt}$ and $\frac{d[CHO^+]}{dt}$ must equal zero. Thus, $[H_3O^+]\,[e^-] = \frac{k_i}{k_r}\,[CH]\,[O]$. (5.3-5)

Since the charges are in balance, we have:

$$[H_3O^+] = [e^-] = [n_+].$$

Equation (5.3-5) therefore becomes:

$$[n_+^2] = \frac{k_i}{k_r}\,[CH]\,[O] \cdot \qquad (5.3\text{-}6)$$

Equation (5.3-6) states that the square of the instantaneous positive-ion concentration is proportional to the product of the instantaneous concentrations of the radicals CH and O. The proportionality constant, k_i/k_r, can be evaluated from the Arrhenius relation with the minimum activation energies assumed to equal the exothermisities of the reactions (2.4-1) and (2.4-3) respectively (Green and Sugden 1963). Thus,

$$\frac{k_i}{k_r} = \frac{A_i}{A_r}\,e^{-E/RT} \quad , \qquad (5.3\text{-}7)$$

where A_i and A_r are the pre-exponential coefficients, and T is the time-mean temperature of positive-ions, which is nearly equal to the local gas temperature (Calcote and King 1955). The activation energy E equals 145 x 4.187 KJ/mol (eqs. 2.4-1 and 2.4-2) and R is the universal gas constant. The ratio (A_i/A_r) can be put equal to a constant, A, since both A_i and A_r are proportional to $T^{\frac{1}{2}}$. Thus, expression (5.3-6) can be written as:

$$[n_+]^2 = A\,e^{-E/RT}\,[CH]\,[O] \qquad (5.3\text{-}8)$$

We recall that $[n_+]^2$ can be taken as proportional to the reaction rate (see section 2.4). Thus, if the "reaction range" λ has the physical meaning we have ascribed to it, we expect that it can be related to the quantities on the R.H.S. of eq. (5.3-8). Since in the present prediction procedure we do not calculate the concentration of the radicals such as CH and O, it is necessary to relate their concentrations to other available quantities. In order to do this we have to introduce additional assumptions.

For convenience, let us re-write eq. (5.3-8) as:

$$\left(\frac{d}{dt}\ [H_2O]\right)_i \approx A\, e^{-E/RT}\, [CH]\, [O]\ , \qquad (5.3\text{-}9)^*$$

where the approximation sign comes from the relation between $[n_+]^2$ and $\left(\frac{d}{dt}\ [H_2O]\right)_i$ given by eq. (2.4-6). Let the symbols $\tilde{\alpha}$, $\tilde{\beta}$ and $\tilde{\gamma}$ stand for the instantaneous concentrations [O], [CH] and $\left([H_2O]\right)_i$ respectively. We can then write eq. (5.3-9) as:

$$\frac{d}{dt}\ \tilde{\gamma} \approx \tilde{\alpha}\,\tilde{\beta}\, A\, e^{-E/RT} \qquad (5.3\text{-}10)$$

If we split the instantaneous quantities $\tilde{\alpha}$, $\tilde{\beta}$ and $\tilde{\gamma}$ in conventional fashion, as:

$$\tilde{\alpha} = \alpha + \alpha' \ ,$$
$$\tilde{\beta} = \beta + \beta' \ ,$$
$$\tilde{\gamma} = \gamma + \gamma' \ ,$$

and substitute them in eq. (5.3-10) and time-average we get:

$$\frac{d}{dt}\ \gamma \approx A\, e^{-E/RT}\, (\alpha\beta + \langle\alpha'\beta'\rangle) \ . \qquad (5.3\text{-}11)$$

* See the footnote on page 26.

Equation (5.3-11) highlights the important role the concentration fluctuations play in controlling the chemical reaction rates. In particular, the reaction rate can be either reduced or enhanced by the correlation term $<\alpha'\beta'>$ depending on whether it is negative or positive.

As an illustration, we can imagine two reacting materials $\tilde{\alpha}$ and $\tilde{\beta}$ pass a point of observation at different times, i.e. they are never in contact with each other. Time-mean values α and β are measured. But it is seen that $\alpha\beta$ is equal to $- <\alpha'\beta'>$ in this case, a result which predicts no chemical reaction. On the other hand, if the two materials are initially premixed and discharge from a point source, during their subsequent turbulent mixing with the surrounding atmosphere their concentration fluctuations should be positively correlated. We should then expect on the basis of this effect their reaction rate would be considerably higher than if there were no fluctuations, or if the flow was non-turbulent. Both of these cases, though mathematically true, lack the physical reality because the role of molecular diffusivity in dissipating the correlation $<\alpha'\beta'>$ has been neglected. This decay of concentration fluctuations is analogous to the decay of turbulence kinetic energy; the first is effected through molecular diffusion and the latter by molecular viscosity. The time-rates of decay of both quantities are controlled by large-scale dynamics which involves neither molecular diffusion nor viscosity (Batchelor 1959, Csanady 1967, Tennekes and Lumley 1972). Accordingly, the dissipation term in the g equation (section 3.2) has been modelled as proportional to $g\varepsilon/k$ (Table 3.2.4) where ε/k is the time-scale of the large turbulence-eddies.

It is thus expected that the time-mean rate of reaction $d\bar{Y}/dt$ in eq. (5.3-11) should be proportional to the decay rate of $\alpha'\beta'$ To calculate this rate rigorously, five partial differential equations for the dependent variables $\langle\alpha'\beta'\rangle$, $\langle\alpha'^2\rangle$, $\langle\beta'^2\rangle$, α and β must be solved simultaneously with the other equations, as has been suggested by Hilst et al (1973). In the present analysis, the two mathematical models for the chemical reaction (sec. 3.2.4) and concentration fluctuations (sec. 3.2.6) allow us to calculate α, β, $\langle\alpha'^2\rangle$ and $\langle\beta'^2\rangle$ (sec. 3.2.7), but no information about $\langle\alpha'\beta'\rangle$ can be obtained. For this reason we shall postulate here that the rate of decay of $\langle\alpha'\beta'\rangle$ is proportional to that of g; this permits the rate of reaction, $d\bar{Y}/dt$, to be taken as proportional to dg/dt.

As we have explained earlier, the "reaction range" λ is expected to be related to the quantities on the R.H.S. of eq. (5.3-8). To be concrete we shall now assume λ to be proportional to both $[Ae^{-E/RT}]$ and $[dg/dt]$. Since λ is dimensionless (see eq. 5.3-2), the term $[dg/dt]$ needs to be modelled in a dimensionless form. One way of doing this is to write $[dg/dt]$ as $[g/f^2]\,[t_K/t]$, where t equals ε/k and t_K is the Kolmogorov's time-scale, $t_K \equiv (\nu/\varepsilon)^{\frac{1}{2}}$. The Kolmogorov's time-scale is the smallest scale occuring in turbulent motion; it decreases with increasing the dissipation rate of turbulence energy. Thus a fairly general expression for λ may be written as:

$$\lambda = A\, e^{-E/RT}\,[g/f^2]^{B_1}\,[t_K/t]^{B_2} \quad , \qquad (5.3\text{-}12)$$

where B_1 and B_2 are constants of proportionality. A, B_1 and B_2 were found by correlating the measured and predicted values of P at many locations in the furnace (150 points from 4 sets of results), using

the least square method, as*:

$$A = 1.2, \quad B_1 = 1, \quad B_2 = 1$$

It may be noted that equation (5.3-12) can also be written in terms of the length-scales instead of the time-scales as:

$$\lambda = A\, e^{-E/\mathcal{R}T} \left[g/f^2\right]^{B_1} / \left[\ell/\eta\right]^{2B_2/3}, \qquad (5.3\text{-}13)$$

where ℓ is the turbulence length-scale proportional to the size of large eddies (eq. 3.2-8), and η is the Kolmogorov's microscale, $\equiv \nu^{\frac{3}{4}}/\varepsilon^{\frac{1}{4}}$. It should perhaps be pointed out that the quantity λ has been introduced to allow us to calculate P in the present procedure, it does not appear to have any physical significance.

5.3.3 Accuracy and convergence criteria

(a) Accuracy. The accuracy of the numerical solution was checked in the following way. Some computations were performed first with a coarse grid and then with a relatively fine grid. When the difference between the two results was acceptably small, it was concluded that a sufficiently accurate solution was reached. Both grids were non-uniformly distributed; the first was 15 x 15 and the second 20 x 30, with the larger number of nodes in the radial direction. Details of the grid-node distribution are given in tables 5.3.a and 5.3.b. The computer storage required for the 20 x 30 grid was, for the present problem, about 60K, which is the maximum storage that the computer used (CDC 6600) permits.

---

*It should be pointed out here that the above values of A, B_1 and B_2 differ slightly from those published earlier (Elghobashi and Pun 1974) where they were given as 1.1, 1.1, 1. respectively. The reason is that at the time of the earlier publication, the experimental results of flames III and IV were not included in the optimisation of the constants.

Table 5.3.a

15 x 15 grid		
*I or J	z/D	r/R
1	0	0
2	.05	.03
3	.12	.08
4	.21	.11
5	.40	.17
6	.58	.25
7	.78	.28
8	1.2	.34
9	1.7	.40
10	2.5	.51
11	3.3	.62
12	4.7	.73
13	6.3	.84
14	7.8	.95
15	9.9	1.

Table 5.4.b

20 x 30 grid					
I or J	z/D	r/R	I or J	z/D	r/R
1	0	0	16	5.6	.26
2	.05	.01	17	6.3	.28
3	.12	.02	18	7.1	.31
4	.21	.03	19	8.7	.34
5	.40	.04	20	9.9	.40
6	.58	.06	21	-	.46
7	.78	.07	22	-	.52
8	.97	.09	23	-	.58
9	1.3	.10	24	-	.64
10	1.7	.12	25	-	.70
11	2.2	.14	26	-	.76
12	2.8	.16	27	-	.83
13	3.3	.18	28	-	.89
14	3.9	.20	29	-	.95
15	4.7	.23	30	-	1.

*I and J are the numbers of grid lines in the axial and radial directions respectively.

In figs. 5.3.a and 5.3.b, the effect is displayed of the grid size on the distributions along the furnace axis of f, T, u/u_1, ℓ/R for flame A (Table 2.6). Also shown on fig. 5.3.a are the experimental values of f (El-Mahallawy et al 1973) for the same flame. Figure 5.3.c compares the predicted radial profiles of T, u/u_1 for the two grids at the axial locations of 0.21D and 3.3D. On the whole, the results from the coarse and the fine grids do not differ significantly, except perhaps at locations close to the burner where the gradients in both the axial and radial directions are very steep. On this basis the 15 x 15 grid was considered accurate enough and all the computations to be reported later were carried out with this more economical grid.

(b) Convergence. Convergence of the numerical process was measured by reference to two criteria. The first was the monotonic decrease of the quantity $\Delta\phi$ defined as:

$$\Delta\phi \equiv \frac{\phi^n - \phi^{n-1}}{\phi_{ref}} \quad , \qquad (5.3\text{-}14)$$

where ϕ^n and ϕ^{n-1} denote the values at a node of the variable ϕ at two successive iterations and ϕ_{ref} is a suitable reference value of ϕ. The second criterion was based on the use of a residual source R_s defined as:

$$R_s \equiv \left| \phi_P - \sum_{i=N,S,E,W} c_i \phi_i - d_\phi \right| \quad , \qquad (5.3\text{-}15)$$

where ϕ is the value of ϕ at the grid node P; N, S, E, W are the

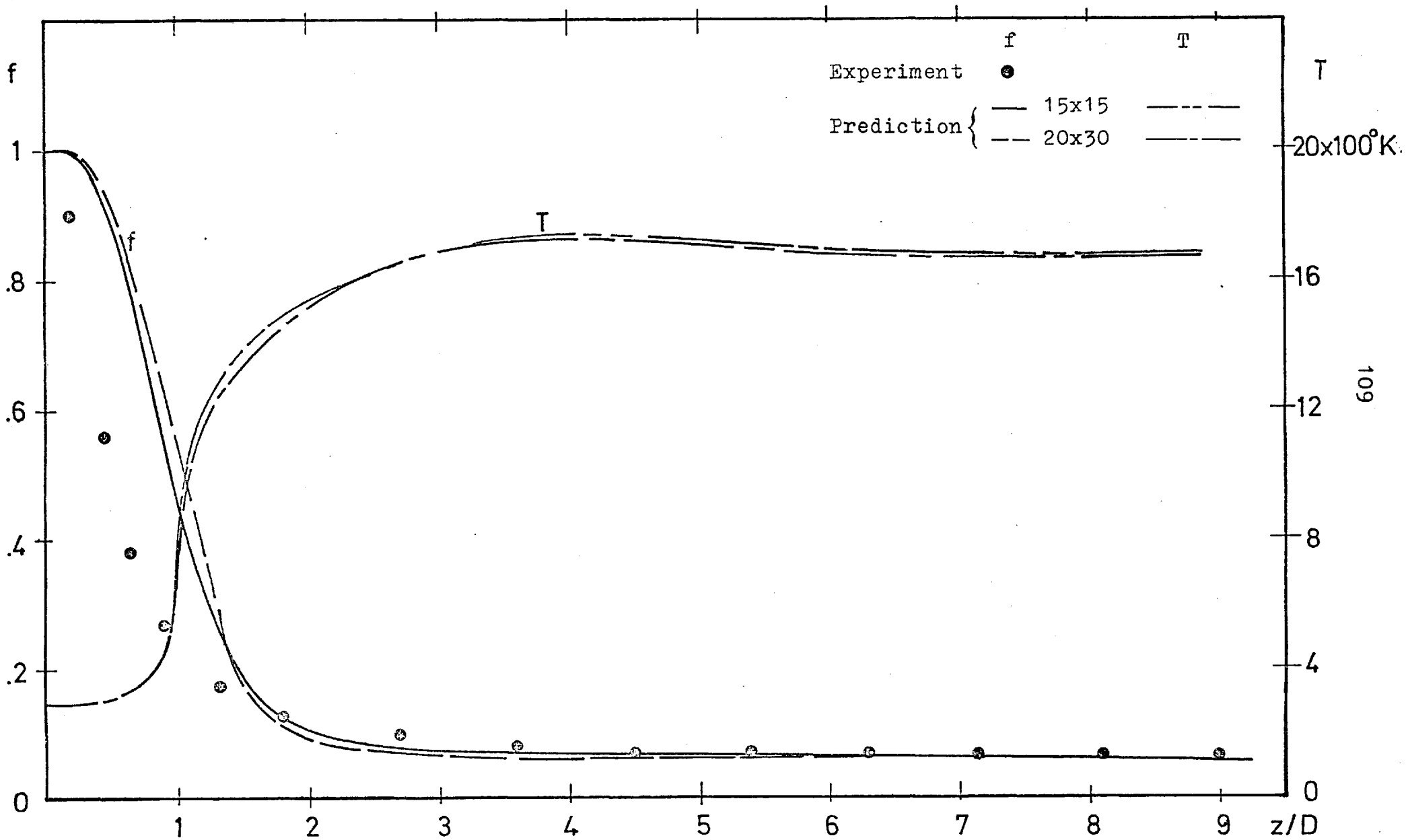
f
T
Experiment
Prediction
15x15
20x30
f
T
20x100°K
1
.8
.6
.4
.2
0
16
12
8
4
0
1
2
3
4
5
6
7
8
9
z/D

Fig.5.3.a

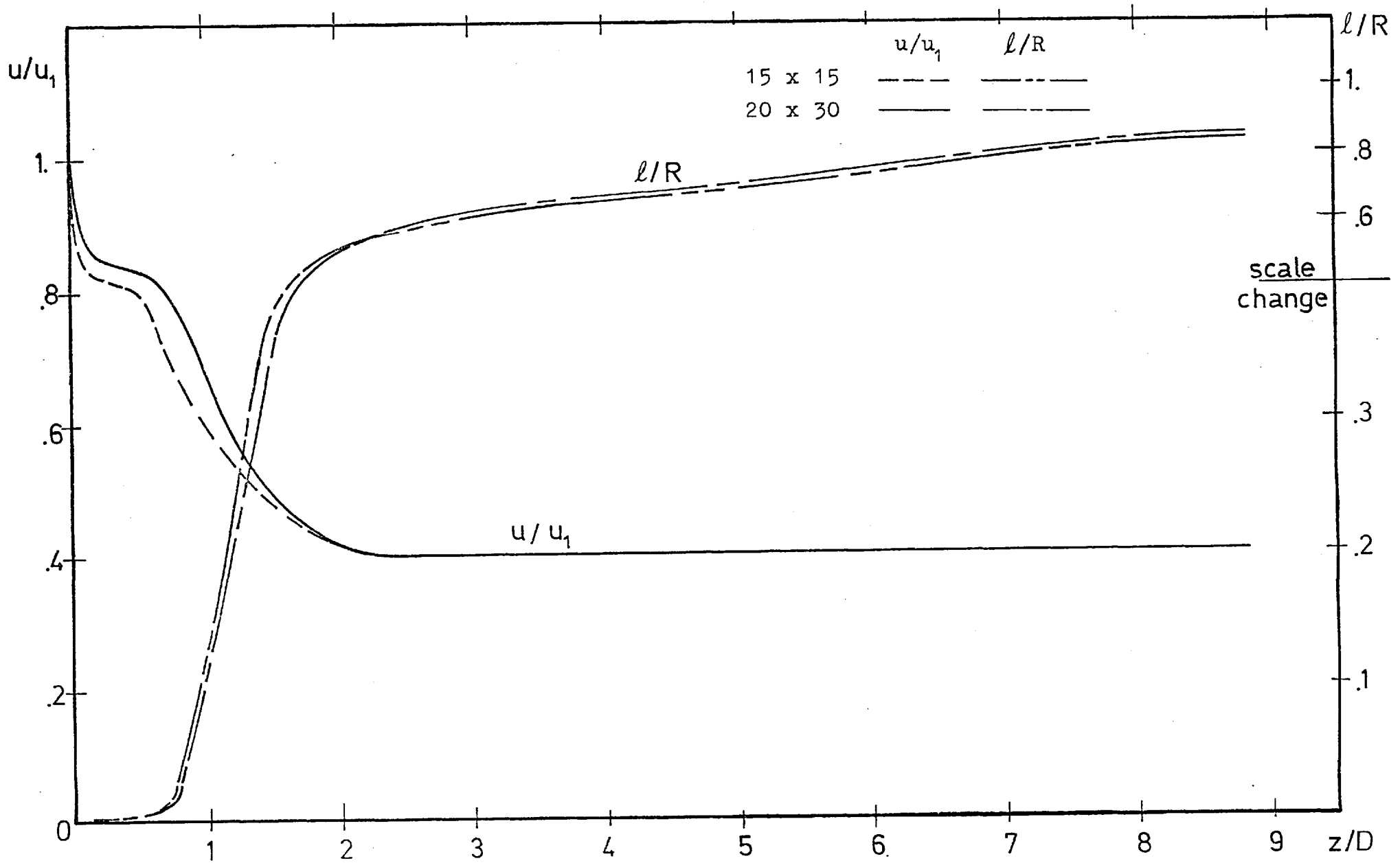

Fig.5.3.b

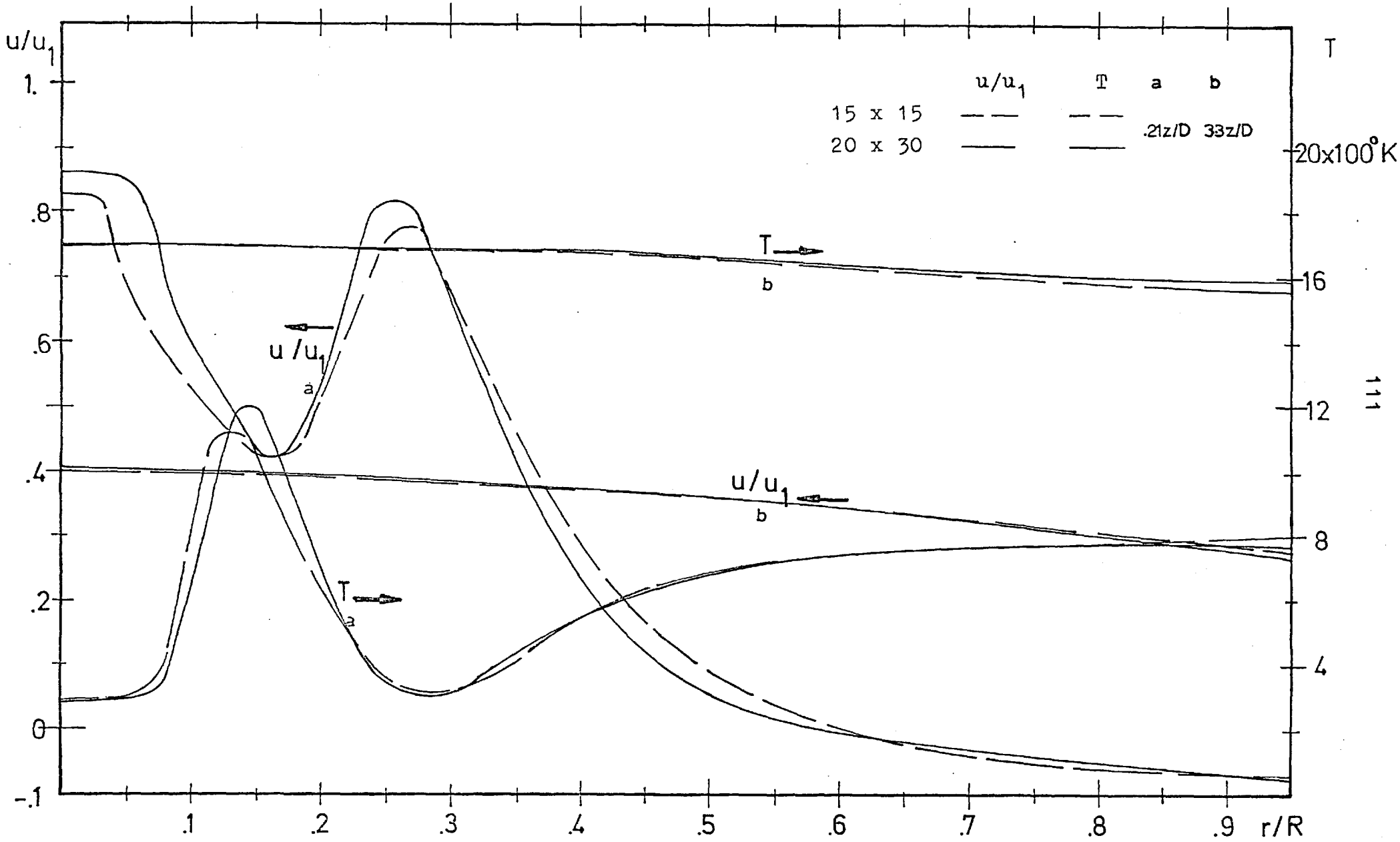
u/u1
T
u/u1 T a b
15 x 15
20 x 30
.21z/D 33z/D
20x100°K
1.
.8
.6
.4
.2
0
-.1
16
12
8
4
T
b
u/u1
a
u/u1
b
T
a
.1
.2
.3
.4
.5
.6
.7
.8
.9
r/R

Fig.5.3.c

neighbouring nodes; c_i's are coefficients representing the influence of convective and diffusive fluxes, and d_ϕ is the source term. When the numerical process has converged $R_{s,max}$ should be less than a substantially small value.

5.3.4 Computer time

The computer time required depended directly on two factors: the number of grid points and the number of iterations necessary for achieving convergence. For a 15 x 15 grid, about 400 iterations were needed to obtain a converged solution and the typical time on the CDC 6600 was 540 seconds. The time required for a 20 x 30 grid was 1140 seconds for 446 iterations.

5.4 Results and discussions

All the components of the prediction method have now been introduced. We shall proceed to present the results of some of the predictions obtained for flames I, II, III, IV and A of Table 2.6. The different inlet conditions of these flames were chosen in such a way so as to allow the effects of Reynolds number, air/fuel ratio and velocity ratio to be studied. Where no suitable measurements are available we shall qualitatively examine the computations.

5.4.1 Discussion of the computations

This discussion refers to figures 5.4, 5.5, 5.6 and 5.7 for flames I, II, III and IV respectively, and comments apply to all 4 flames unless specifically mentioned otherwise. Each figure contains 15 contour

plots (a, b, c .... to) for the following fifteen quantities, all of which, with the exception of temperature T, are dimensionless. The discussion is necessarily qualitative since no suitable measurements are available for these quantities.

Plot	Quantity
a	$\psi^* = \psi/\psi_{ref}$
b	$u^* = u/u_1$
c	$v^* = v/u_1$
d	$k^* = k^{1/2}/u$
e	$\ell^* = \ell/R$
f	$\mu^* = \mu_{eff}/\mu$
g	f
h	T
i	$\rho^* = \rho/\rho_0$
j	$\omega^* = (\omega/r)/(\omega/r)_{ref}$
k	$g^* = g^{1/2}/f$
l	$T'^* = \langle T'^2 \rangle^{\frac{1}{2}}/T$
m	$m^*_{ox} = m_{ox}/m_{ox,0}$
n	$m^*_{fu} = m_{fu}/m_{fu,1}$
o	$m^*_{pr} = m_{pr}/m_{inert,0}$

The quantities ψ_{ref} and $(\omega/r)_{ref}$ are respectively the values of ψ at point D, and of (ω/r) at point D' of fig. 5.2.b.

The stream function

From figures 5.4.a, 5.5.a, 5.6.a, 5.7.a it can be seen that the length of the recirculation zone is nearly the same, about 1.2D, for the four different conditions. Also the maximum mass-flow rate of the recirculating products of combustion is about 40% of the total inlet mass flow rate. For the range of inlet conditions studied (Re varied from 15200 to 25000) the predictions suggest that, as in isothermal flows, the length of recirculation zone in a turbulent, sudden-expansion, reacting flow is mainly a function of the expansion ratio.

Axial and radial velocities

Figures 5.4.b, 5.5.b, 5.6.b, 5.7.b show that at a distance of about 3.3D from the burner, the axial-velocity fields become fully developed. The rate of decay of u with distance along the center line depends on the ratio of the inlet-stream momenta (air to fuel). Flame II (momenta ratio = 10.4) exhibits the fastest rate of decay; u^* has a value of 0.5 at a distance of 1.7D from the burner, while for flame I (momenta ratio = 26.3) u^* has a value 0.5 at about 3D.

The radial velocity distributions (figs. 5.4.c,5.5c,5.6c,5.7c) indicate, as expected, that v has a maximum positive ($v^* = .08$) at the lower boundary of the recirculation eddy and a maximum negative ($v^* = -.08$) at the left boundary of the eddy.

Vorticity/radius

The contours of vorticity/radius (figs. 5.4.j, 5.5.j, 5.6.j, 5.7.j)

display plausible behaviour: close to the burner, ω/r attains a high positive value at r/R equals about 0.1 (point B of fig. 5.2.a) where $\partial u/\partial r$ is negative and is much larger than dv/dz. At a radial location of r/R equals about 0.2 (point C of fig. 5.2.a) ω/r becomes negative; here du/dr is positive and $\partial v/\partial z$ is negligible. Far downstream from the burner (z/D>4) ω/r approaches a fully developed profile with a high value near the furnace wall which decreases as we move towards the axis.

Intensity and length scale of turbulence

Common to all of the four flames are the two locations of high ($k^* \geq 10$) turbulence intensity (figs. 5.4.d, 5.5.d, 5.6.d, 5.7.d). The first at an axial distance of about 0.8D from the burner and at a radial position of about 0.7R, the second is closer to the wall and at an axial distance of 1.2D. As expected these two zones are where $\partial u/\partial r$ is maximum and u is minimum, at the center and close to the reattachment of the recirculating eddy.

The shear layer between the main flow and the boundaries of the eddy (r/R = 0.3 to 0.5) is characterised by the high values of the turbulence kinetic energy (contours of $k^* = 1, .5$ and $u^* = 0.2, 0.3$).

The turbulence length-scale (figs. 5.4.e, 5.5.e, 5.6.e, 5.7.e) exhibits a uniform distribution near the wall; this is a consequence of the wall-function treatment (section 3.3.2), namely at the nearest node to the wall the length scale is proportional to the distance from the wall.

A highly dissipative region characterised by the small values of the length scale (ℓ^* = .027 to .07) exists between the fuel and air streams (r/R = 0.1 to 0.25) close to the burner (up to a distance of 1D). As will be seen later in the discussion this region is particularly significant in promoting chemical reaction.

The distribution of the length scale along the axis shows a steep increase from ℓ^* = .02 at z = .78D to ℓ^* = .29 at z = 1.2D; these two locations mark the axial positions of the center and the end of the recirculating eddy. This result accords with the findings of Günther and Lenze (1973): that the length scale attains its maximum at the station of maximum recirculating flow rate. Downstream from the zone of recirculation, the length scale continues to increase, but at a much slower rate, till the end of the furnace where it attains a value of 0.8R ($\approx$ 80mm).

The effective viscosity

The effective viscosity distributions (figs. 5.4.f, 5.5.f, 5.6.f, 5.7.f) show a zone of high μ_{eff} ($\overset{*}{\mu} \approx 10^3$) located at an axial distance of 0.78D from the burner and at r = 0.5R. This is a region of high generation of k as explained earlier.

Of the four flames, flame III has the highest inlet air velocity (21 m/sec) and consequently largest value of $\overset{*}{\mu}$ (1216). The inlet air velocity, and not the total mass flow rate, influences μ_{eff} because the air stream is in contact with the recirculation zone; thus the higher the air velocity the larger the gradient $\partial u/\partial r$. The large values of μ_{eff} (10^3 times the laminar viscosity) in that region and hence of

the exchange coefficients for heat and mass transfer point out the important role of the recirculation of hot combustion products in heating the incoming air (flame stabilizing effects).

For all the four flames, the computed exchange coefficients for the mixture fraction f in the recirculation zone vary between .03 and .04 m^2/sec; these values accord with the measurements of Lenze (1971-pp.92) for a confined, town-gas, turbulent diffusion flame.

Time-mean mixture fraction

(i) Flame A. In fig. 5.3.a, the predicted distribution of f along the axis of the furnace for flame A of table 2.6 is displayed; also shown are the measurements of El-Mahallawy et al (1973) for the same flame.

At far downstream locations, $z/D \geqslant 1.5$, good agreement is observed. Close to the inlet where the gradients in both the axial and radial directions are steep, the measurements exhibit a faster axial decay-rate than the predictions. It is possible that measurements in this region were subject to larger errors because of the critical need to locate the sampling probe more accurately there. The measured and predicted radial profiles are compared in fig. 5.8.a at three axial locations of z/D values of .21, 1.7 and 2.5. Again agreement is good at the two locations of z/D of 1.7 and 2.5 between prediction and measurement. At the station nearest the burner, z/D = .21, the agreement is less good, particularly close to the axis.

(ii) Flames I, II, III and IV

The predictions of f (figs. 5.4.g, 5.5.g, 5.6.g, 5.7.g) show that the rate of decay of the mixture fraction with distance along the axis depends mainly on the inlet air/fuel ratio. Flame II, the fuel-richest of the four flames exhibits the lowest rate of decay of f, while flame I, the leanest, shows the highest rate. The rates for flames III and IV fall between the above two extremes.

Intensity of fluctuations of the mixture fraction

It is appropriate here to consider the probability density function $p(\tilde{f})$ when we examine the distributions of the intensity of fluctuations $g^{\frac{1}{2}}/f$ (figs. 5.4.k, 5.5.k, 5.6.k, 5.7.k).

For all four flames, $g^{\frac{1}{2}}/f$ attains its maximum value (≈ 3)* in a region very close to the burner ($z \leqslant .4D$) at a radial location of about 0.3R. In this region, because the f values are relatively low ($\leqslant .01$), $p(\tilde{f})$ will be characterised by large values of the delta function A_0 (see fig. 3.2.g); i.e. the instantaneous mixture fraction $\tilde{f}$ fluctuates between values corresponding to air and products at one side and fresh air at the other, with large proportion of time spent at the latter.

As we move downwards towards the axis, for example to a radial location of 0.2R where $g^{\frac{1}{2}}/f$ equals about 1. and f approaches f_{st}, $\tilde{f}$ experiences fluctuations between fuel and products at one end and air

---

*this seemingly high value still lies well below the physical upper-limit imposed on g, namely $g \leqslant f(1-f)$

and products at the other, with the diminshing of the delta function A_0, closer to the axis, where f attains large values (≈ 0.5) corresponding to the fuel-rich zone, $\overline{g^2}/f$ decreases and $p(\tilde{f})$ approaches a normal Gaussian distribution ($A_0 = A_1 = 0$, see fig. 3.2.e).

Far downstream from the burner, beyond an axial distance of 4.7D up to the end of the furnace, f becomes less than f_{st} and the intensity $\overline{g^2}/f$ attains an approximately uniform value of about .16. In that region $p(\tilde{f})$ is expected to have a peaked Gaussian distribution (fig. 3.2.f).

Time-mean values and fluctuations of temperature

Figures (5.4.h, 5.5.h, 5.6.h, 5.7.h) show that the field of the time-mean temperature can be divided into three distinct zones: the first extends from the burner up to an axial distance of 1D; in this zone steep gradients exist in the radial direction and the temperature of the recirculating combustion products (in the region of r = .5R to R) is higher than that of the unreacted fuel near the axis. This zone is also characterised by large fluctuation of temperature ($T'^* \approx 1.$, figs. 5.4.1, 5.5.1, 5.6.1, 5.7.1). It can be seen that the maximum fluctuations occur at a larger radial distance (0.3R) from the axis than that of the maximum time-mean temperature (0.15R) where the turbulence length-scale is much smaller.

The second zone follows the first and extends to an axial distance of 1.7D; in that region the time-mean temperature along the axis becomes higher than that of the combustion products, but the maximum

value of T occurs away from the axis at a radial location of 0.1R. The temperature fluctuations at the axis exhibit steep gradient because relatively large-scale air vortices have been introduced by turbulent mixing into the smaller-scale region of the fuel jet; these vortices have been preheated by the combustion products.

In the last zone which occupies the rest of the furnace, the maximum value of T occurs along the axis where the fluctuations in both temperature and concentration decay gradually.

As expected, the time-mean temperature at the exhaust end of the furnace is inversely proportional to the inlet air/fuel ratio, being maximum for flame I (22.9) and minimum for flame II (15.4).

It should be remarked here that although we have neglected the heat transfer to the furnace wall in the computations (see section 3.2.4), the predicted maximum values of the time-mean temperature are, on the whole, 20 to 30% lower than those measured by Günther and Lenze (1973) for a similar flame. This discrepancy may perhaps be explained by reference to the following three points:

1. Günther and Lenze used a 10 mm. diameter fuel-jet in a relatively large furnace (450 mm. diameter), so that the condition of the free jet was fulfilled to a great extent, and hence the turbulence length-scale, especially along the axis, would be much smaller than that in the present study where a 20 mm. jet is issuing into a 200 mm. diameter furnace. A smaller length-scale results in smaller-amplitude fluctuations of temperature and consequently in higher time-mean values.

2. The predicted values of the fluctuations of the mixture fraction may be higher than their actual values (the constants c_{g1} and c_{g2} have the same values used in predicting non-reacting flows). This would result in lower values for the time-mean temperature.

3. In calculating the time-mean temperature from eq. (3.2-46), the instantaneous specific heat was assumed to depend on the local time-mean temperature instead of the instantaneous one. This would underestimate the time-mean temperature at locations where the values of either one of the delta functions of $p(\tilde{f})$ is large.

In order to provide a further, but fairly crude check on the predictions, a simple enthalpy balance for the furnace was carried out under the experimental conditions of the four flames. Table 5.4 below displays the four different values of the exhaust temperature (averaged over the exit plane) obtained: from the predictions, from an enthalpy balance for adiabatic walls, from an enthalpy balance for non-adiabatic walls, and from the measurements using a thermocouple (Comark-type 1602). The predictions are in satisfactory agreement with those from the enthalpy-balance calculations for the adiabatic case. The discrepancy between the thermocouple measurements and the non-adiabatic case is thought to be due mainly to thermocouple error (no correction for radiation and conduction losses was made).

Table 5.4

flame	average exhaust temperature ^{o}K			
	enthalpy balance adiabatic wall	predictions adiabatic wall	enthalpy balance non-adiabatic	thermocouple measurements
I	1234	1190	1102	1073
II	1642	1590	1479	1138
III	1400	1300	1277	1088
IV	1560	1500	1404	1173

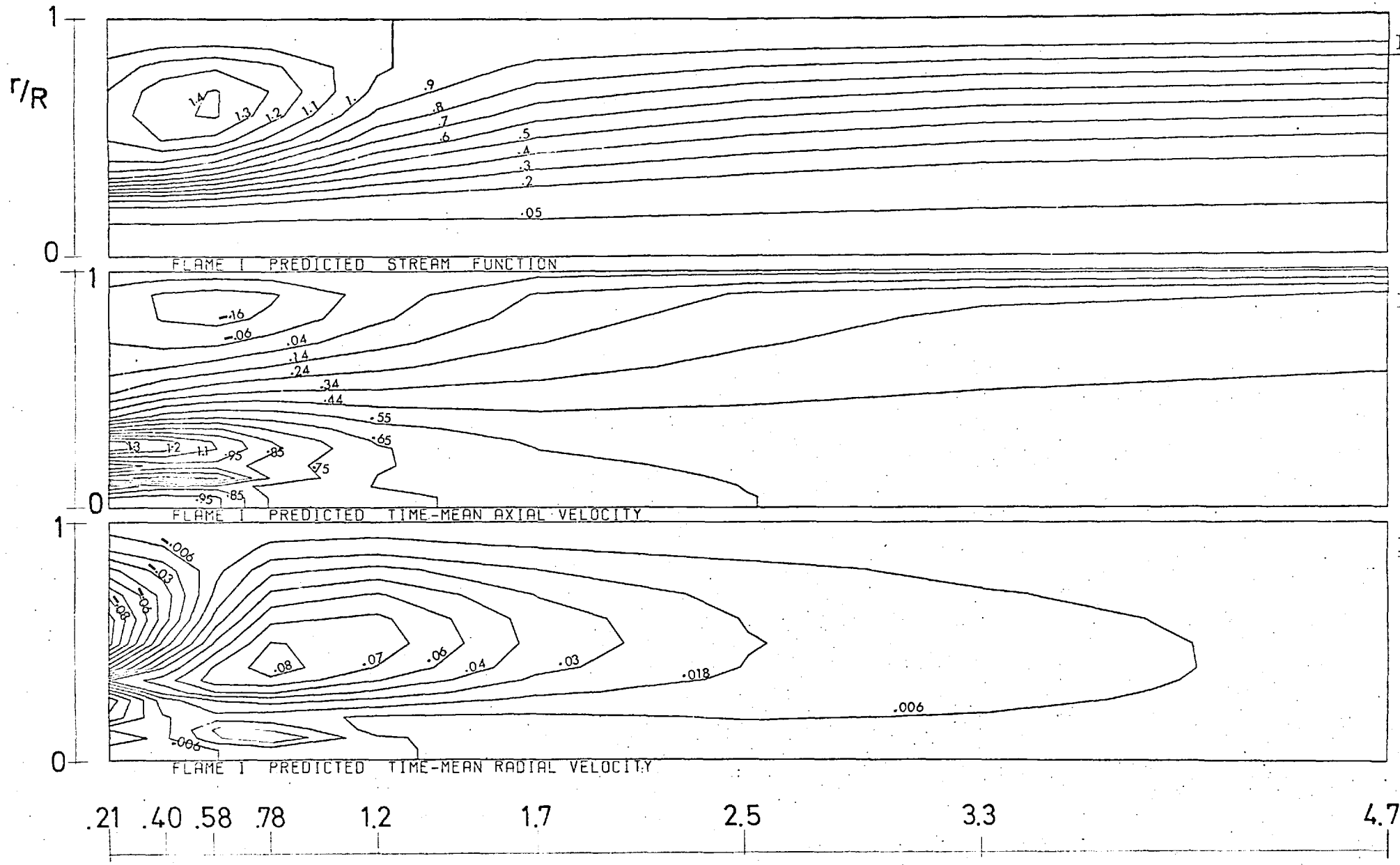
1
r/R
0
1.4
1.3
1.2
1.1
1.
.9
.8
.7
.6
.5
.4
.3
.2
.05
FLAME I PREDICTED STREAM FUNCTION
Fig.5.4.a
ψ^*
1
0
-.16
-.06
.04
.14
.24
.34
.44
.55
.65
1.3
1.2
1.1
.95
.85
.75
.95
.85
FLAME I PREDICTED TIME-MEAN AXIAL VELOCITY
Fig.5.4.b
u^*
1
0
-.006
-.03
-.06
-.08
.08
.07
.06
.04
.03
.018
.006
-.006
FLAME I PREDICTED TIME-MEAN RADIAL VELOCITY
Fig.5.4.c
v^*
.21
.40
.58
.78
1.2
1.7
2.5
3.3
4.7
z/D

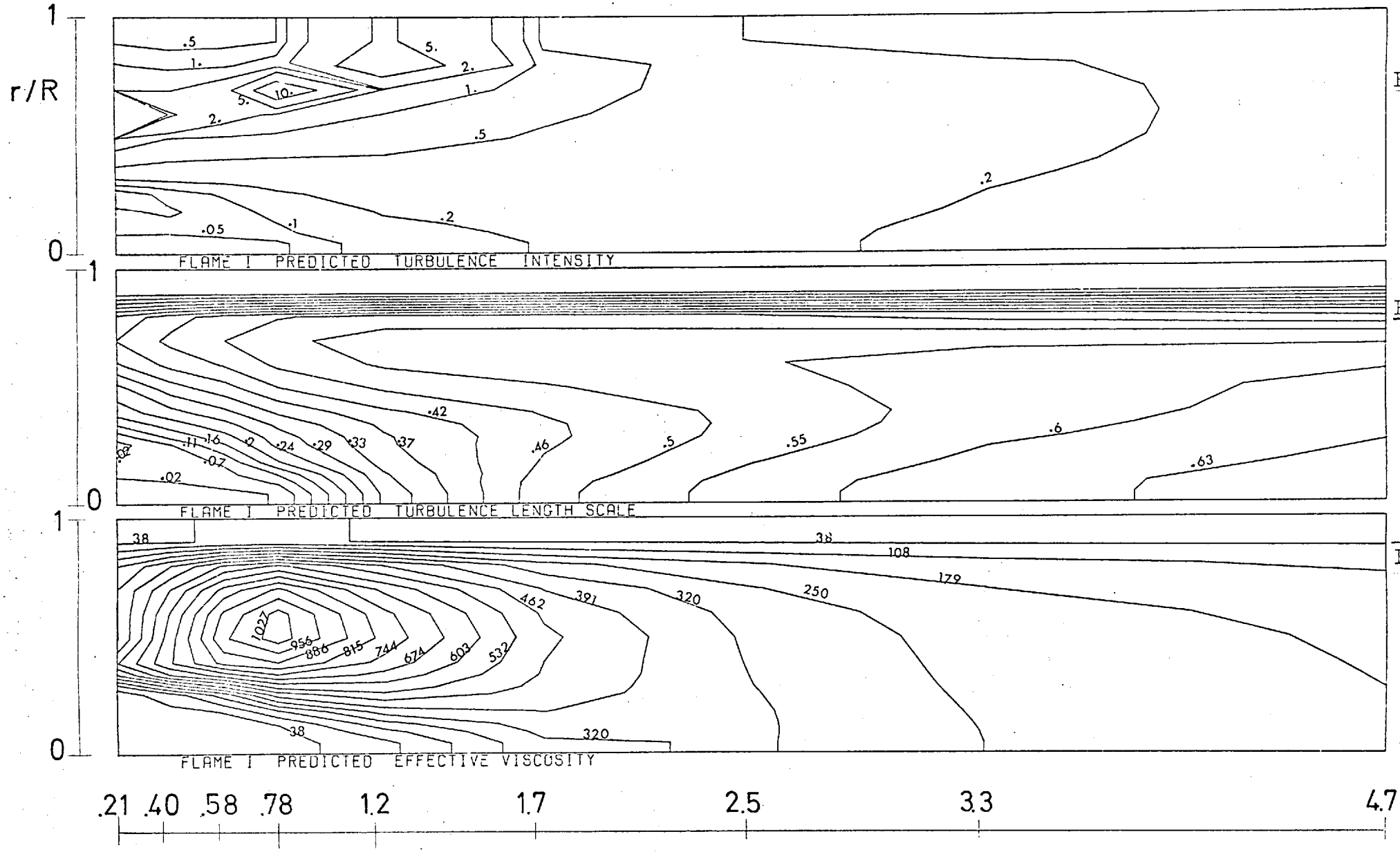

Fig.5.4.d

k^*

Fig.5.4.e

ℓ^*

Fig.5.4.f

μ^*

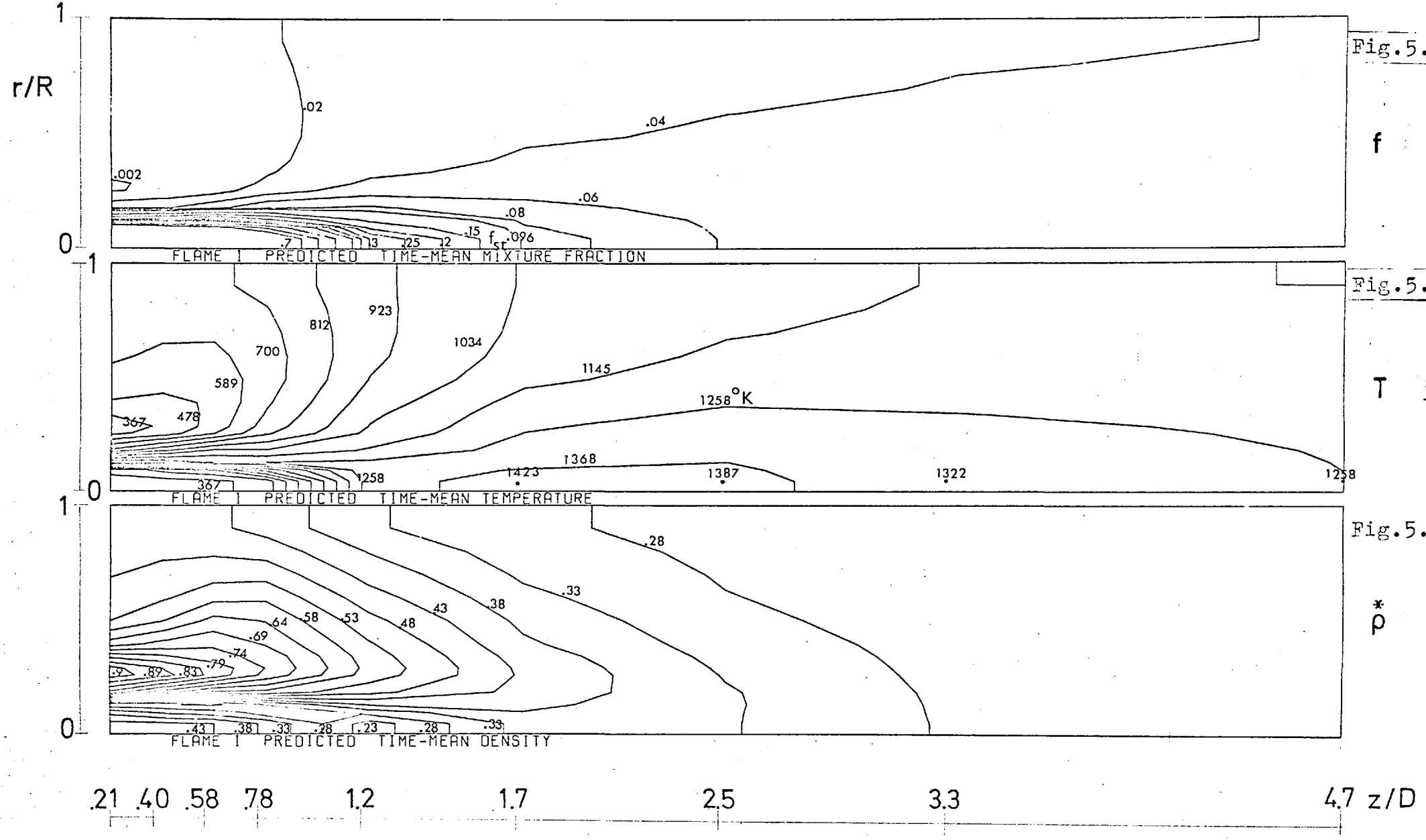
r/R
1
0
.002
.02
.04
.06
.08
.15
.096
.7
.13
.25
.12
f_{st}
FLAME I PREDICTED TIME-MEAN MIXTURE FRACTION
f
Fig.5.4.g
367
478
589
700
812
923
1034
1145
1258°K
1368
1423
1387
1322
1258
FLAME I PREDICTED TIME-MEAN TEMPERATURE
T
Fig.5.4.h
.28
.33
.38
.43
.48
.53
.58
.64
.69
.74
.79
.83
.89
.9
FLAME I PREDICTED TIME-MEAN DENSITY
ρ^*
Fig.5.4.i
.21 .40 .58 .78 1.2 1.7 2.5 3.3 4.7 z/D

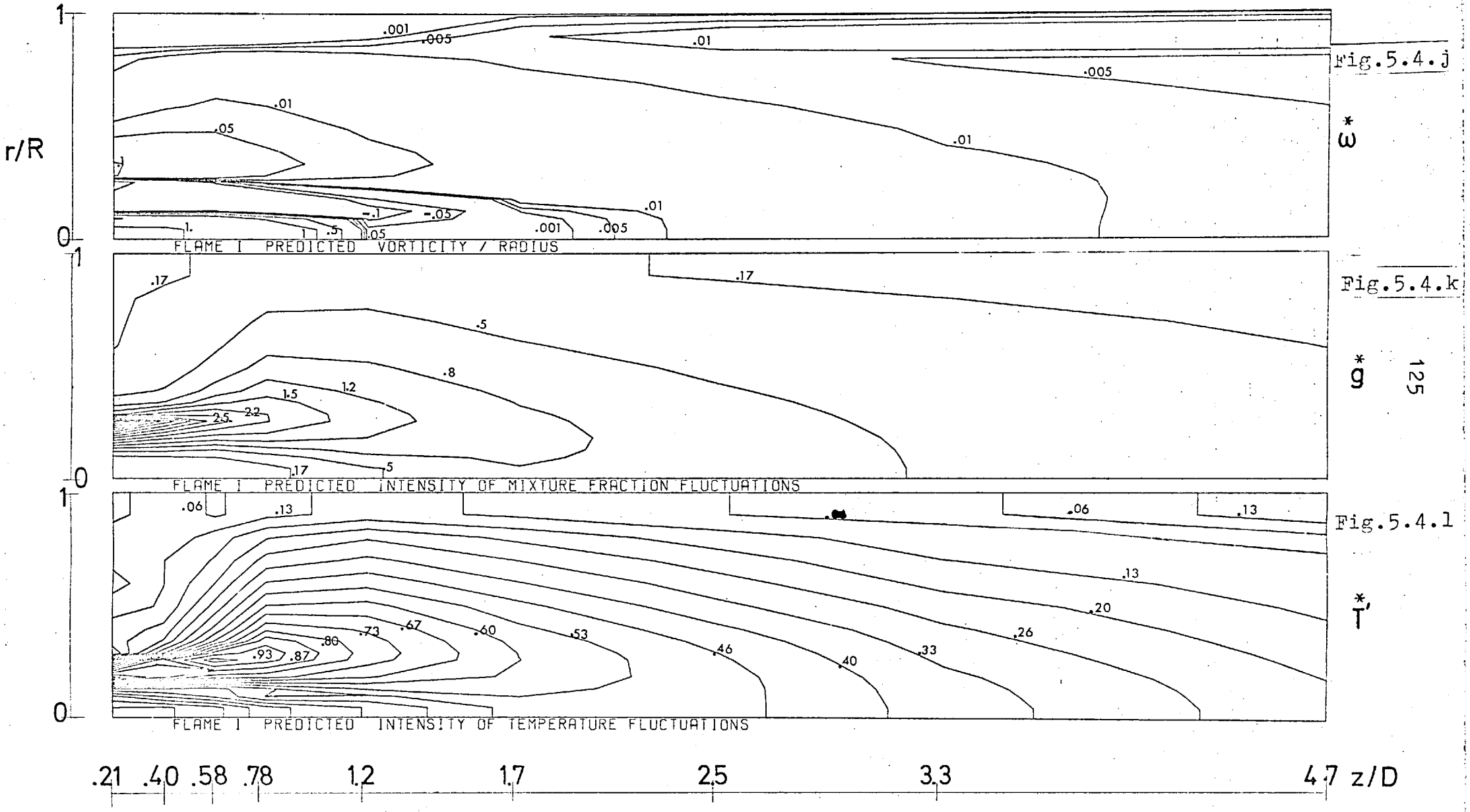
r/R
1
0
.001
.005
.01
.005
.01
.05
.01
.01
.001
.005
FLAME I PREDICTED VORTICITY / RADIUS
Fig.5.4.j
$\dot{\omega}^*$
.17
.17
.5
.8
1.5
1.2
2.5
2.2
.17
.5
FLAME I PREDICTED INTENSITY OF MIXTURE FRACTION FLUCTUATIONS
Fig.5.4.k
g^*
125
.06
.13
.06
.13
.13
.20
.26
.33
.40
.46
.53
.60
.67
.73
.80
.87
.93
FLAME I PREDICTED INTENSITY OF TEMPERATURE FLUCTUATIONS
Fig.5.4.l
T'^*
.21 .40 .58 .78 1.2 1.7 2.5 3.3 4.7 z/D

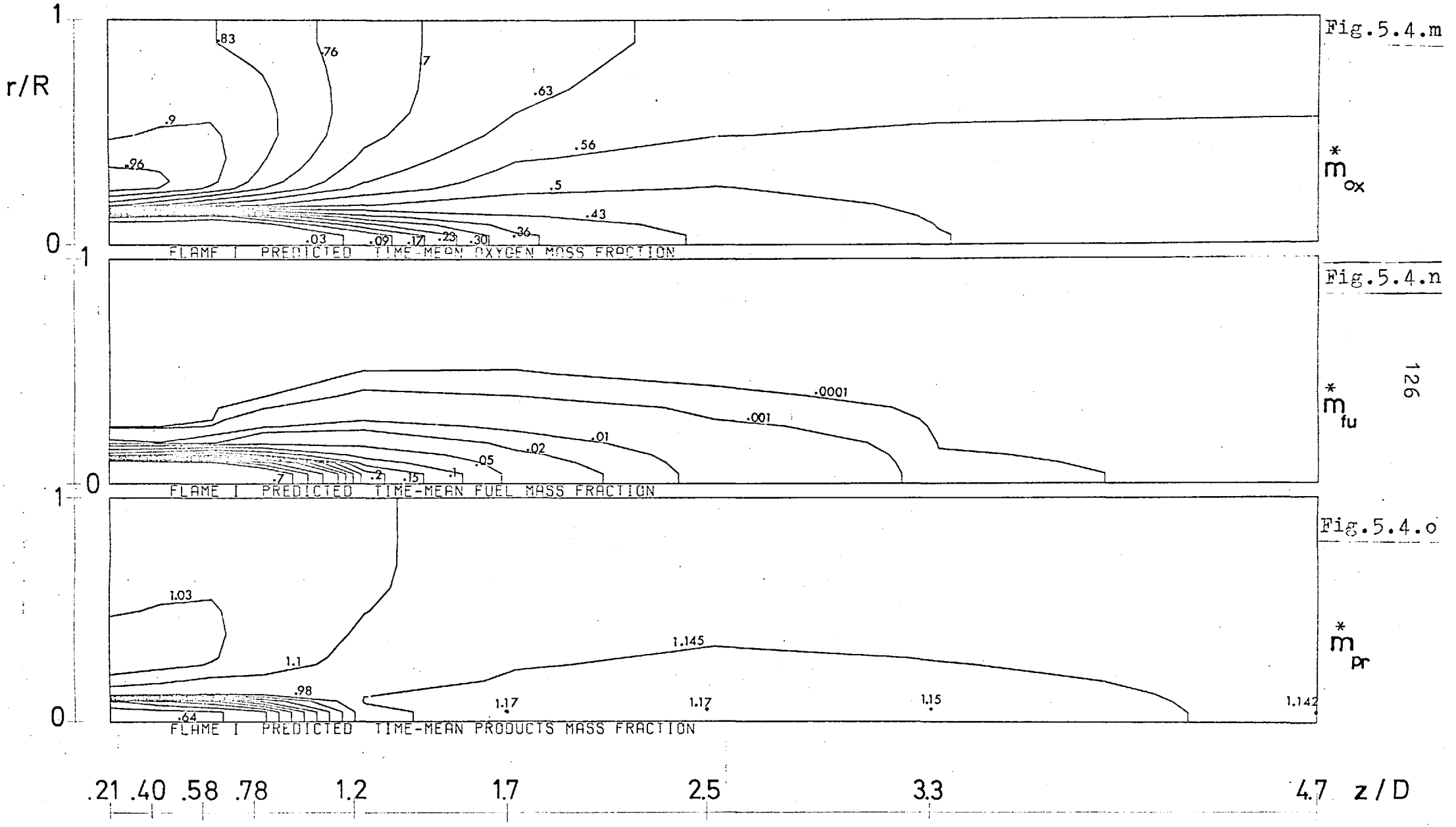

Fig.5.4.m

Fig.5.4.n

Fig.5.4.o

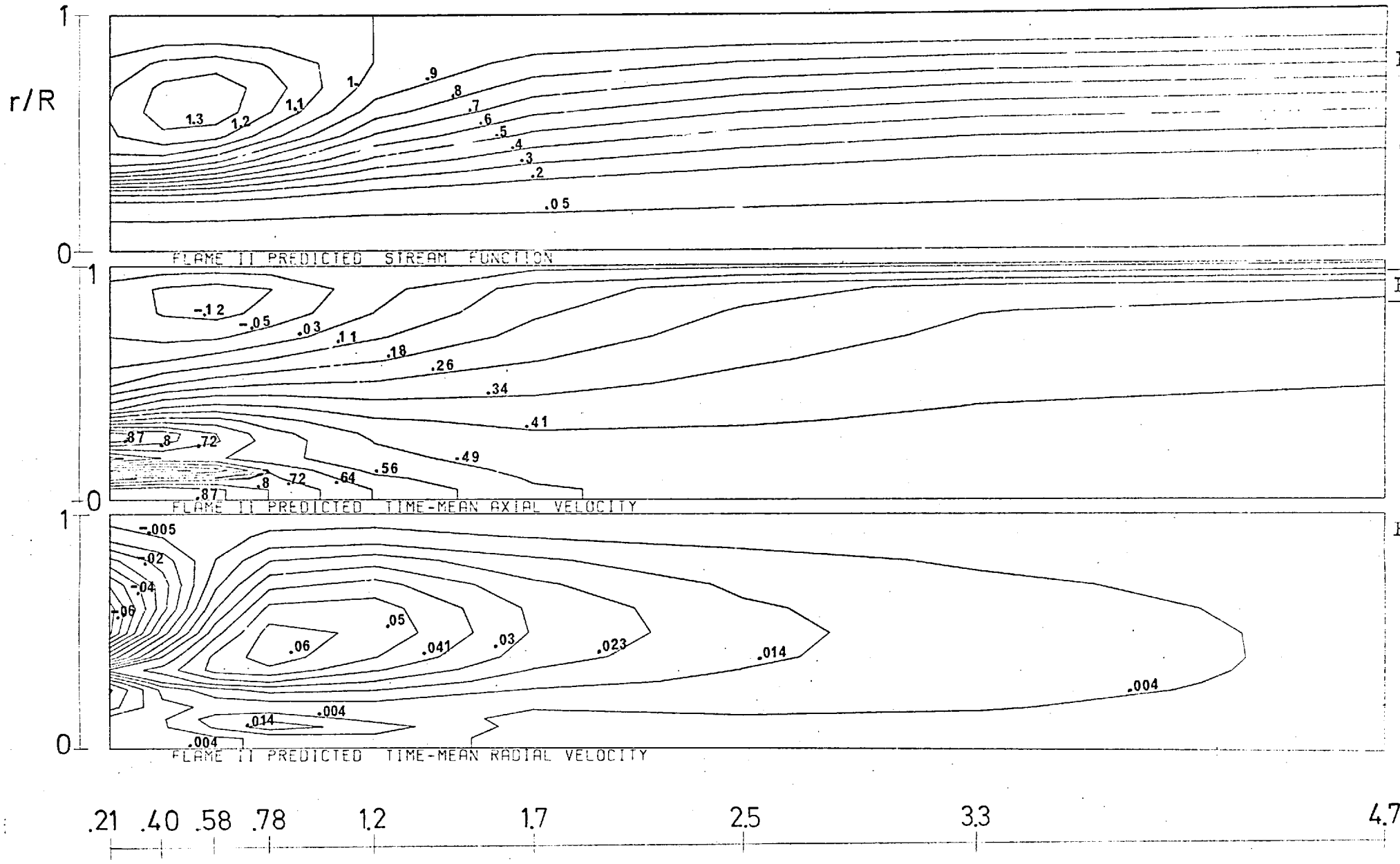

Fig.5.5.a

ψ^*

Fig.5.5.b

u^*

Fig.5.5.c

v^*

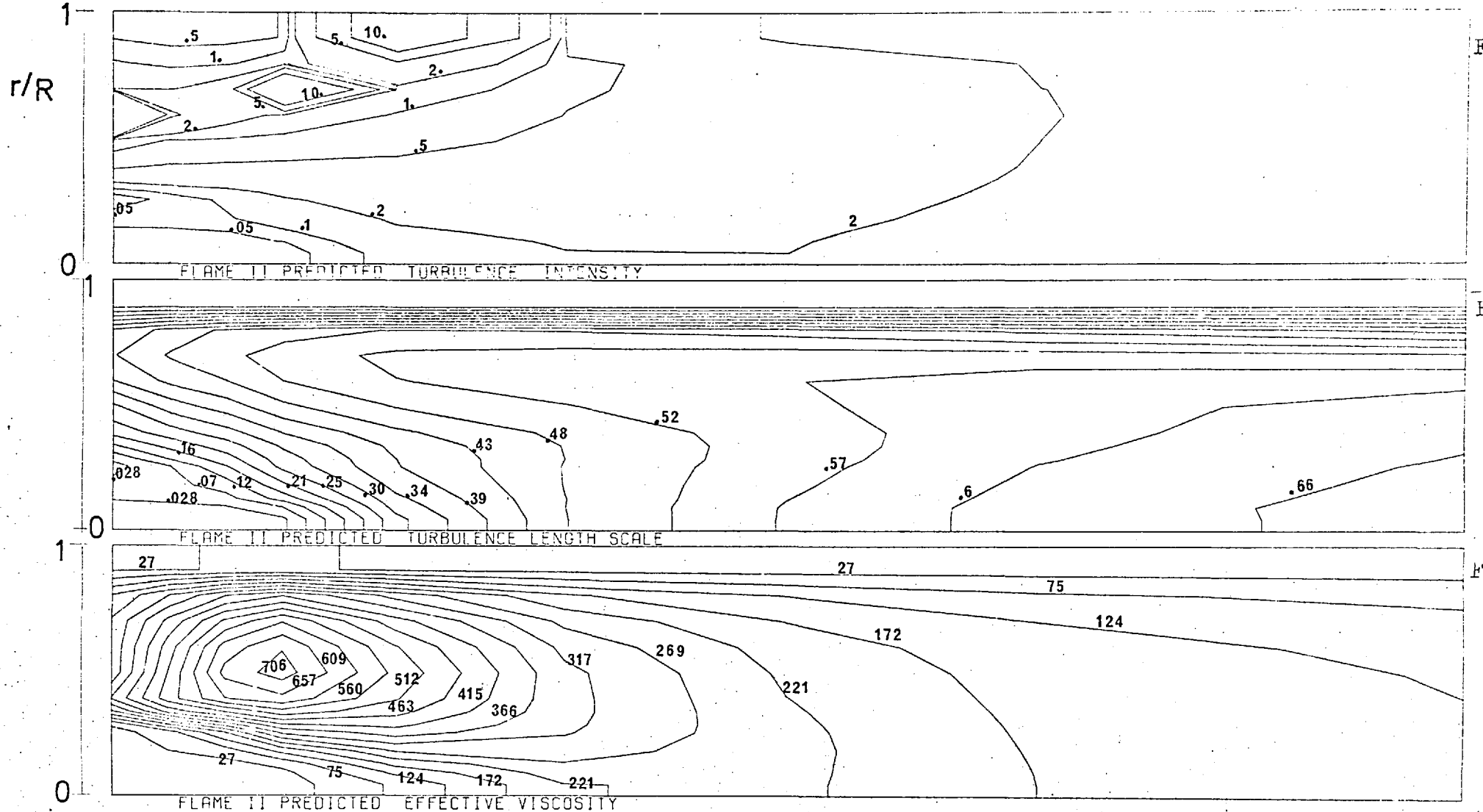

Fig.5.5.d

k^*

Fig.5.5.e

ℓ^*

Fig.5.5.f

μ^*

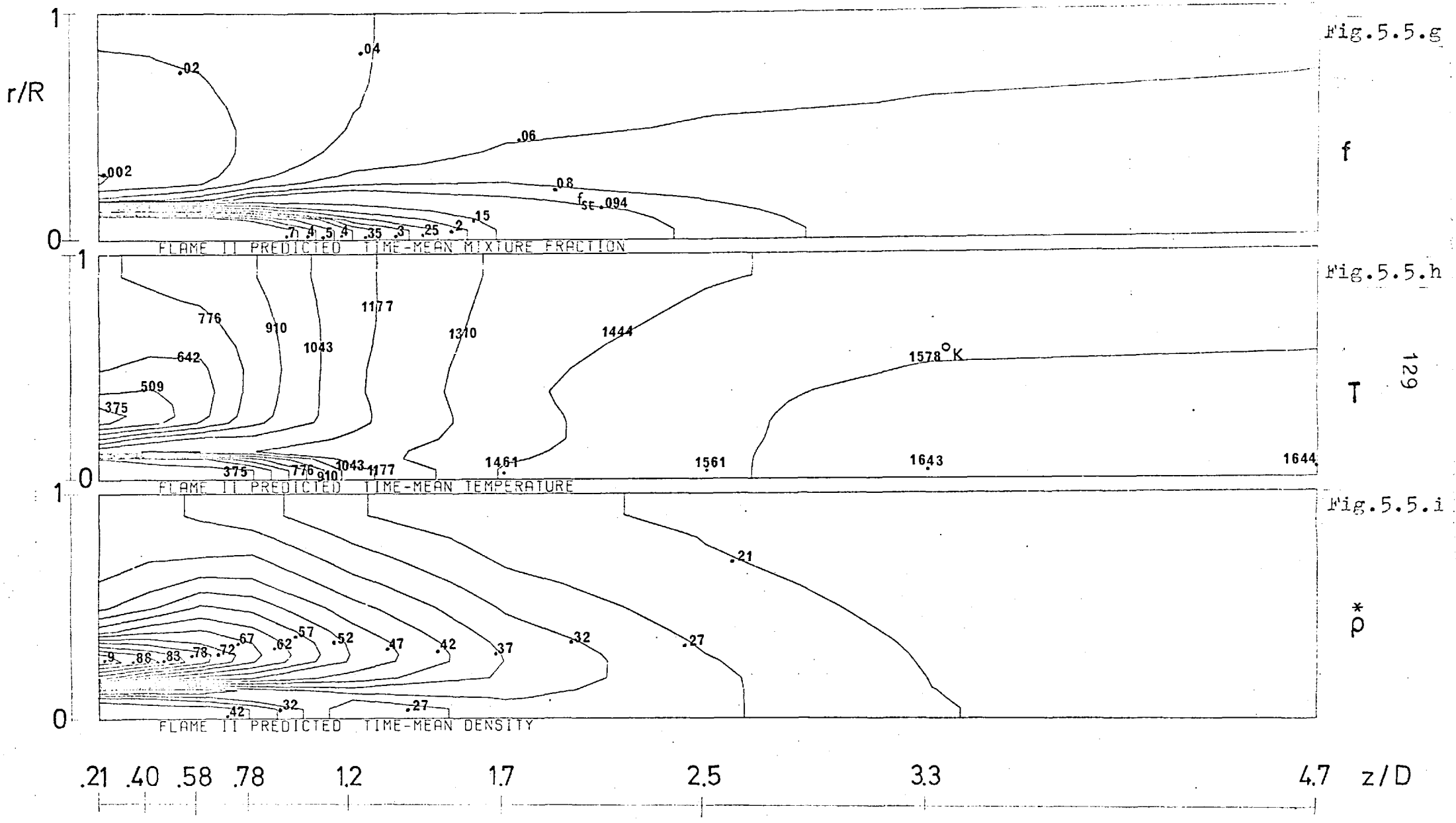

Fig.5.5.g

Fig.5.5.h

Fig.5.5.i

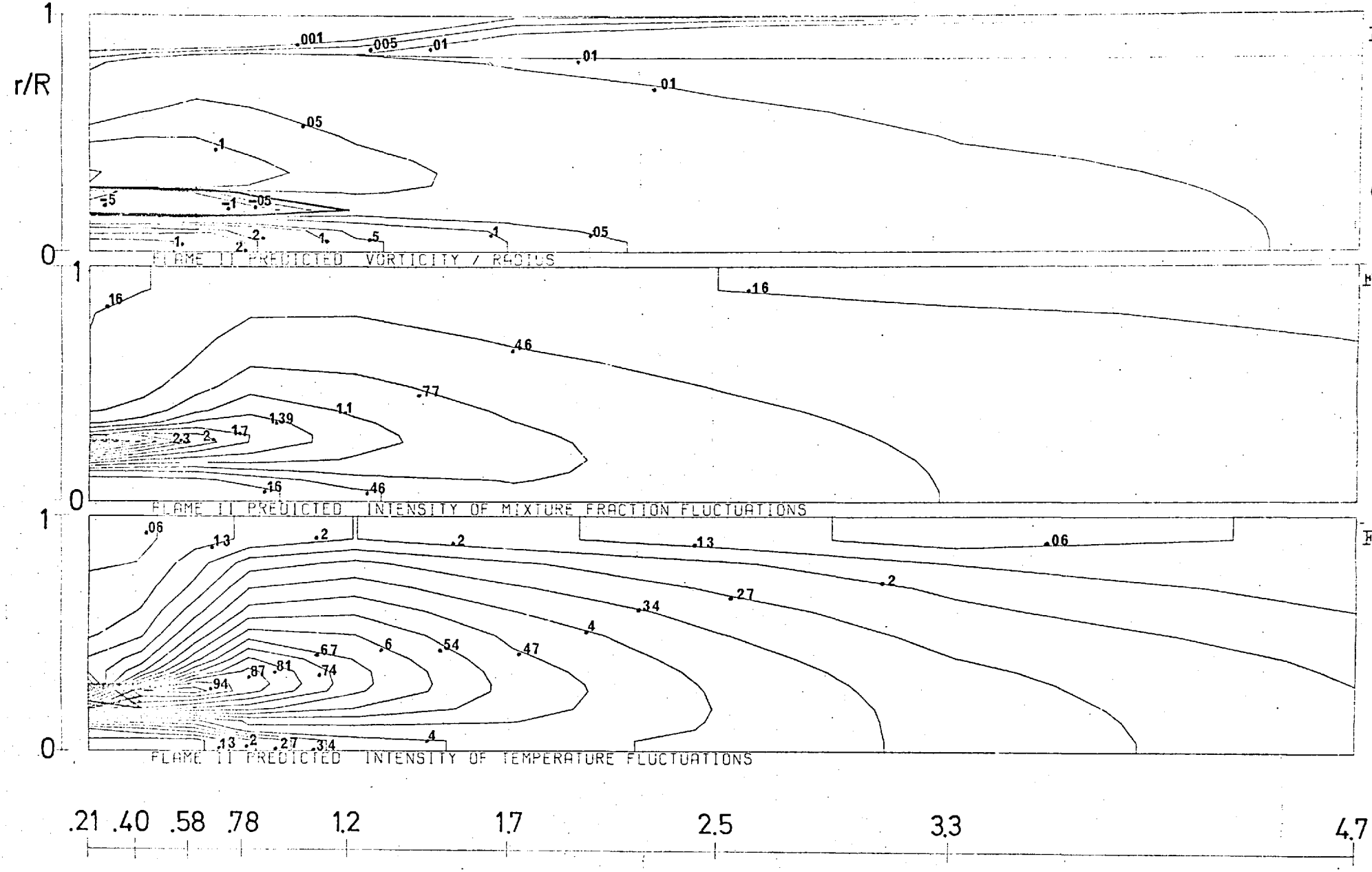
r/R
1
0
.001
.005
.01
.01
.01
.05
.1
.5
.1
.05
.1
.2
.2
.1
.5
.1
.05
FLAME II PREDICTED VORTICITY / RADIUS
ω^*
Fig.5.5.j
.16
.16
.46
.77
1.1
1.39
1.7
2
2.3
.16
.46
FLAME II PREDICTED INTENSITY OF MIXTURE FRACTION FLUCTUATIONS
g^*
Fig.5.5.k
.06
.13
.2
.2
.13
.06
.2
.27
.34
.4
.47
.54
.6
.67
.74
.81
.87
.94
.4
.13
.2
.27
.34
FLAME II PREDICTED INTENSITY OF TEMPERATURE FLUCTUATIONS
$T^{*'}$
Fig.5.5.l
.21
.40
.58
.78
1.2
1.7
2.5
3.3
4.7
z/D

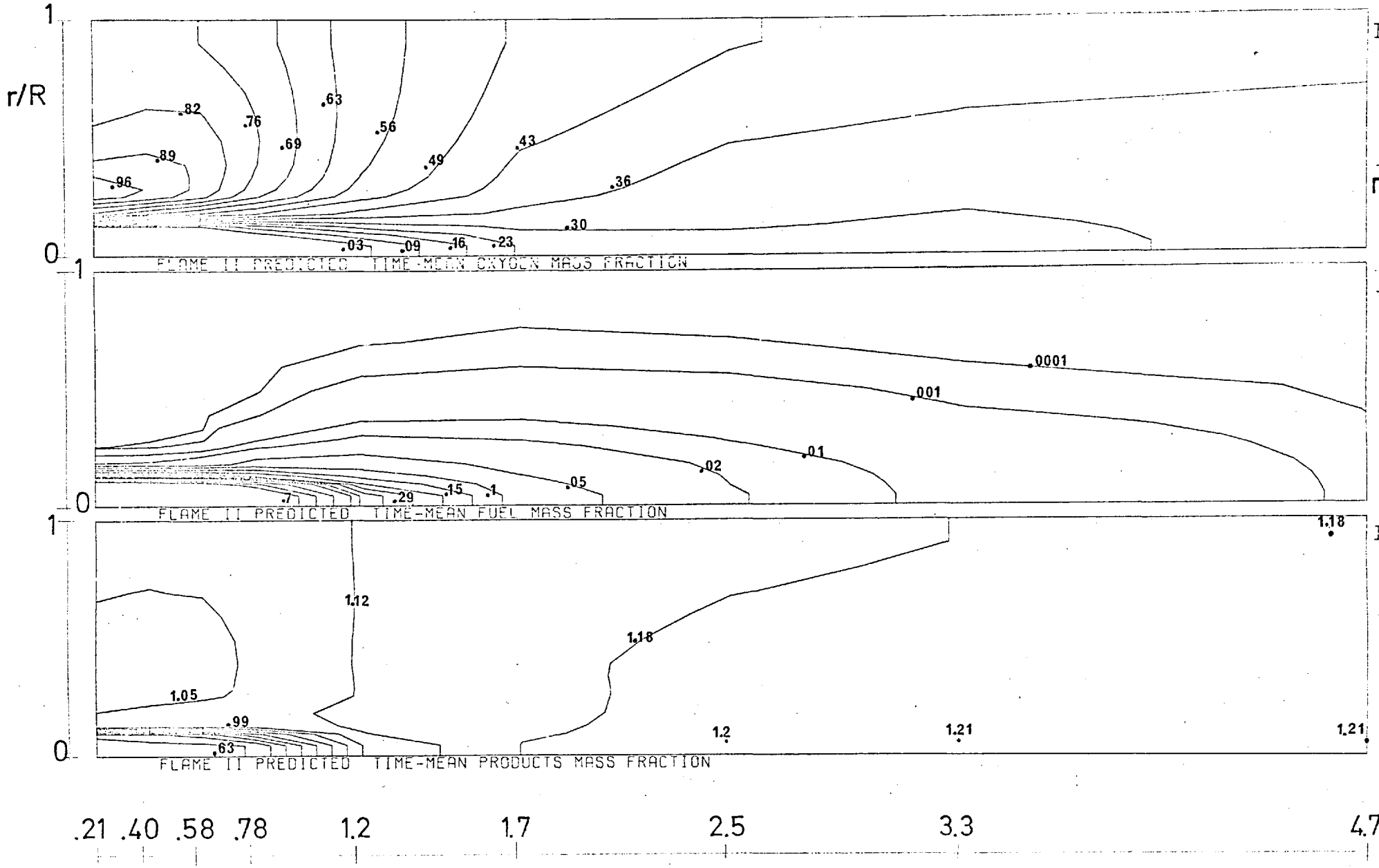

Fig.5.5.m

$\dot{m}^*_{ox}$

Fig.5.5.n

$\dot{m}^*_{fu}$

Fig.5.5.o

$\dot{m}^*_{pr}$

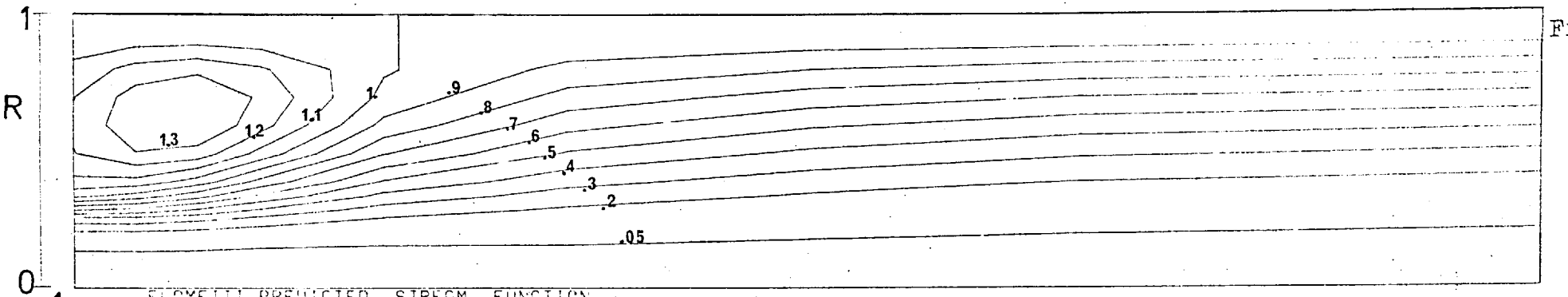

Fig.5.6.a

ψ^*

FLAME III PREDICTED STREAM FUNCTION

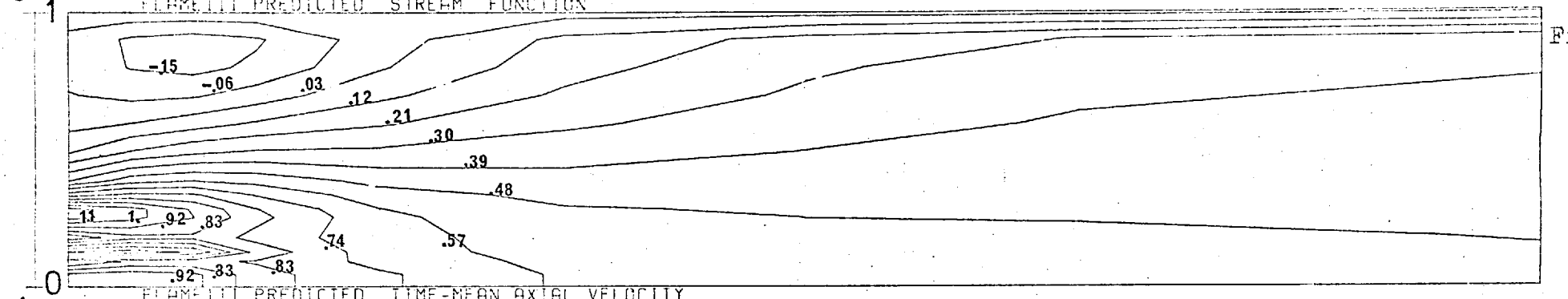

Fig.5.6.b

u^*

FLAME III PREDICTED TIME-MEAN AXIAL VELOCITY

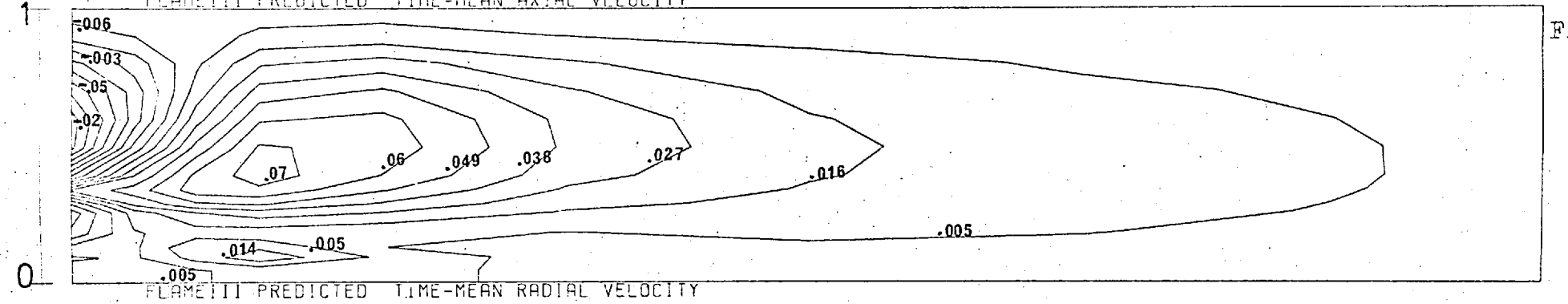

Fig. 5.6.c

v^*

FLAME III PREDICTED TIME-MEAN RADIAL VELOCITY

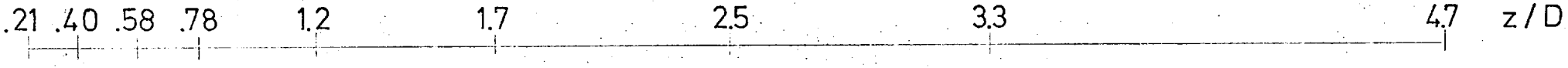

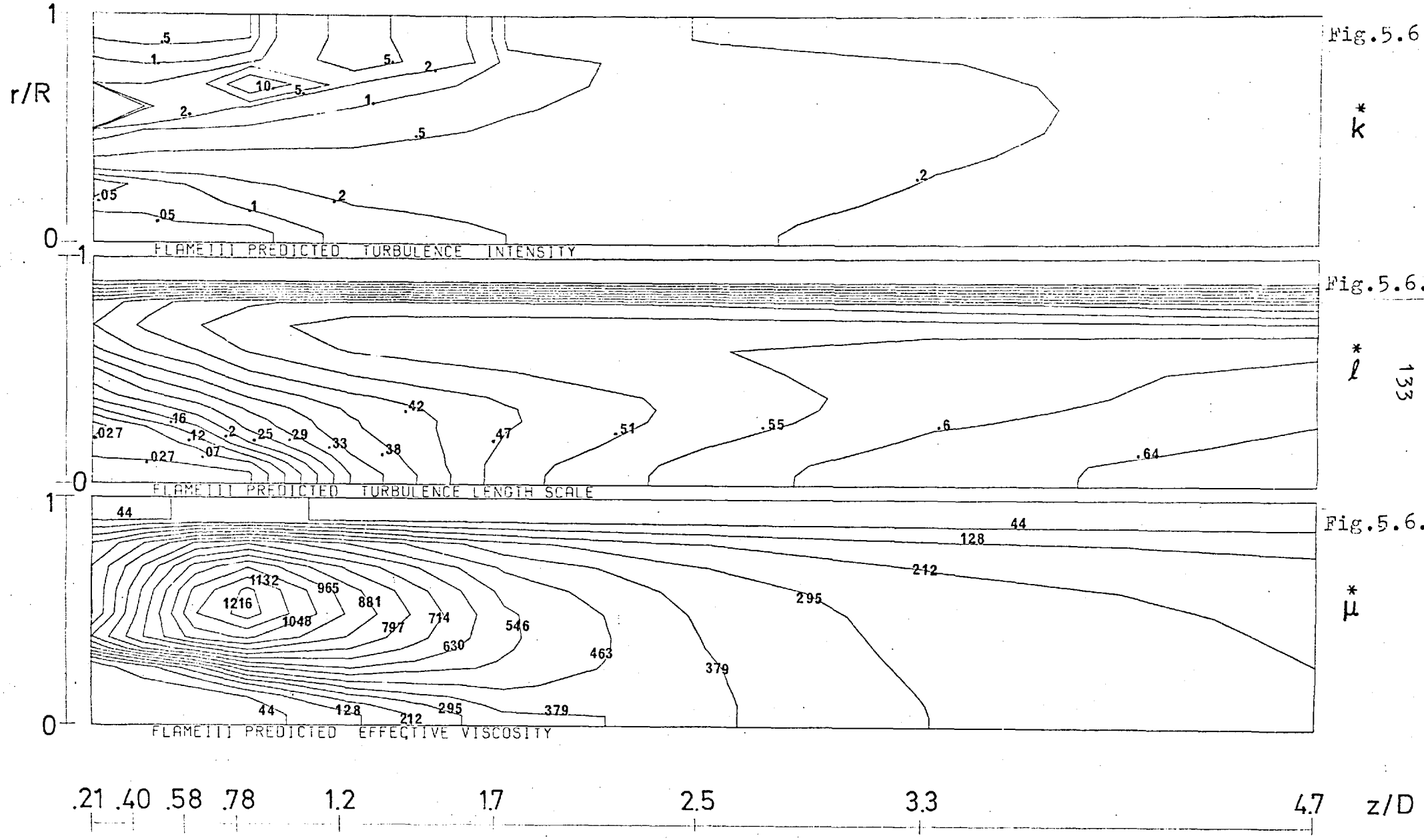
r/R
1
0
.5
1.
5.
2.
10.
5.
1.
2.
.5
.2
.05
.05
1
.2
FLAMEIII PREDICTED TURBULENCE INTENSITY
Fig.5.6.d
k*
1
0
.42
.16
.12
.2
.25
.29
.33
.38
.47
.51
.55
.6
.64
.027
.027
.07
FLAMEIII PREDICTED TURBULENCE LENGTH SCALE
Fig.5.6.e
ℓ*
1
0
44
44
128
212
295
379
463
546
630
714
797
881
965
1048
1132
1216
44
128
212
295
379
FLAMEIII PREDICTED EFFECTIVE VISCOSITY
Fig.5.6.f
μ*
.21
.40
.58
.78
1.2
1.7
2.5
3.3
4.7
z/D

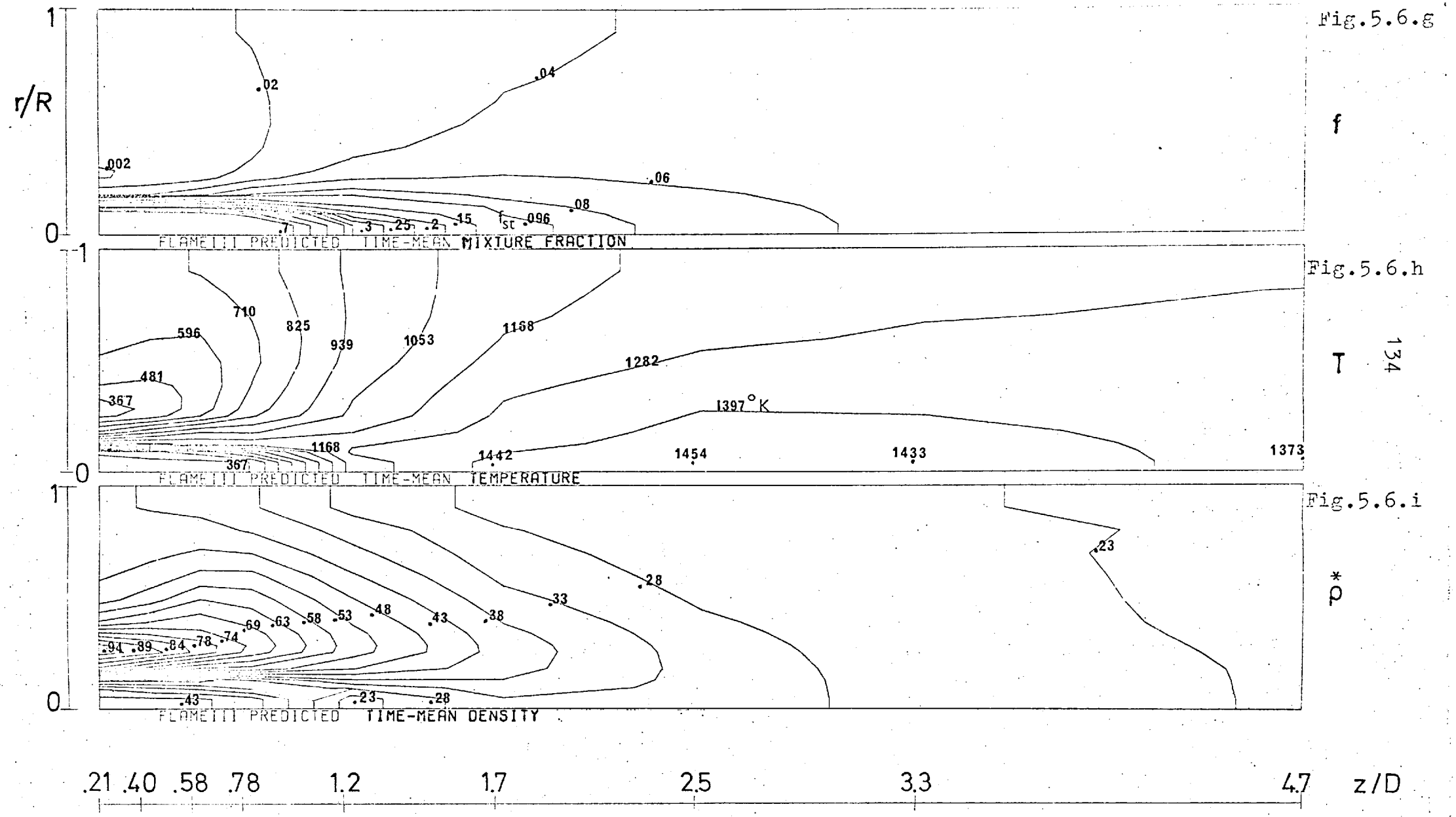
r/R
1
0
.002
.02
.04
.06
.08
.096
f_{st}
.15
.2
.25
.3
.7
FLAMEIII PREDICTED TIME-MEAN MIXTURE FRACTION
f
Fig.5.6.g
-1
0
367
481
596
710
825
939
1053
1158
1168
1282
1397°K
1442
1454
1433
1373
FLAMEIII PREDICTED TIME-MEAN TEMPERATURE
T
Fig.5.6.h
.23
.28
.33
.38
.43
.48
.53
.58
.63
.69
.74
.78
.84
.89
.94
FLAMEIII PREDICTED TIME-MEAN DENSITY
ρ^*
Fig.5.6.i
.21 .40 .58 .78 1.2 1.7 2.5 3.3 4.7 z/D

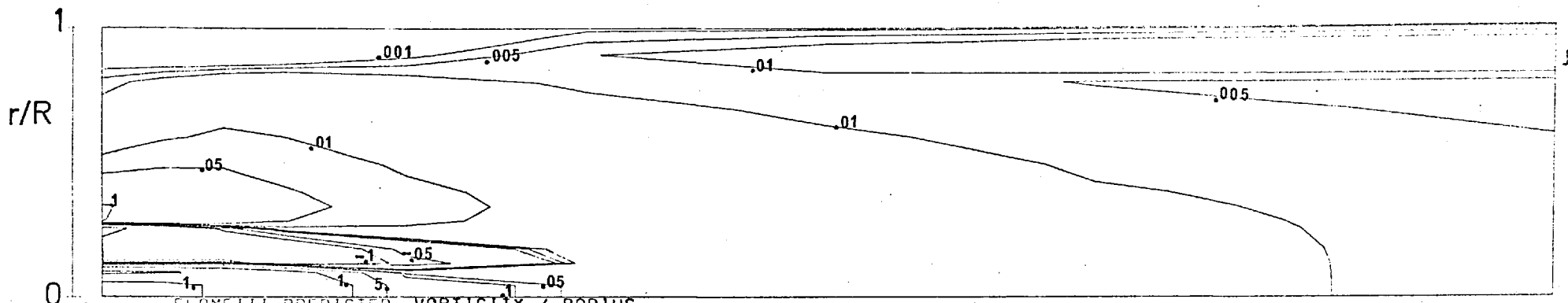

FLAME III PREDICTED VORTICITY / RADIUS

Fig.5.6.j

$\overline{\omega}^*$

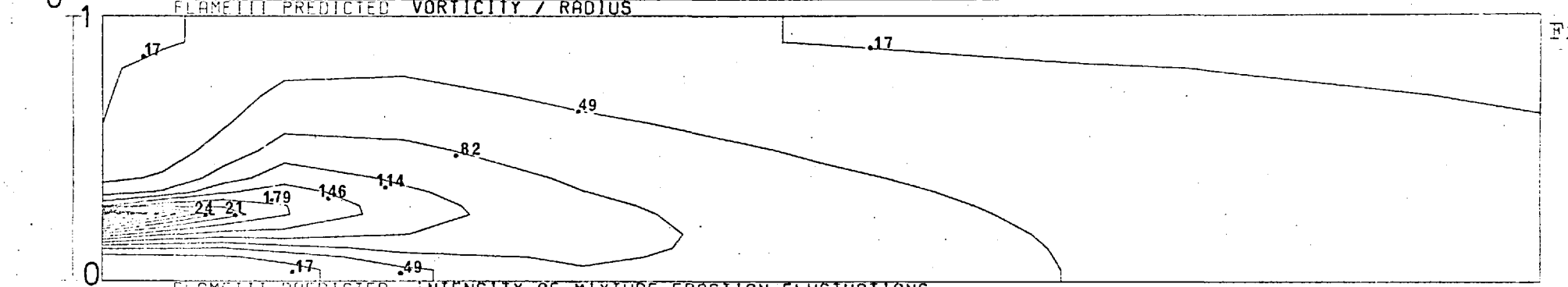

FLAME III PREDICTED INTENSITY OF MIXTURE FRACTION FLUCTUATIONS

Fig.5.6.k

g^*

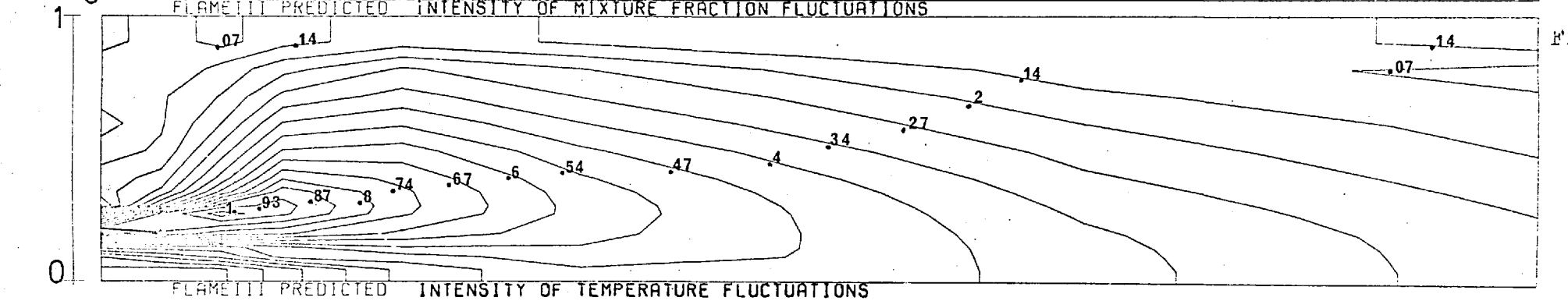

FLAME III PREDICTED INTENSITY OF TEMPERATURE FLUCTUATIONS

Fig.5.6.l

$T^{*\prime}$

.21 .40 .58 .78 1.2 1.7 2.5 3.3 4.7 z/D

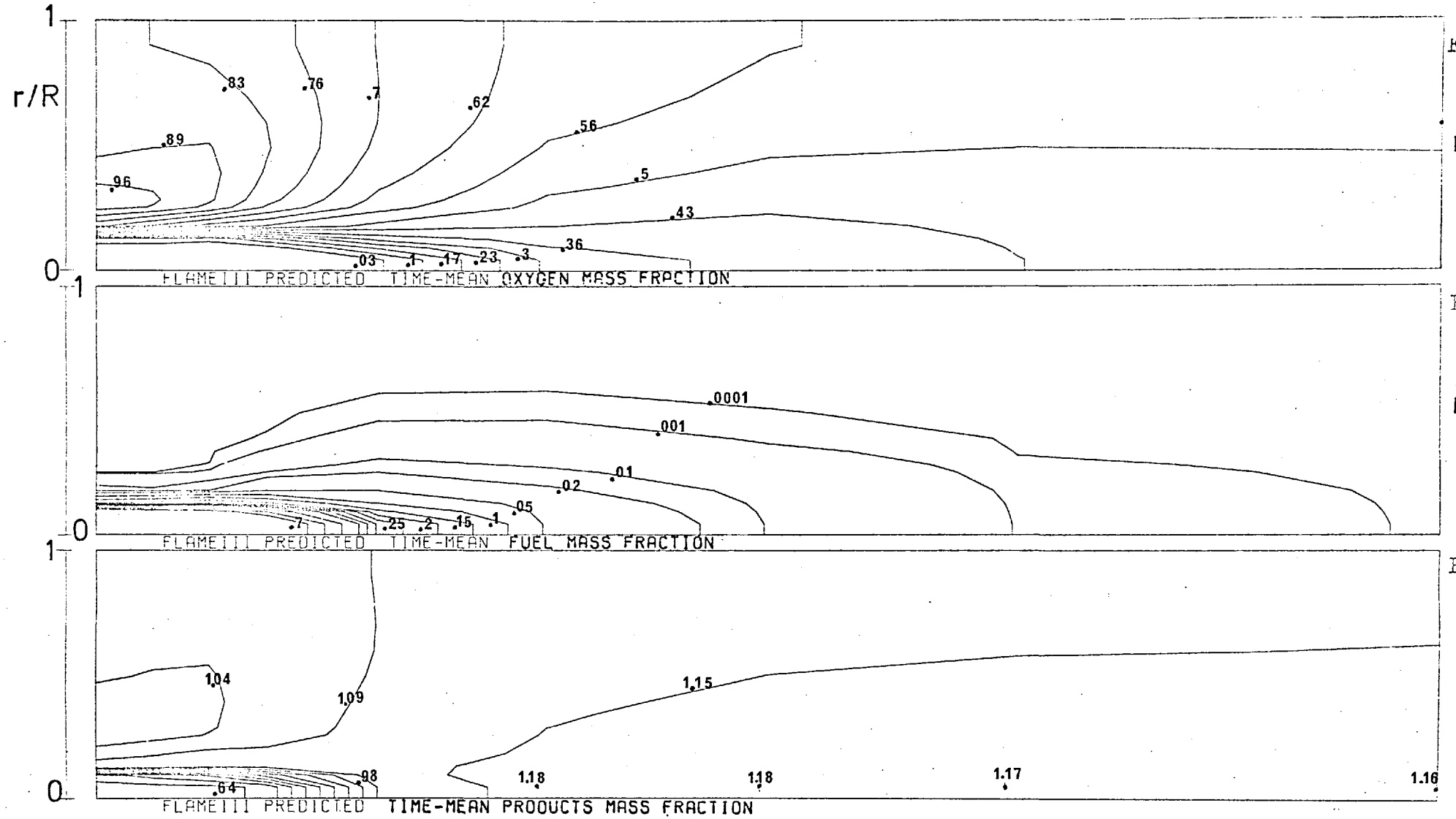

Fig.5.6.m $\dot{m}^*_{ox}$

Fig.5.6.n $\dot{m}^*_{fu}$

Fig.5.6.o $\dot{m}^*_{pr}$

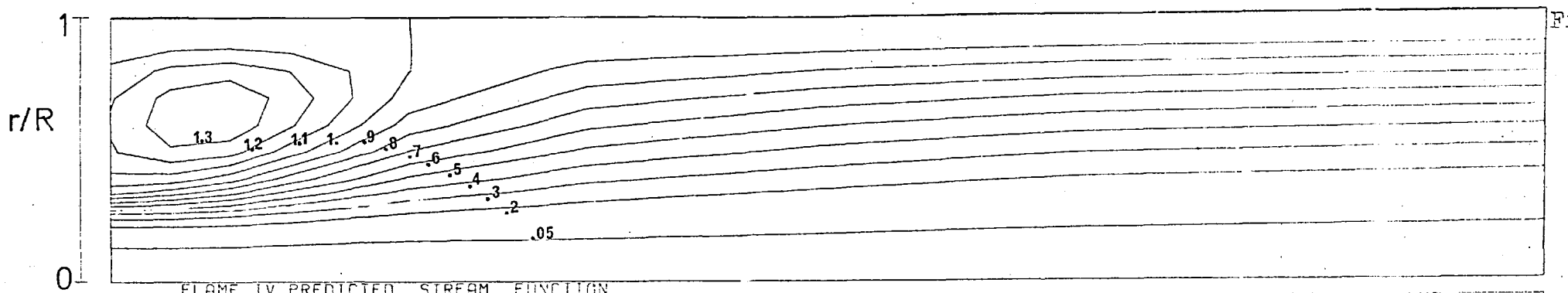

FLAME IV PREDICTED STREAM FUNCTION

Fig.5.7.a

ψ^*

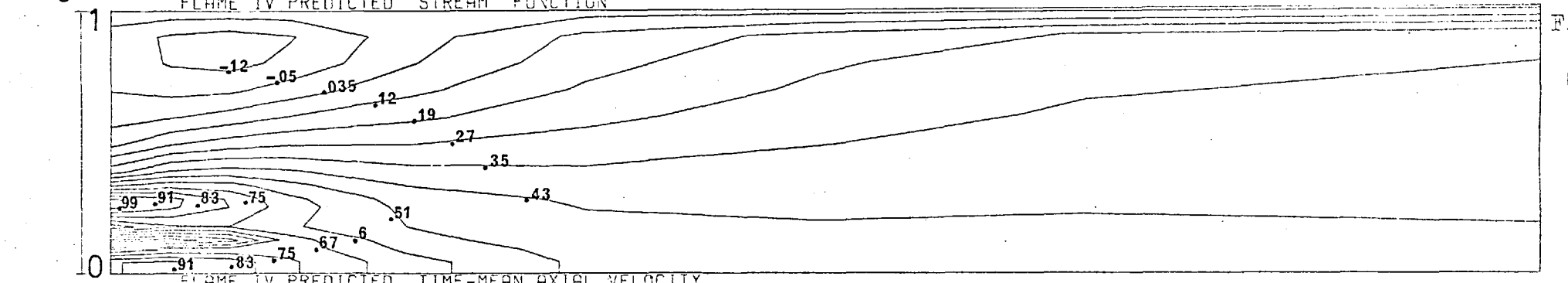

FLAME IV PREDICTED TIME-MEAN AXIAL VELOCITY

Fig.5.7.b

u^*

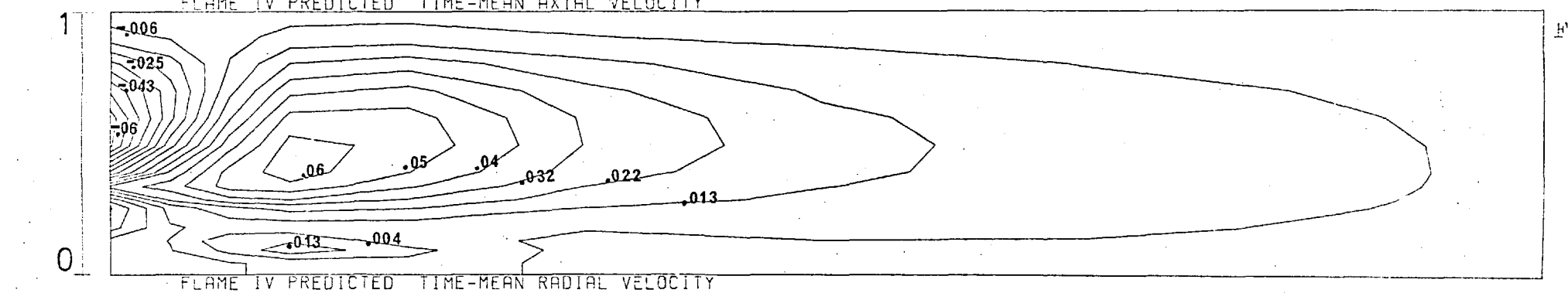

FLAME IV PREDICTED TIME-MEAN RADIAL VELOCITY

Fig.5.7.c

v^*

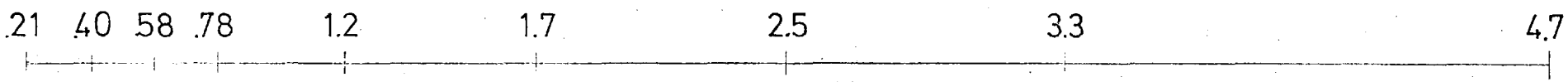

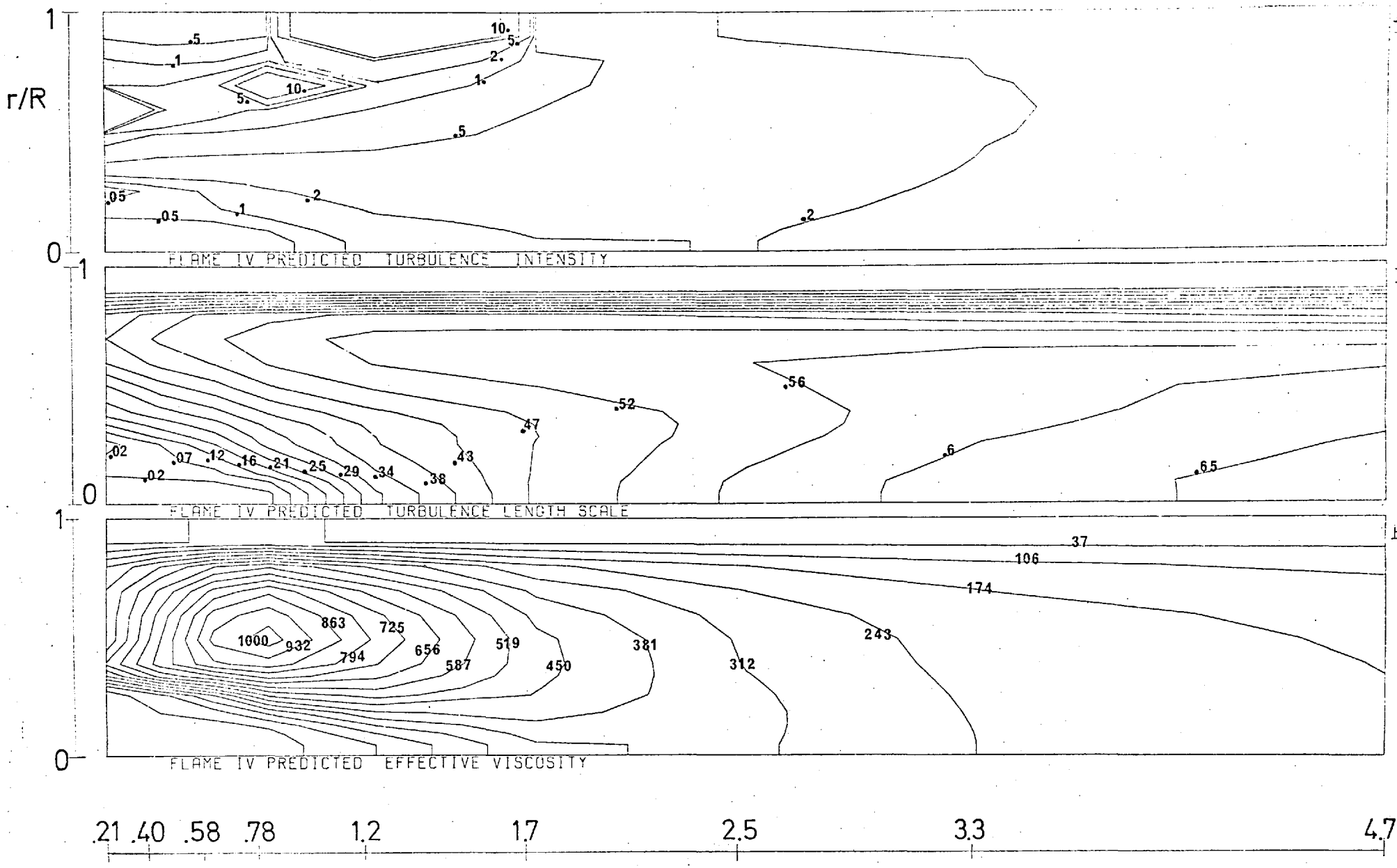

Fig.5.7.d

k^*

Fig.5.7.e

ℓ^*

Fig.5.7.f

μ^*

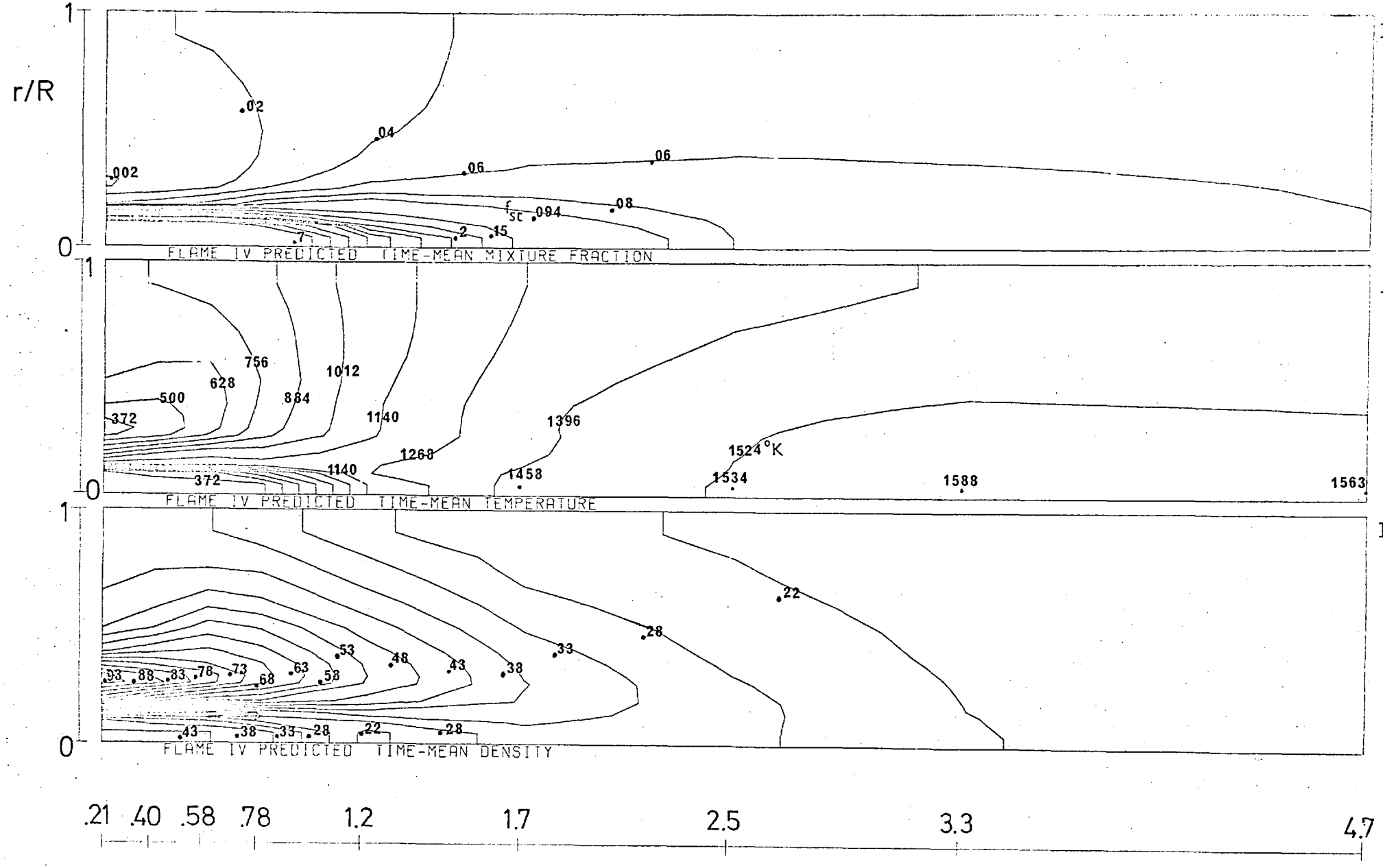
r/R
1
0
.02
.04
.06
.06
.002
.08
f_{st} .094
.7
.2
.15
FLAME IV PREDICTED TIME-MEAN MIXTURE FRACTION
Fig.5.7.g
f
1
0
756
628
1012
500
884
372
1140
1396
1268
1524°K
1140
1458
1534
1588
1563
372
FLAME IV PREDICTED TIME-MEAN TEMPERATURE
Fig.5.7.h
T
1
0
.22
.28
.53
.48
.43
.38
.33
.93
.88
.83
.78
.73
.68
.63
.58
.43
.38
.33
.28
.22
.28
FLAME IV PREDICTED TIME-MEAN DENSITY
Fig.5.7.i
ρ^*
.21
.40
.58
.78
1.2
1.7
2.5
3.3
4.7
z/D

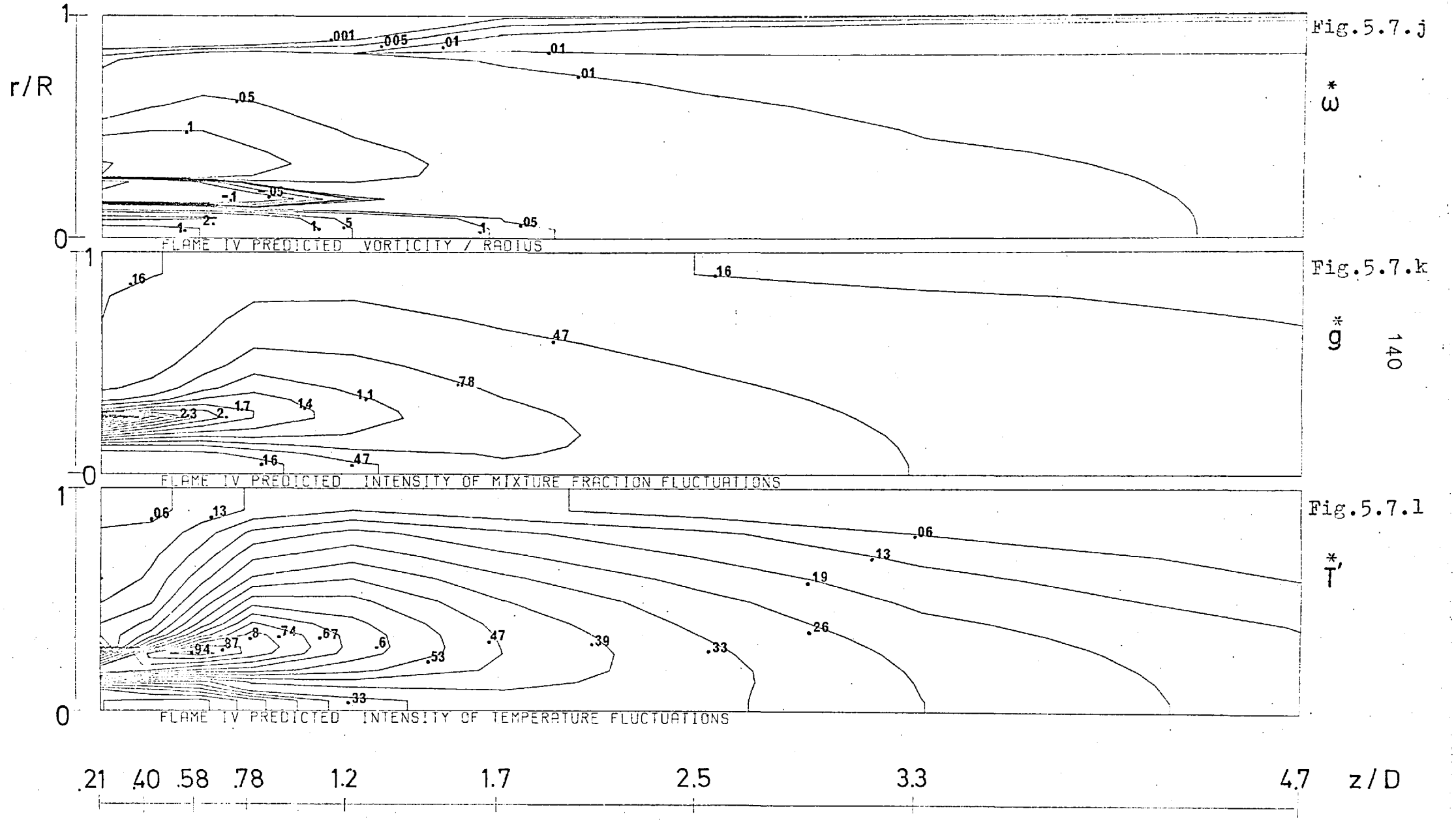

Fig.5.7.j

ω^*

Fig.5.7.k

g^*

Fig.5.7.l

$T^{*\prime}$

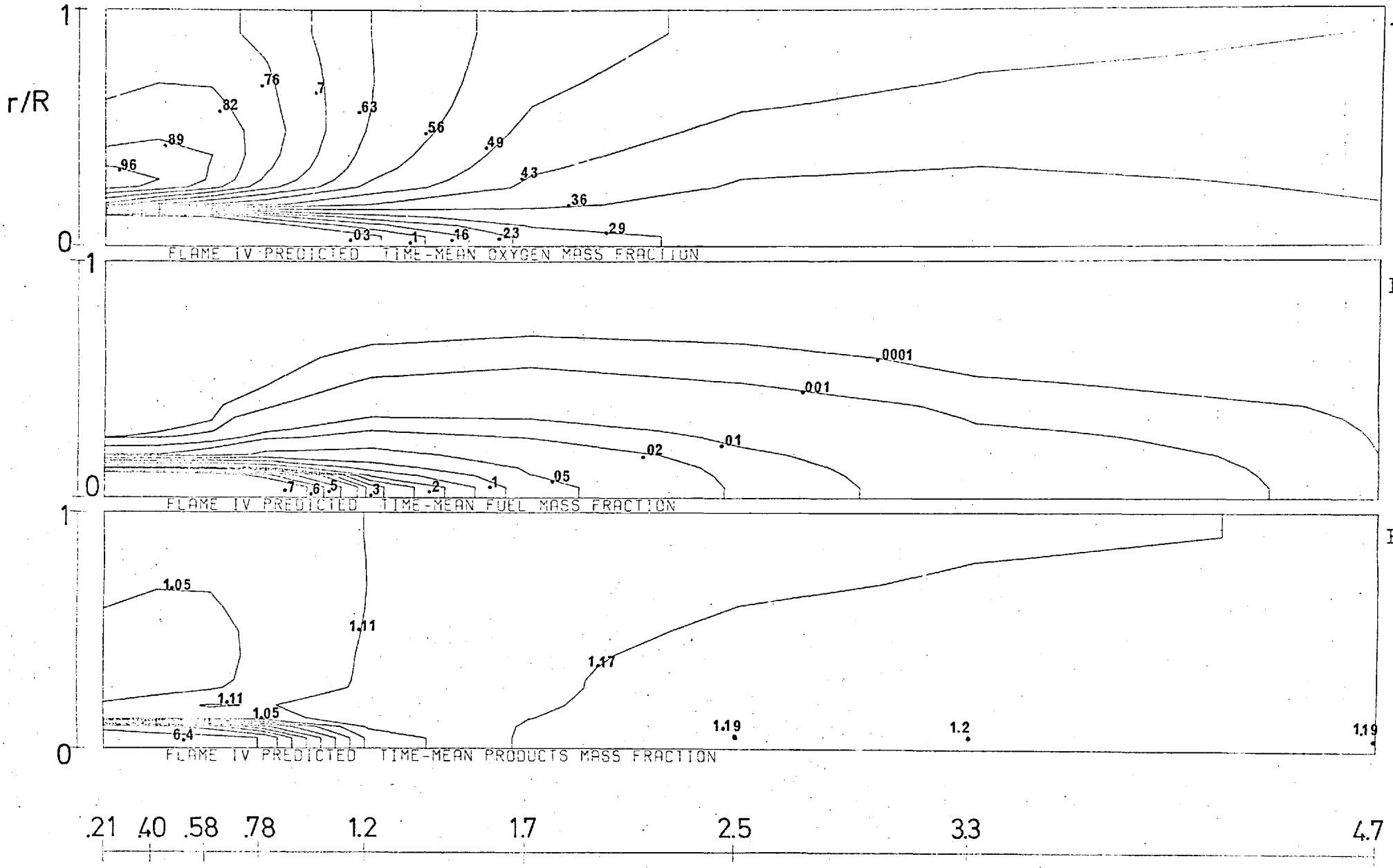

Fig.5.7.m

$\dot{m}^*_{ox}$

Fig.5.7.n

$\dot{m}^*_{fu}$

Fig.5.7.o

$\dot{m}^*_{pr}$

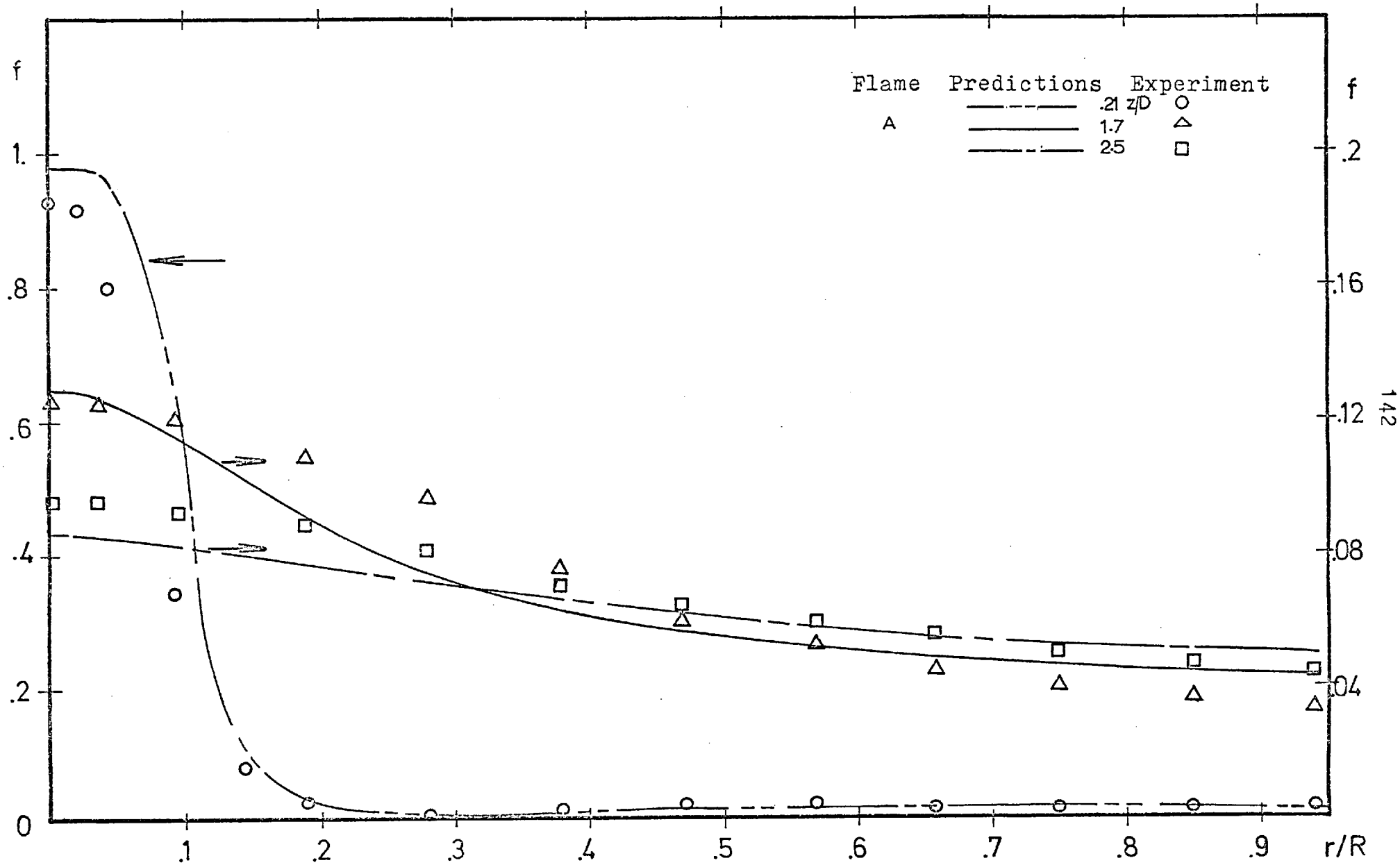
f
1.
.8
.6
.4
.2
0
.1
.2
.3
.4
.5
.6
.7
.8
.9
r/R
Flame Predictions Experiment
A
.21 z/D
1.7
2.5
f
.2
.16
.12
.08
.04

Fig.5.8.a

Time-mean density

It can be seen from figs. 5.4.i, 5.5.i, 5.6.i, 5.7.i that the density of the combustion products at the exhaust end of the furnace is less than the initial fuel-density by a factor of about 2 and less than the initial air-density by a factor of about 4.5. It is also noticed that the density distribution along the axis has a small peak at about 1.5D from the burner, this is due to the introduction by turbulent mixing of air vortices to the jet axis as explained earlier.

Time-mean mass fractions of oxygen, fuel and products

From figs. (5.4.m,n, 5.5.m,n, 5.6.m,n, 5.7.m,n) we see the expected overlapping near the axis of fuel and oxygen concentrations; this is supported by the currently available experimental data (for example Vranos et al 1969). The mass fraction of the products (figs. 5.4.o, 5.5.o, 5.6.o, 5.7.o) exhibits a peak far downstream from the burner near the axis where the time-mean temperature is also the highest.

5.4.2 Probability of chemical reaction P

The distributions of both the measured and the predicted P are displayed in figs. 5.8.b to 5.8.j. In these figures the symbols represent the experimental data and lines denote the computations.

(i) Measurements

Figures 5.8.b to 5.8.h show that the measured probability of reaction varies from less than 0.001 to about 0.45. Generally, P decreases with

distance from the burner and attains a maximum, in all four flames, at about the same axial location, z/D = .4, and at radial locations of 0.14R for flame I (the leanest of all flames) and of .18R for the otner three flames.

If we take the reaction zone as being the zone with values of P higher than say, .001, we see that close to the burner the measured radial width of this zone is about 0.2R. This zone is formed by two cylindrical envelopes at some distance from the axis. As we move downstream from the burner, this radial thickness increases, the inner envelope falls towards and eventually cuts the axis, while the outer envelope pushes outwards, reaching a maximum radial distance before falling back towards the axis and reducing the reaction-zone width. This variation agrees qualitatively with that deduced from the reaction-rate profiles measured by Vranos et al (1969) and describes the "flame brush" associated with turbulent diffusion flames.

It is interesting to note that the reaction zone begins to spread significantly in the radial direction, as expected, only after the end of the recirculating zone of hot products at z/D = 1.2 (fig. 5.8.e).

In order to study the effects on P of Reynolds number and of the inlet air/fuel ratio, the variations of P along the axis for flames I, II and IV are plotted in figs. 5.8.i and j.

Flame II has a Reynolds number of 15200 and flame IV's Reynolds number is 40% higher (21200). The inlet air/fuel ratios for the two flames (15.4 and 16.9 respectively) differ by only 5%. Figure 5.8.i

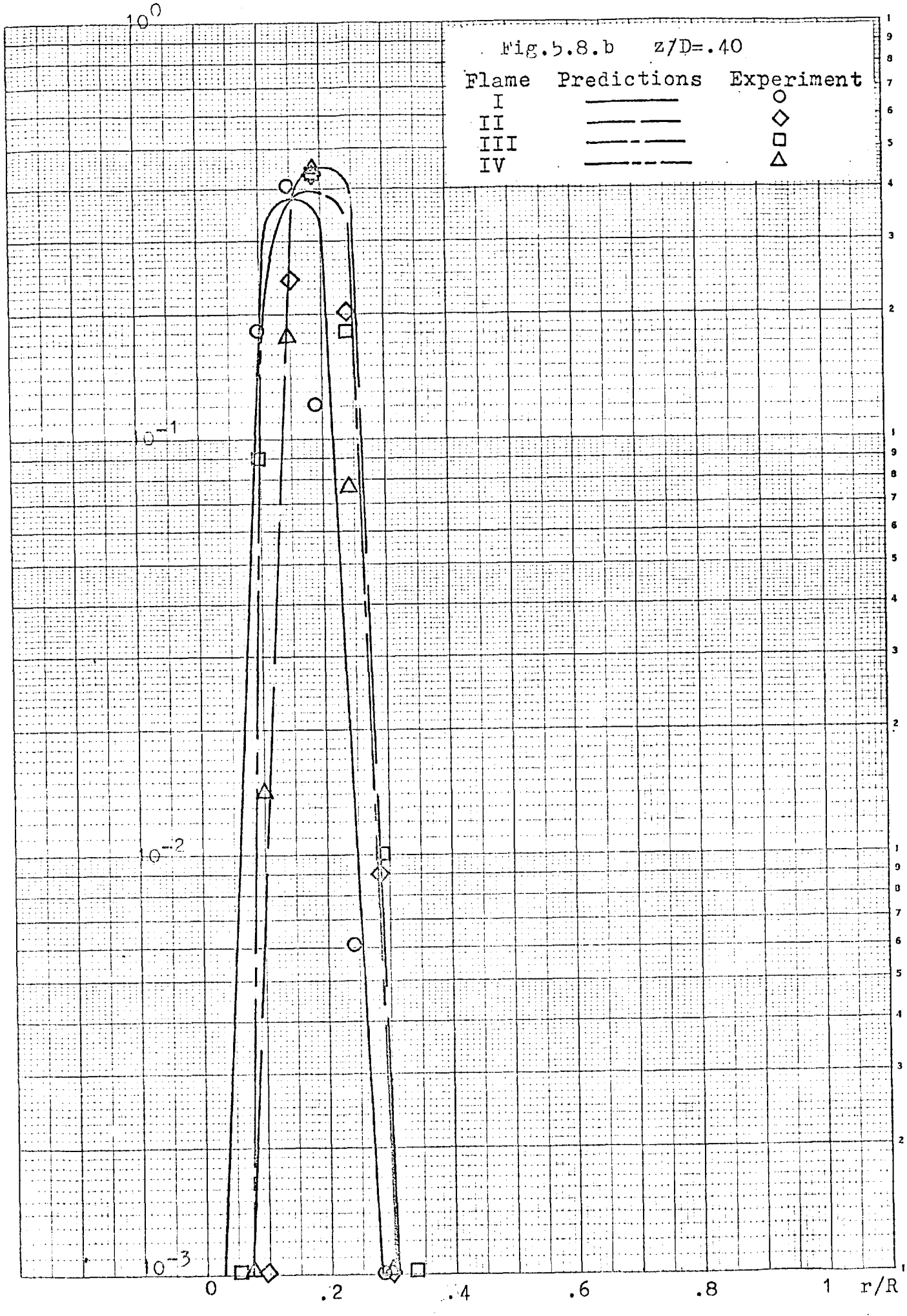
P
10^0
10^{-1}
10^{-2}
10^{-3}
Fig.5.8.b z/D=.40
Flame Predictions Experiment
I
II
III
IV
0
.2
.4
.6
.8
1
r/R

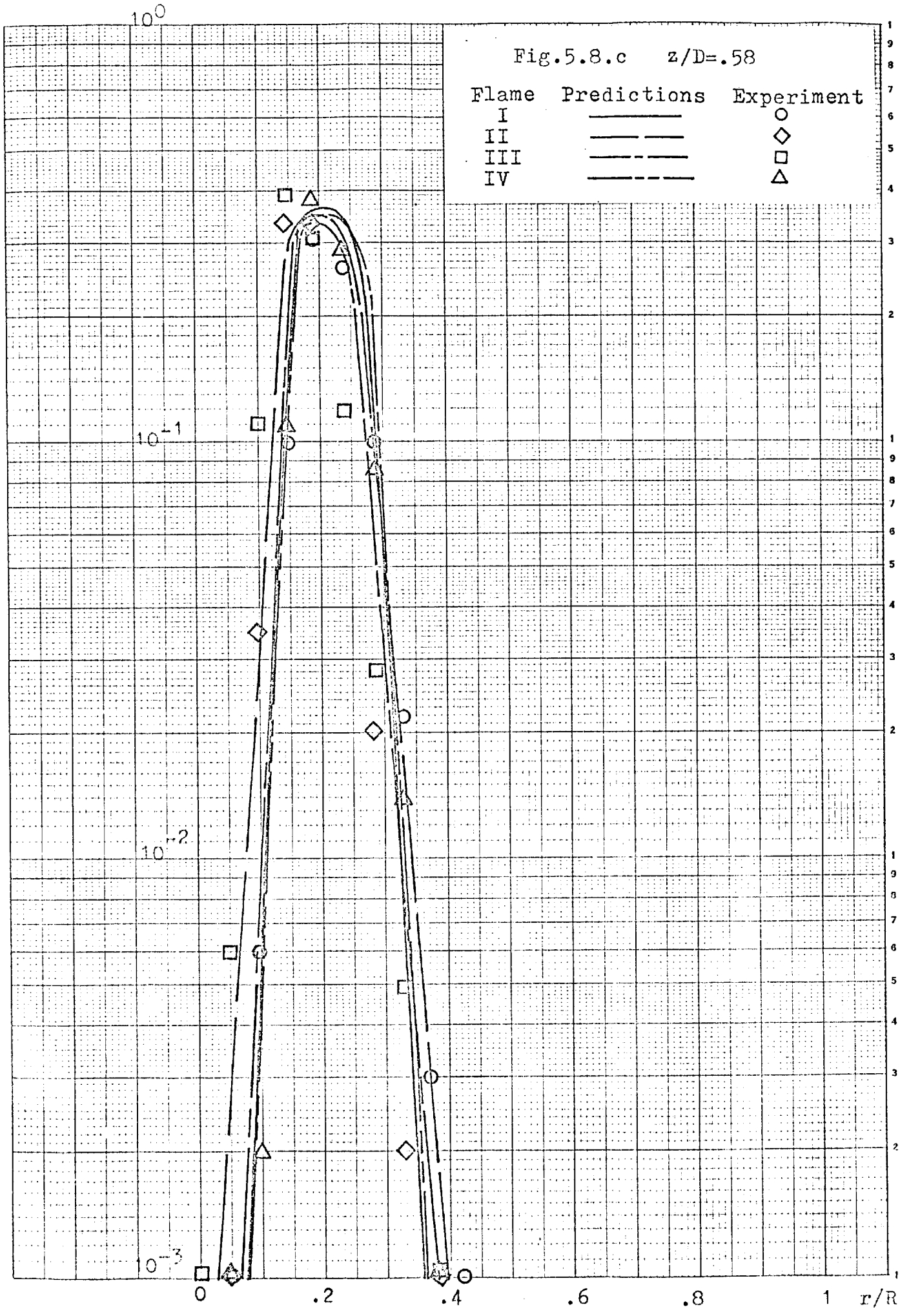
P
10^{0}
10^{-1}
10^{-2}
10^{-3}
Fig.5.8.c z/D=.58
Flame Predictions Experiment
I
II
III
IV
0
.2
.4
.6
.8
1
r/R

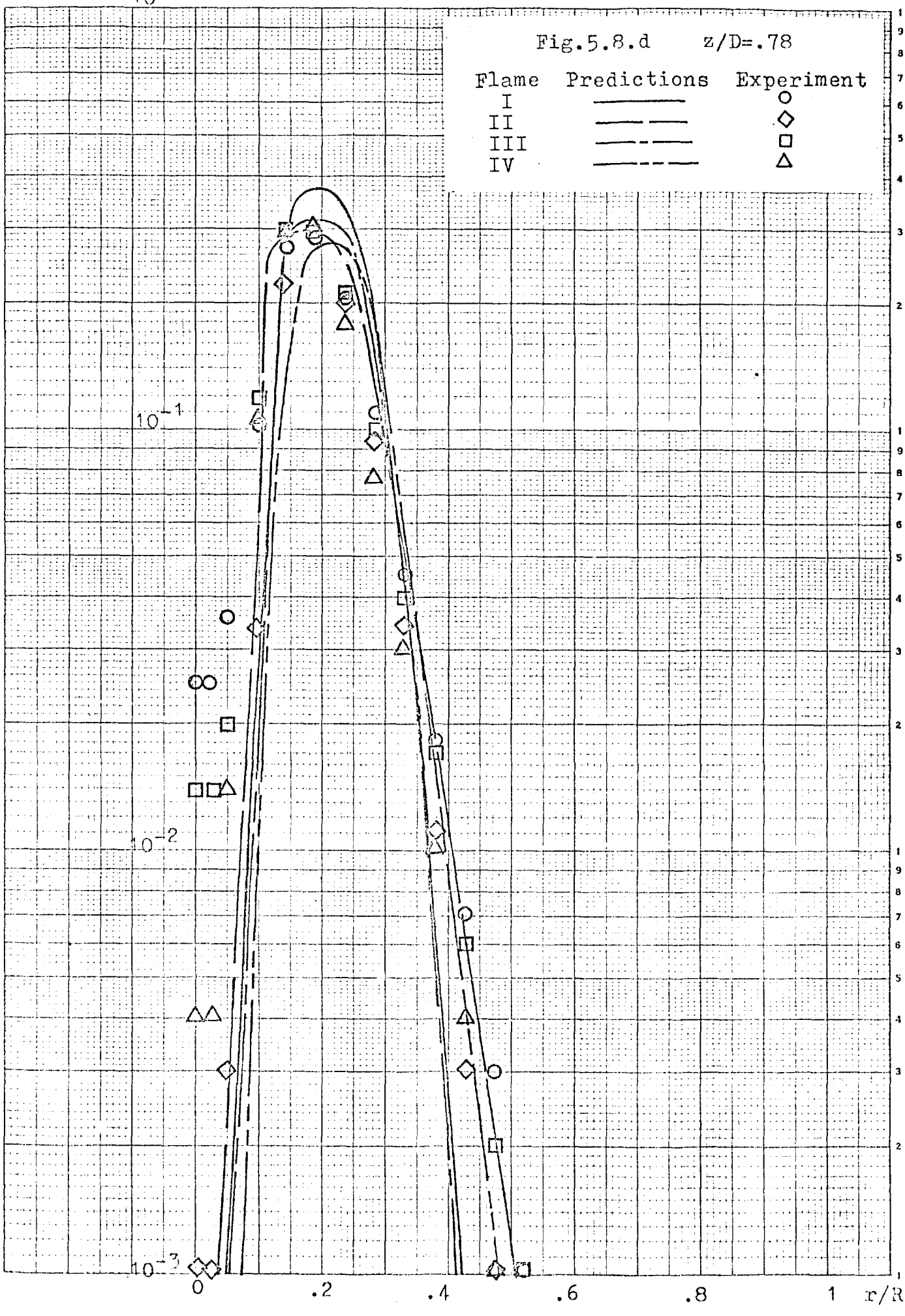
P
10^0
10^{-1}
10^{-2}
10^{-3}
Fig.5.8.d z/D=.78
Flame Predictions Experiment
I
II
III
IV
0
.2
.4
.6
.8
1
r/R

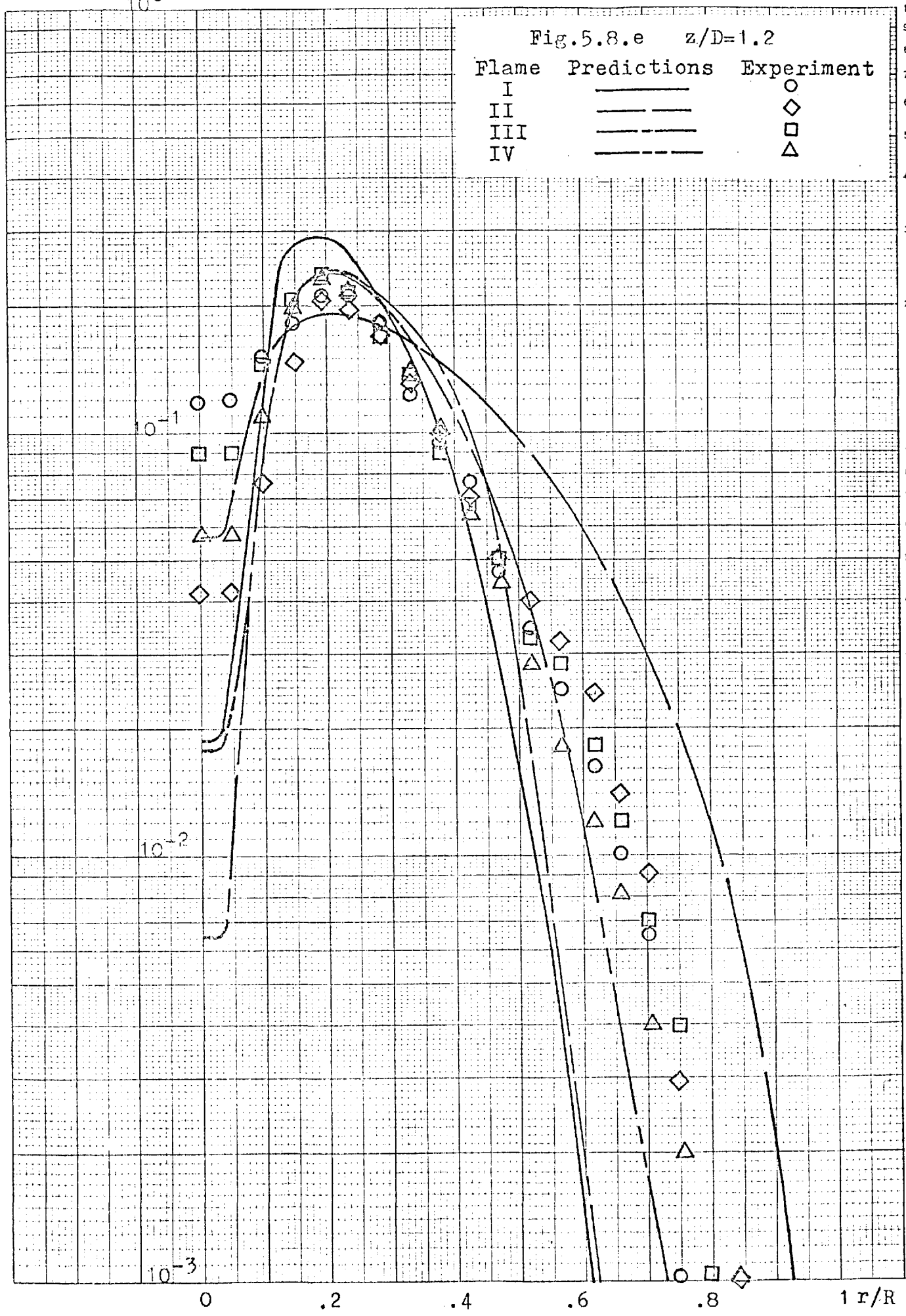
P
10^0
10^{-1}
10^{-2}
10^{-3}
Fig.5.8.e z/D=1.2
Flame Predictions Experiment
I
II
III
IV
0
.2
.4
.6
.8
1 r/R

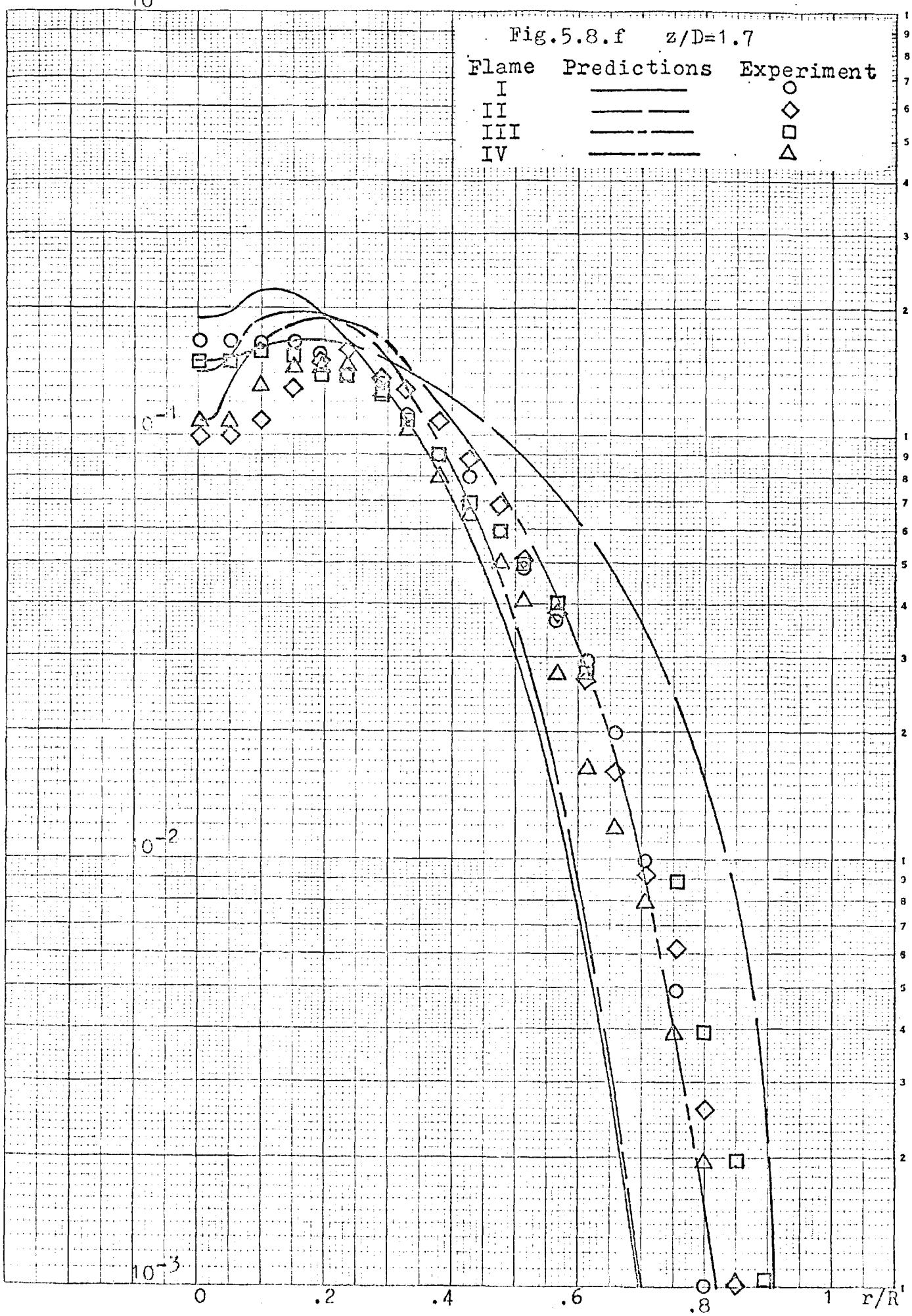
P
10^0
10^{-1}
10^{-2}
10^{-3}
Fig.5.8.f z/D=1.7
Flame Predictions Experiment
I
II
III
IV
0
.2
.4
.6
.8
1
r/R

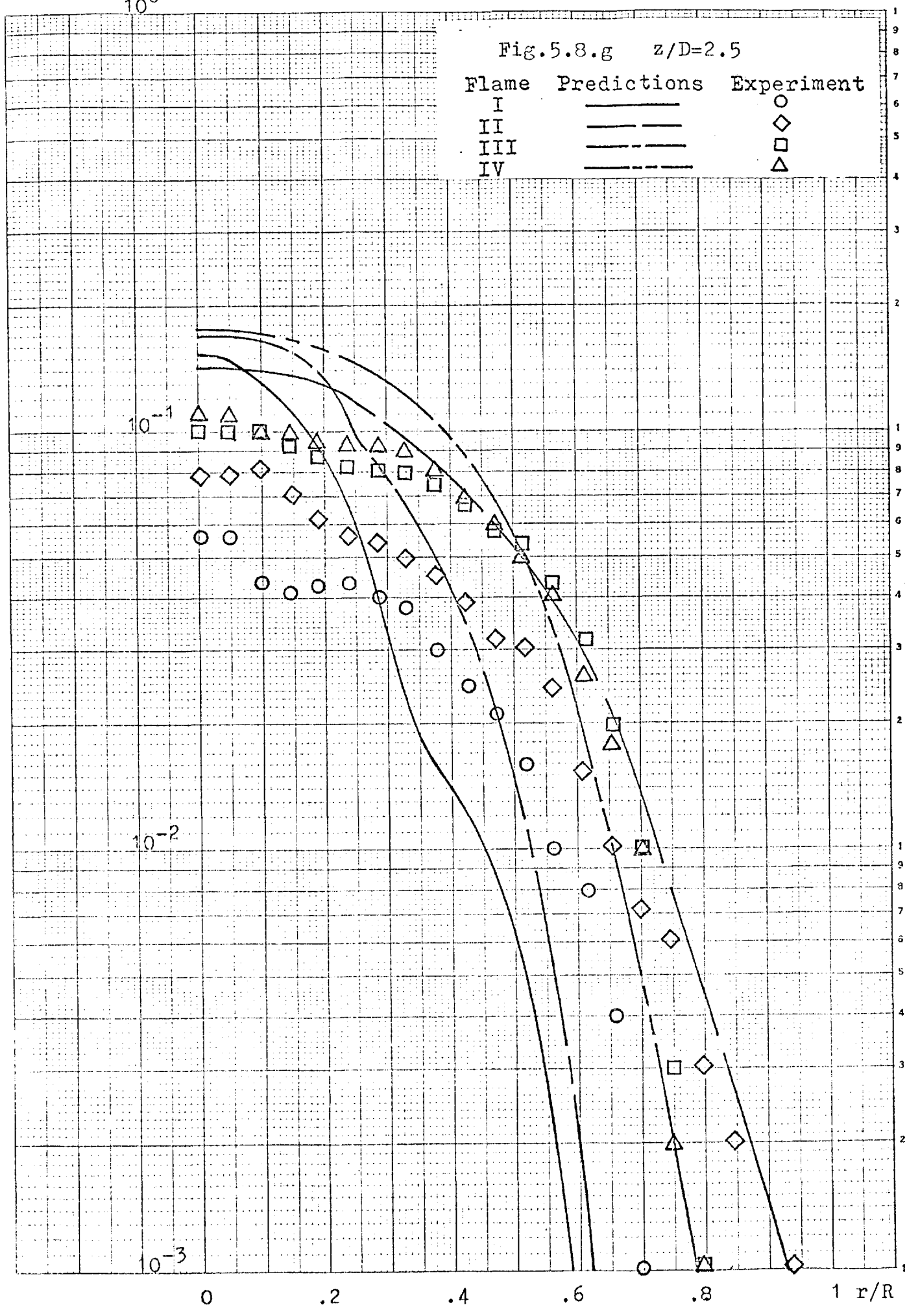
P
10^0
10^{-1}
10^{-2}
10^{-3}
Fig.5.8.g z/D=2.5
Flame Predictions Experiment
I
II
III
IV
0
.2
.4
.6
.8
1 r/R

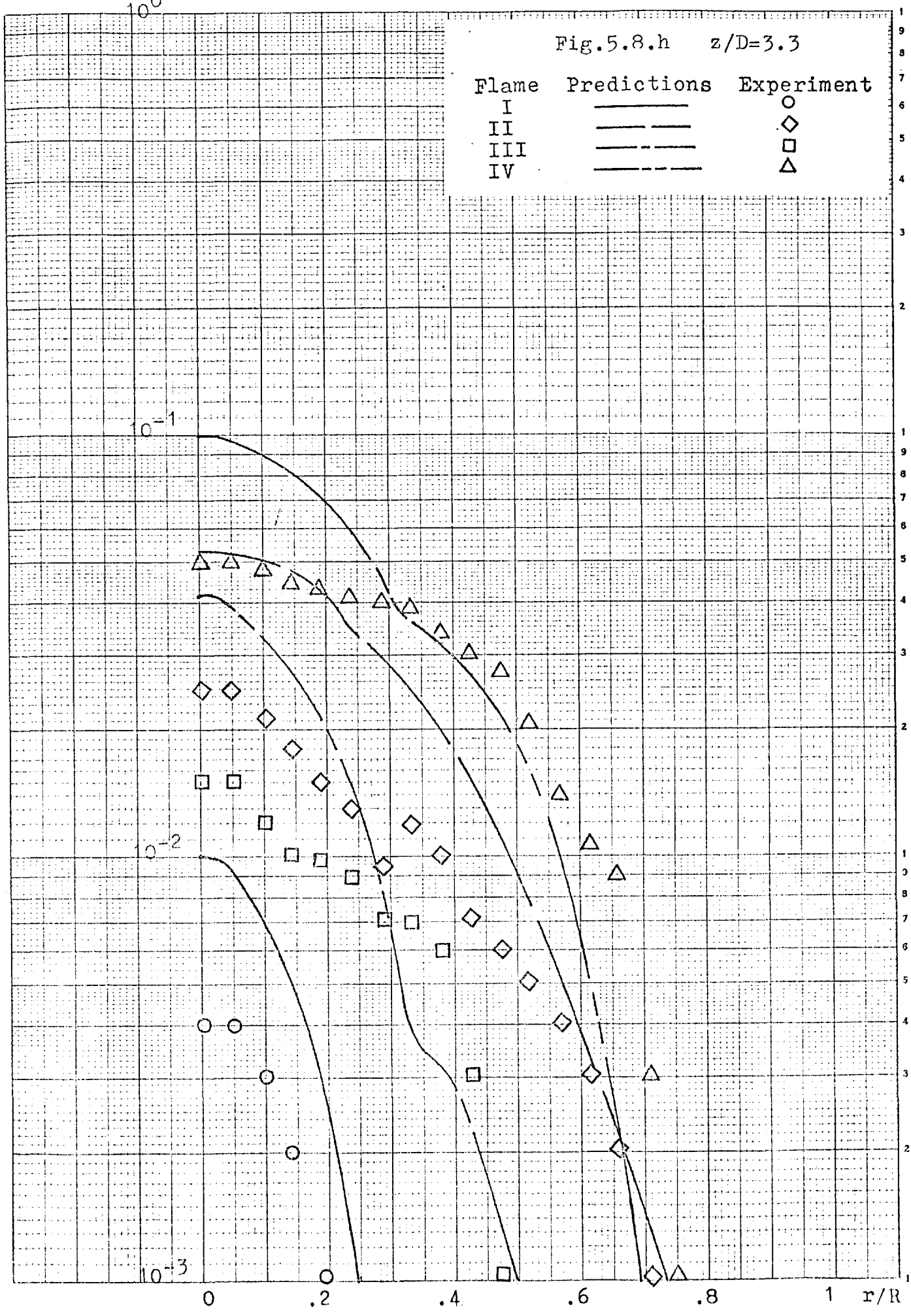
P
10^0
10^{-1}
10^{-2}
10^{-3}
0
.2
.4
.6
.8
1
r/R
Fig.5.8.h z/D=3.3
Flame
Predictions
Experiment
I
II
III
IV

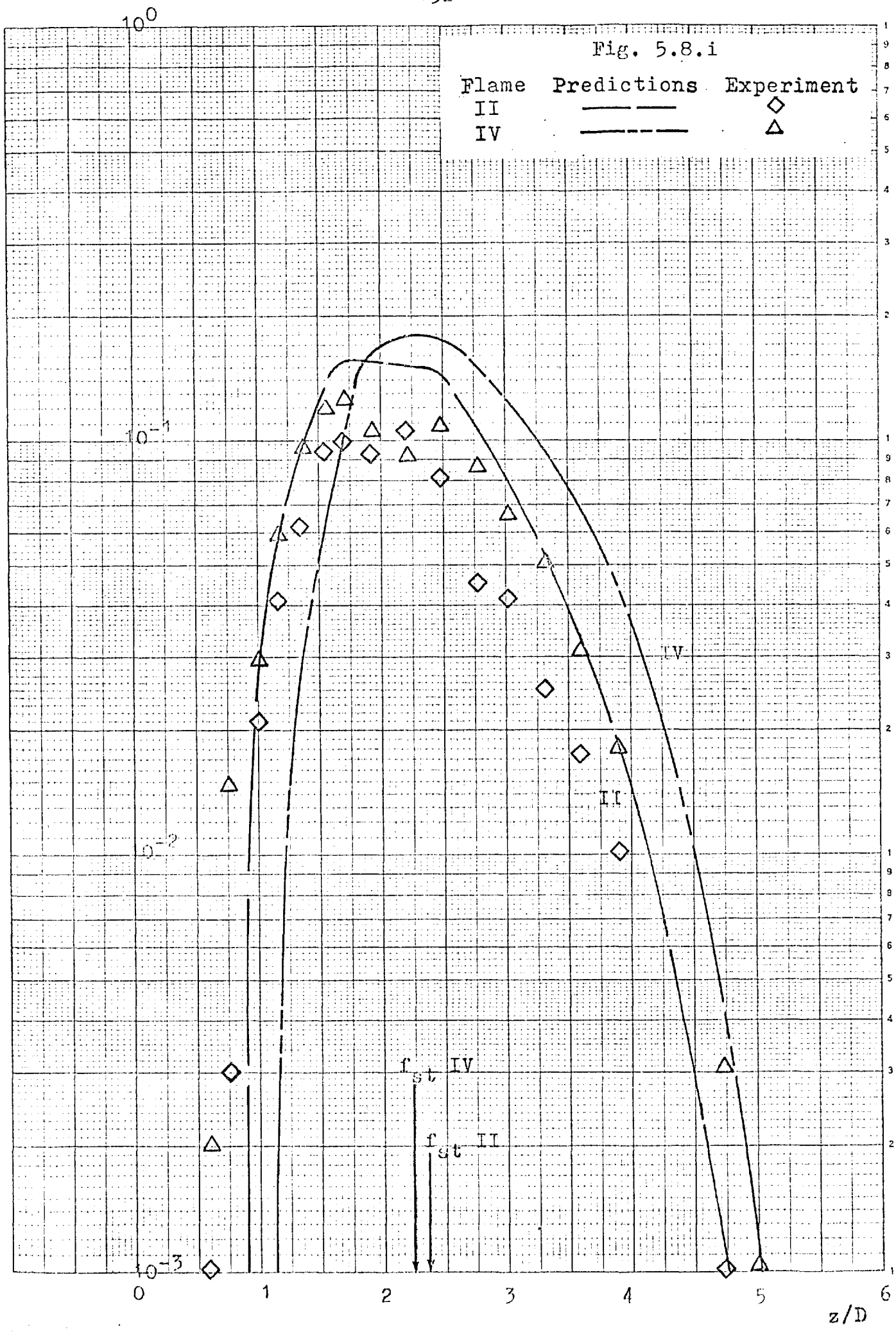
P
10^0
10^{-1}
10^{-2}
10^{-3}
Fig. 5.8.i
Flame Predictions Experiment
II
IV
IV
II
f_{st} IV
f_{st} II
0 1 2 3 4 5 6
z/D

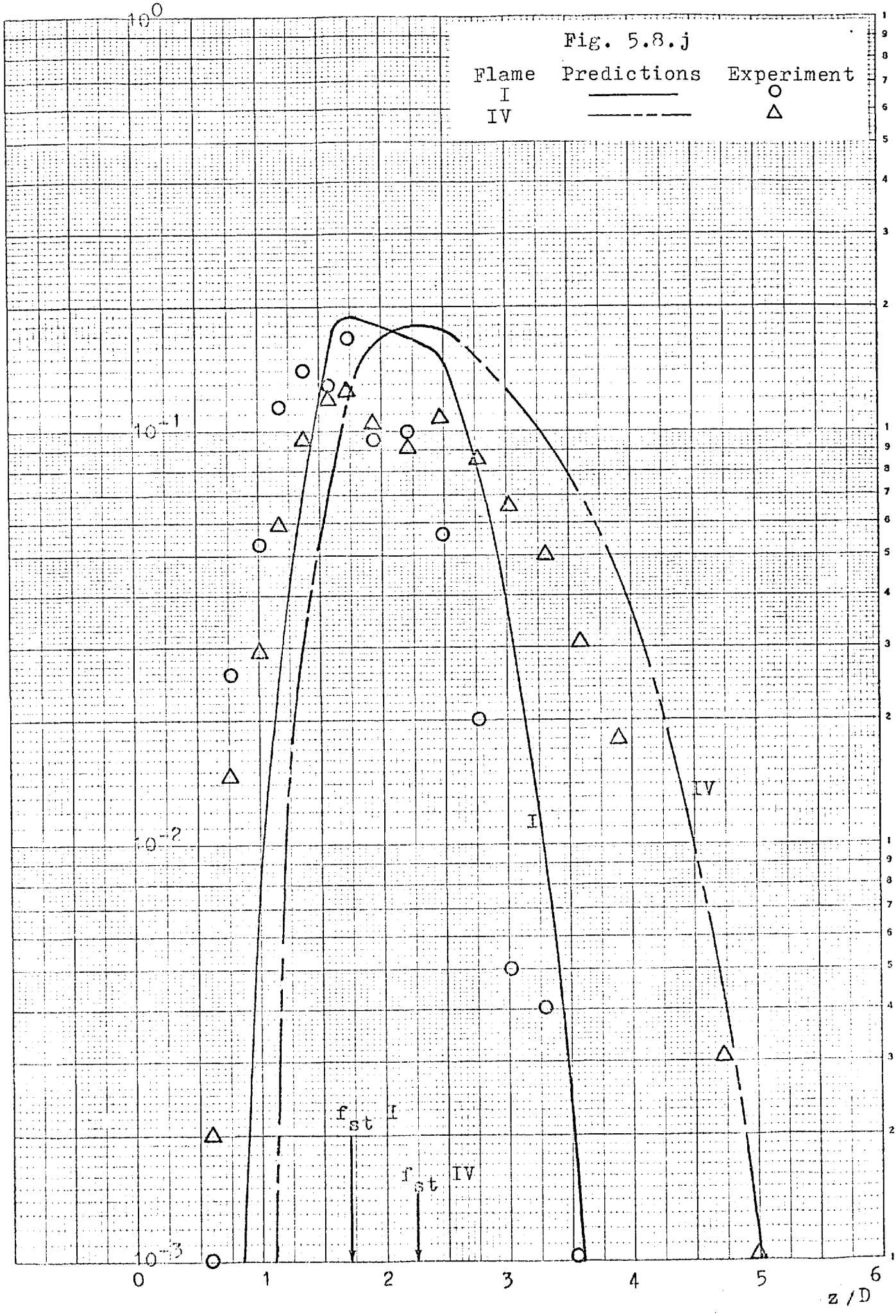
P
Fig. 5.8.j
Flame Predictions Experiment
I
IV
10^{0}
10^{-1}
10^{-2}
10^{-3}
I
IV
f_{st} I
f_{st} IV
0
1
2
3
4
5
6
z / D

shows that both these flames attain a P value of .001 at nearly the same axial location, 4.75D and 5D; i.e., the length of the reaction zone is observed to be rather insensitive to Reynolds number variation.

A comparison is made between flames I and IV in fig. 5.8.j; the inlet air/fuel ratios for the two are 22.9 and 16.9 respectively, the first being 40% leaner than the second. The two flames have about the same Reynolds number. The measured values of P indicate that the reaction zone of flame IV extends to 5D downstream the burner, while that of flame I extends only to 3.5D. As anticipated, increasing the inlet air/fuel ratio shortens the length of the reaction zone.

In summary, the measurements indicate that the extent of the "flame brush" can be readily established by using the ionization probe.

(ii) Predictions, discussion and comparison with measurements

The radial distribution of P (figs. 5.8.b to 5.8.h) show that the predicted values and locations of the maximum P agree well with measurements at sections close to the burner ($z/D \leq 1.7$) but less well at sections farther downstream. The radial width of the reaction zone is predicted within the range of experimental uncertainity which is estimated to be of the order of 10%. It should be noted that the measured values of P at the two sections of $z/D = 1.2$ and $z/D = 1.7$ (figs. 5.8.e and 5.8.f), indicate that away from the axis, P is only slightly influenced by the different conditions of the four flames, while the predictions show pronounced effect.

The above discrepancies between measurements and predictions far

downstream from the burner and away from the axis may be attributed to the simplifying assumptions introduced in the formulation of λ, especially in treating the kinetics of ionization which are believed to have significant effects in those regions.

The predicted distributions of P along the axis are shown in figs. 5.8.i and 5.8.j. The agreement between measurements and predictions is on the whole fairly good. The predicted locations of f_{st} on the axis coincide with the predicted and are very close to the measured, maximum-P-value points for flames I and II, but in flame IV the measured maximum-P-point occurs nearer the burner.

5.4.3 Typical variation of λ

For completeness, the variation of λ along the axis of the furnace for flame II is shown in fig. 5.8.k along with the quantities it depends on: $g^{\frac{1}{2}}/f$, ℓ/η, T and the quantity it affects: P. Also shown in figs. 5.8.l and 5.8.m are the radial profiles of these quantities for the same flame, at two different axial locations (z = .78D, z = 2.5D). It is seen that the temperature does not influence λ significantly (the value of the term $e^{-E/\mathcal{R}T}$ in eq. (5.3-13) is about 0.9 at most points in the field).

If we write the ratio ℓ/η as $[Re_{turb}]^{\frac{3}{4}}$, then λ is proportional to $[Re_{turb}]^{-\frac{1}{2}}$ and to $[g/f^2]$.

5.5 Conclusions

(i) The predictions of the time-mean mixture fraction agree fairly

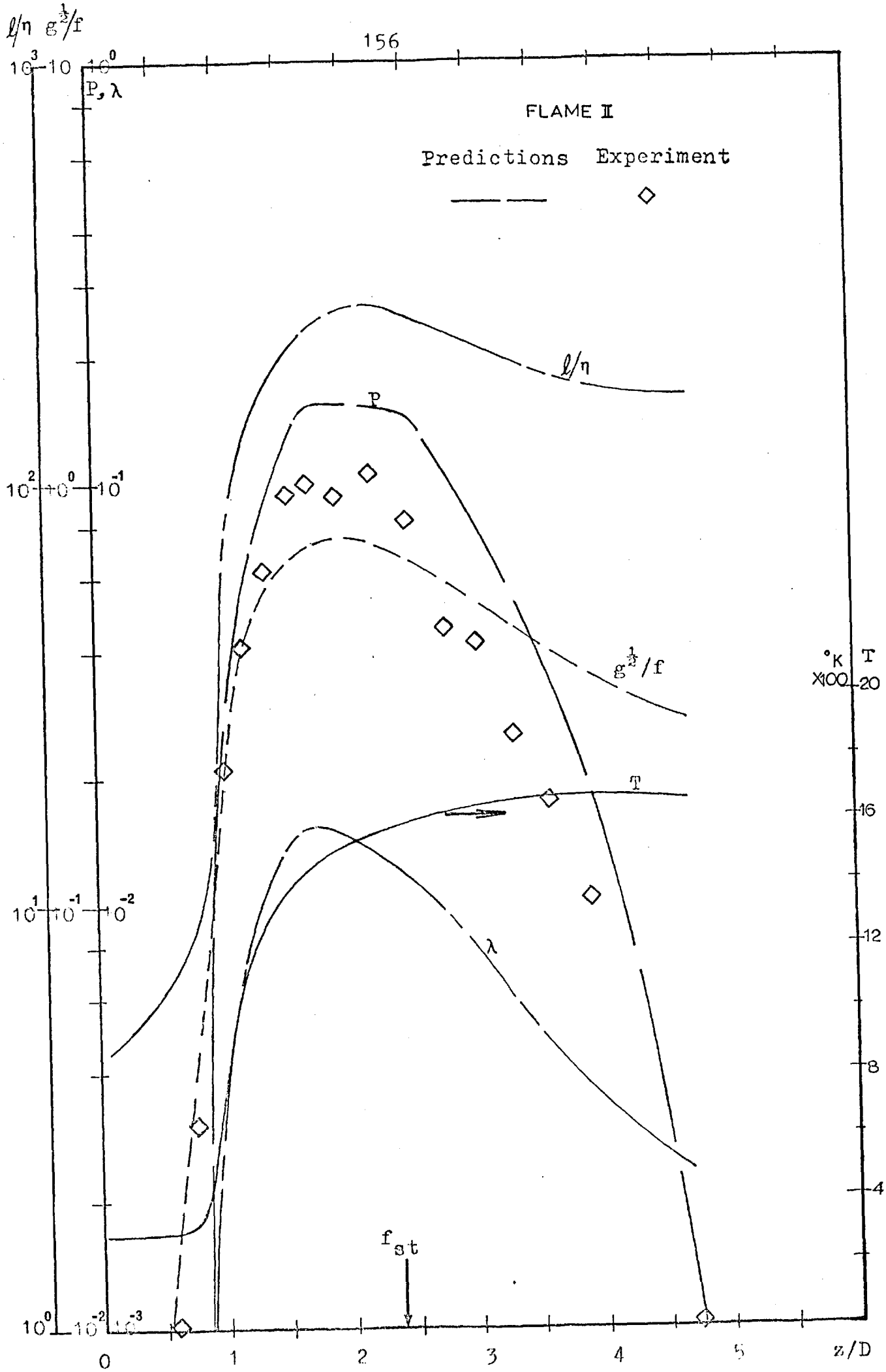
ℓ/η $g^{\frac{1}{2}}/f$
P, λ
FLAME II
Predictions Experiment
ℓ/η
P
$g^{\frac{1}{2}}/f$
T
λ
f_{st}
°K T X100
z/D

Fig.5.8.k

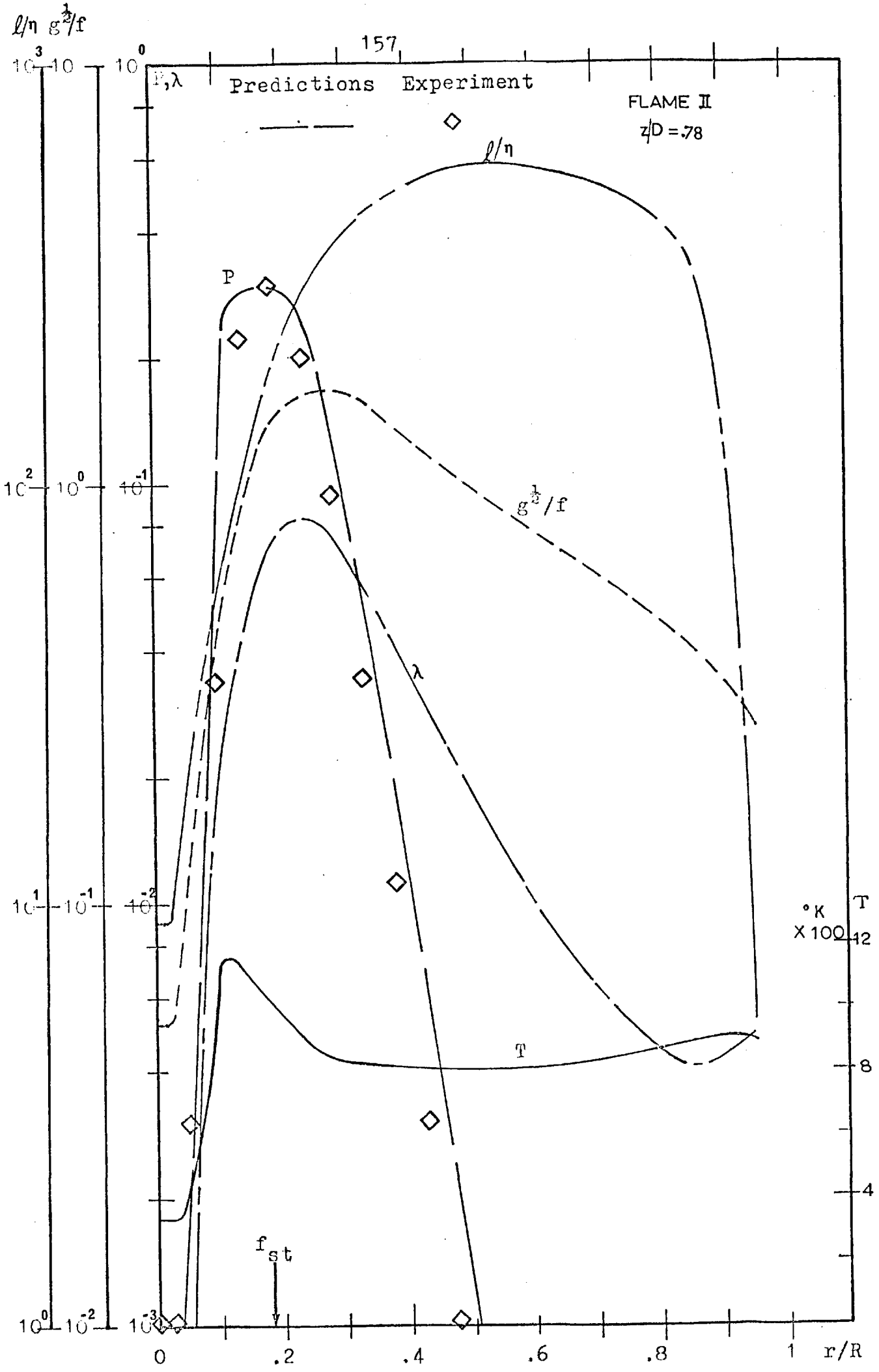
ℓ/η g^½/f
P,λ
Predictions Experiment
FLAME II
z/D = .78
ℓ/η
P
g^½/f
λ
T
°K X 100
T
f_st
r/R
0
.2
.4
.6
.8
1
12
8
4

Fig.5.8.1

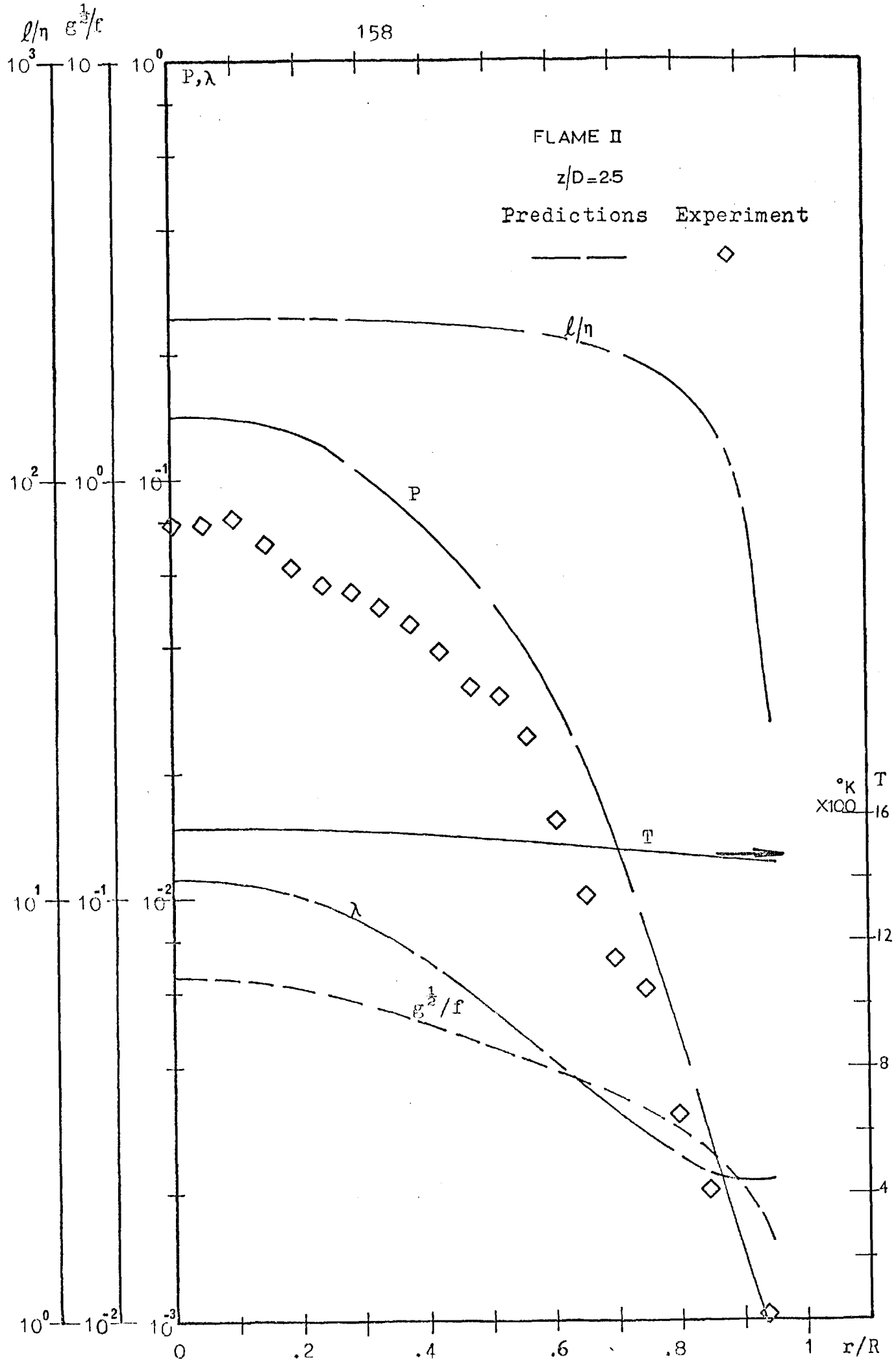
ℓ/η
g^½/f
P,λ
FLAME II
z/D=2.5
Predictions
Experiment
ℓ/η
P
T
λ
g^½/f
°K
X100
T
16
12
8
4
10^3
10^2
10^1
10^0
10^0
10^-1
10^-2
10^-3
10^0
10^-1
10^-2
0
.2
.4
.6
.8
1
r/R

Fig.5.8.m

well with measurements on the whole; in the small zone close to the burner around the axis rather poor agreement is however noted. The experimental data obtained are not sufficient to allow us to diagnose the possible sources of this discrepancy.

(ii) Since no direct measurements are available for concentration fluctuations of stable species in turbulent flames, it is not possible to check the predictions of g. The good agreement between measurements and predictions of g in isothermal flows (chapter 4) is the only available confirmation; one is however reluctant to extrapolate this conclusion to include turbulent flames until more evidence is available.

(iii) The clipped Gaussian distribution proposed for the concentration fluctuations has proved to be realistic, in that its use yields predicted time-mean values of the mass fractions and of the density all exhibiting the expected behavious. The predicted values of the time-mean temperatures are somewhat lower than available measurements for similar flows. This is thought to be mainly due to the high level of temperature fluctuations.

(iv) The measurements of the probability of reaction under the conditions investigated indicate that the highest values of P occur in a region close to the burner in a relatively thin layer away from the axis. This finding is supported by the data of Vranos et al (1969). The predicted concentration fluctuations at that location experience a high time-rate of decay due to the large gradients of f and the small-scale turbulence.

(v) The assumptions made in predicting P, and hence the extent of the flame brush, produce results which on the whole compare reasonably

well with the measurements.

(vi) It should be pointed out that the measured values of P depend on the comparator discrimination-level (section 2.4.4) and are therefore arbitrary. Consequently, the values of the constants A, B_1 and B_2 (eq. 5.3-13) are valid under the present measurement conditions.

CHAPTER 6

CLOSURE

6.1 Concluding remarks

The main conclusions that can be drawn from the present study are the following.

6.1.1 Theoretical

(a) The use of the k-ε turbulence model, together with the modelled g equation, enables acceptable predictions to be made for the time-mean motion, the time-mean concentration and fluctuations of concentration in 2-dimensional, turbulent isothermal recirculating flows.

(b) The hydrodynamic and thermodynamic properties of confined, axi-symmetrical, gaseous turbulent diffusion flames can be predicted by the employment of the turbulence model of (a) above together with two additional mathematical models: one for the chemical reaction and the other for the concentration fluctuations. The influences on the time-mean density of the fluctuations in both concentration and temperature can and should be accounted for.

The predictions made compare favourably with the few measurements that are available.

(c) A procedure has been put forward for calculating the probability of chemical reaction in turbulent diffusion flames. Its use in the

present work has produced predictions which agree fairly well with measurements. Since the procedure makes use of local turbulence quantities only, it is reasonable to expect that the method can be applied more generally to other geometries.

6.1.2 Experimental

The ionization-probe technique proves to be a simple and reliable means of measuring the extent of the turbulent flame-brush.

6.2 Recommendations for future research

6.2.1 Theoretical

In the present prediction method, many simplifying assumptions have been made. These have been imposed mainly through the lack of knowledge of the very complex physics of turbulent flames. The following are suggestions for extending the present line of research:

(a) In order to account for the heat transfer from the combustion-chamber walls, two partial differential equations in a form similar to that of eq. (3.2-3), are required, for the time-mean enthalpy, h, and its mean square fluctucations, $\langle h'^2 \rangle$. Accordingly, we can remove the restriction that a linear relationship exists between the enthalpy and mixture fraction. Of course, the equations for the radiation fluxes have to be solved simultaneously.

(b) The effect of chemical reaction on turbulence has so far been accounted for only through the spatial variation of the time-mean

density. However, there are terms in the exact equations of k and g which represent the explicit influence of the chemical-reaction rate on both quantities (Bray 1973a, 1974). The modelling of these terms is required to assess their effects.

(c) In most practical combustion equipments, swirl is required to achieve combustion stability and to control the extent of the flame. It is therefore recommended to include the equation for swirl in the prediction procedure. Consequently, an adequate turbulence model has to be employed in order to account for the local anisotropy of the flow; i.e., equations for the Reynolds' stresses are required (Roberts 1972).

6.2.2 Experimental

(a) The need exists for measurements of the probability density function of stable-species concentration fluctuations in turbulent diffusion flames in order to assess the validity of the proposed function or its alternatives. It is recognised that this type of measurements requires instantaneous-response probes of high spatial resolution. Determination of this function for temperature fluctuations would be of great importance and might yield useful information about concentration fluctuations.

(b) The use of laser anemometry in measuring the time-mean and fluctuations of velocity seems to be very promising. A combination of these data with those of ionization probes would enable the structure of turbulent flames to be better understood.

REFERENCES

BAKER, R.J., HUTCHINSON, P., KHALIL, E.E. and WHITELAW, J.H. (1974):
"Measurements of three velocity components in a model furnace with and without combustion". Fifteenth Symposium (International) on Combustion, to be published.

BAKER, R.J., HUTCHINSON, P. and WHITELAW, J.H. (1973):
"Preliminary measurements of instantaneous velocity in a two-meter square furnace using a laser anemometer". A.S.M.E. paper 73-HT-34, N.Y.

BATCHELOR, G.K. (1959):
"Small-scale variation of converted quantities like temperature in turbulent fluid". J. Fluid Mech., 5, pp.113-133.

BECKER, H.A. and BROWN, A.P.G. (1969):
"Velocity fluctuations in turbulent jets and flames". Twelfth Symposium (International) on Combustion, pp.1059-1068.

BECKER, H.A., HOTTEL, H.C. and WILLIAMS, G.C. (1963):
"Mixing and flow in ducted turbulent jets". Ninth Symposium (International) on Combustion, the Combustion Institute, pp.7-20.

BECKER, H.A., HOTTEL, H.C. and WILLIAMS, G.C. (1965):
"Concentration intermittency in jets". Tenth Symposium (International) on Combustion, the Combustion Institute, pp.1253-1263.

BECKER, H.A., HOTTEL, H.C. and WILLIAMS, G.C. (1967):
"Concentration fluctuations in ducted turbulent jets". Eleventh Symposium (International) on Combustion, the Combustion Institute, pp.791-798.

BENDAT, J.S. and PIERSOL, A.G. (1971):
"Random data, analysis measurement procedures". Wiley-Interscience, N.Y., p.66.

BILGER, R.W. and KENT, J.H. (1972):
"Concentration fluctuations in turbulent jet diffusion flames". Charles Kolling Research Laboratory, Technical note F-46, The University of Sydney, Australia.

BOUSSINESQ, T.V. (1877):
"Théorie de l'écoulement tourbillant". Mém. Prés. Acad. Sc., 23, Paris, p.46.

BRAY, K.N.C. (1973-a):
"Equations of turbulent combustion - I: Fundamental equations of reacting turbulent flow". University of Southampton, Department of Aeronautics and Astronautics, Southampton, AASU Re. no. 330.

BRAY, K.N.C. (1973-b):
"Equations of turbulent combustion - II: Boundary layer approximation". University of Southampton, Department of Aeronautics and Astronautics, Southampton, AASU Rep. no. 331.

BRAY, K.N.C. (1974):
"Kinetic energy of turbulence in flames". University of Southampton, Department of Aeronautics and Astronautics, Southampton, AASU Rep. no. 332.

BULEWICZ, E.M. (1967):
"Some observations on chemiluminescence and chemi-ionization in flames". Combustion and Flame, 11, pp.297-308.

BURKE, S.P. and SCHUMANN, T.E.W. (1928):
"Diffusion flames". Industrial and Engineering Chemistry, 20, pp.998-1004.

BUSH, W.B. and FENDELL, F.E. (1973):
"On diffusion flames in turbulent shear flows". Project Squid Technical Report TRW-7-PU, Purdue University, Lafayette, Indiana.

CALCOTE, H.F. (1962):
"Ion production and recombination in flames". Eighth Symposium (International) on Combustion, pp.184-199.

CALCOTE, H.F. (1963):
"Ion and electron profiles in flames". Ninth Symposium (International) on Combustion, pp.622-637.

CALCOTE, H.F. and KING, I.R. (1955):
"Studies on ionization in flames by means of Langmuir probes". Fifth Symposium (International) on Combustion, Reinhold, pp.423-434.

CHOMIAK, J. (1970):
"A possible propagation mechanism of turbulent flames at high Reynolds numbers". Combustion and Flame, 15, pp.319-321.

CHOMIAK, J. (1972):
"Application of chemi-luminescence measurement to the study of turbulent flame structure". Combustion and Flame, 18, pp.429-433.

CHUNG, P.M. (1972):
"Diffusion flame in homologous turbulent shear flow". The Physics of Fluids, 15, pp.1735-1746.

CLEMENTS, R.M. and SMY, P.R. (1969):
"Electrostatic-probe studies in a flame plasma". J. Applied Physics, 40, pp.4553-4558.

CSANADY, G.T. (1967):
"Concentration fluctuations in turbulent diffusion". J. Atmospheric Sci., 24, pp.21-28.

DAVYDOV, B.I. (1961):
"On the statistical dynamics of an incompressible turbulent fluid". Dok. Akad. Nauk. SSSR, 136, pp.47-50 (Soviet Physics - Doklady, 6, p.10(1961)).

DENNISTON, D.W. Jnr., OXENDINE, J.R., KNAPSHAEFER, D.H., BURGESS, D.S. and KARLOVITZ, B. (1957):
"Applications of the electronic probe to the study of turbulent flames". J. of Applied Physics, 28, p.70-75.

DONALDSON, C. du P. and HILST, G.R. (1972-a):
"Effect of inhomogeneous mixing on atmospheric photochemical reactions". Environmental Science and Technology, 6, pp.812-816.

DONALDSON, C. du P. and HILST, G.R. (1972-b):
"The effect of the scale of turbulent mixing". Proceeding of the 1972 Heat Transfer and Fluid Mechanics Institute, Stanford University Press, Stanford, California, pp.253-261.

DURST, F, MELLING, A. and WHITELAW, J.H. (1972):
"The application of optical anemometry to measurement in combustion systems". Combustion and flame, 18, pp.197-201.

EBRAHIMI, I. (1967):
"A method for the measurement of the local distribution of turbulence intensity in jet flames". Combustion and Flame, 11, p. 255-259.

EICKHOFF, H.E. (1973):
"Experimental investigation of the influence of combustion on turbulent transport in jet diffusion flames". Combustion Institute European Symposium, Academic Press, pp.513-517.

ELGHOBASHI, S.E. and PUN, W.M. (1974):
"A theoretical and experimental study of turbulent diffusion flames in cylindrical furnaces". Paper presented at the Fifteenth Symposium (International) on Combustion, Tokyo, Japan.

EL-MAHALLAWY, F.M., LOCKWOOD, F.C. and SPALDING, D.B.(1973):
"An experimental and theoretical study of the turbulent mixing in a cylindrical, gas-fired furnace". Combustion Institute European Symposium, Academic Press, pp.633-638.

FAVRE, A. (1965):
"Equations des gaz turbulents compressibles". J. de Mecanique, 4, pp.361-421.

FAVRE, A. (1969):
"Statistical equations of turbulent gases". USAF Contract F61052-67-C-0025.

GLASSTONE, S. (1946):
"Thermodynamics for Chemists". D. Von Nostrand Co., Inc., Princeton, New Jersey.

GOSMAN, A.D. and LOCKWOOD, F.C. (1973):
"Prediction of the influence of turbulent fluctuations on flow and heat transfer in furnaces". Imperial College, Department of Mech. Eng., Report HTS/73/52.

GOSMAN, A.D., PUN, W.M., RUNCHAL, A.K., SPALDING, D.B. and WOLFSHTEIN, M. (1969):
"Heat and mass transfer in recirculating flows". Academic Press.

GREEN, J.A. and SUGDEN, T.M. (1963):
"Some observations on the mechanism of ionization in flames containing hydrocarbons". Ninth Symposium (International) on Combustion, pp. 607-631.

GÜNTHER, R. and LENZE, B. (1973):
"Exchange coefficients and mathematical models of jet diffusion flames". Fourteenth Symposium (International) on Combustion, the Combustion Institute, pp.675-687.

GÜNTHER, R. and SIMON, H. (1969):
"Turbulence intensity, spectral density functions, and Eulerian scales of emission in turbulent diffusion flames". Twelfth Symposium (International) on Combustion, the Combustion Institute, pp.1069-1079.

HANJALIC, K. (1970):
"Two-dimensional asymmetric turbulent flow in ducts". Ph.D. Thesis, University of London.

HANJALIC, K. and LAUNDER, B.E. (1972):
"A Reynolds stress model of turbulence and its application to a asymmetric shear flows". J. Fluid Mech., 52, pp.609.

HARLOW, F.H. and NAKAYAMA, P.I. (1968):
"Transport of turbulence energy decay rate". Los Alamos scientific Laboratory of the University of California, Report LA-3854.

HAWTHORNE, W.R., WEDDELL, D.S. and HOTTEL, H.C. (1949):
"Mixing and combustion in turbulent gas jets". Third Symposium (International) on Combustion, pp.266-288.

HILST, G.R. (1973):
"Solutions of the chemical kinetic equations for initially inhomogeneous mixtures". AIAA paper 73-101, New York, pp.13.

HILST, G.R., DONALDSON, C. du P., TESKE, M., CONTILIANO, R. and FREIBERG, J. (1973):
"The development and preliminary application of an invariant coupled diffusion and chemistry model". A.R.A.P. Report no. 193, prepared under contract NAS1-11433 for NASA.

HINZE, J.O. (1959):
"Turbulence". McGraw-Hill, New York.

KARLOVITZ, B., DENNISTON, D.W., Jnr., KNAPSCHAEFER, D.H. and WELLS, F.E. (1953):
"Studies on turbulent flames. A. Flame propagation across velocity gradients. B. Turbulence measurement in flames". Fourth Symposium (International) on Combustion, pp.613-620.

KEELER, R.N. PETERSEN, E.E. and PRAUSNITZ, J.M. (1965):
"Mixing and chemical reaction in turbulent flow reactors". A.I.Ch.E., 11, pp.221-227.

KENT, J.H. and BILGER, R.W. (1972):
"Turbulent diffusion flames". Charles Kolling Research Laboratory Technical note F-37, Department of Mechanical Engineering, The University of Sydney, Australia.

KUHNERT, D. and GÜNTHER, R. (1973):
"Turbulent scale of OH-radiation". Combustion Institute European Symposium, Academic Press, pp.518-523.

KUNUGI, M. and JINNO, H. (1959):
"Measurements of fluctuating flame temperature". Seventh Symposium (International) on Combustion, pp.942-948.

LAUFER, J. (1953):
"The structure of turbulence in fully developed pipe flow". NACA Rep. 1174.

LAUNDER, B.E. and SPALDING, D.B. (1972):
"Mathematical model of turbulence". Academic Press, London.

LAUNDER, B.E. and SPALDING, D.B. (1974):
"The numerical computations of turbulent flows". Computer Methods in Applied Mechanics and Engineering, 3, pp.269-289.

LENZE, B. (1971):
"Turbulenzverhalten und Ungemischtheit von Strahlen und Strahlflammen". Ph.D. Thesis, Universitat Karlsruhe.

MATTON, G. (1957):
"Ionization studies of flames stabilized in rapid flow; measurement of ionic density in the flame". Sixth Symposium (International) on Combustion, pp.770-773.

MOTT-SMITH, H.M. and LANGMUIR, I. (1926):
"The theory of collectors in gaseous discharges". Physical Review, 28, pp.727-763.

NAGUIB, A.S. (1973):
"Private communication", Imperial College.

O'BRIEN, E.E. (1971):
"Turbulent mixing of two rapidly reacting chemical species". The Physics of Fluids, 14, pp.1326-1331.

ODIDI, A.O. (1974):
"The influence of turbulence on the time-mean rate of chemical reactions". Ph.D. Thesis, University of London.

POMPEI, F. and HEYWOOD, J.B. (1972):
"The role of mixing in bunrer generated carbon monoxide and nitric oxide". Combustion and Flame, 19, pp.407-418.

PUN, W.M. and SPALDING, D.B. (1967):
"A procedure for predicting the velocity and temperature distributions in confined, steady, turbulent, gaseous, diffusion flame". Paper presented at the International Astronautical Federation Meeting at Belgrade, September 1967.

RHODES, R.P. and HARSHA, A.P.T. (1972):
"On putting the 'turbulent' in turbulent reacting flow". AIAA Paper no. 72-68, New York.

RICHARDSON, J.M., HOWARD, JR., H.C. and SMITH, JR., R.W. (1953):
"The relation between sampling-tube measurements and concentration fluctuations in a turbulent gas jet". Fourth Symposium (International) on Combustion, Williams and Wilkins, pp.814-817.

ROBERTS, L.W. (1972):
"Turbulent swirling flows with recirculation". Ph.D. Thesis, University of London.

RODI, W. (1970):
"Basic equations for turbulent flow in Cartesian and cylindrical coordinates". Imperial College, Dept. of Mech. Eng., Report BL/TN/A/36.

RODI, W. (1971):
"On the equation governing the rate of turbulent energy dissipation". Imperial College, Dept. of Mech. Eng., Report TM/TN/A/14.

RODI, W. and SPALDING, D.B. (1970):
"A two parameter model of turbulence and its application to free jets". Warme und Stoffubertragung, 3, pp.85.

SALA, R. and SPALDING, D.B. (1973):
"A mathematical model for an axisymmetrical diffusion flame in a furnace". La Rivista dei Combustibili, 27, pp.180-186.

SHVAB, V.A. (1948):
"Relation between the temperature and velocity fields of the flame of a gas burner". Gos. Energ. izd., Moscow-Leningrad.

SMITH, R., STAFFORD, C.M. and WINEFORDNER, J.D. (1969):
"Temperature profiles of turbulent hydrogen diffusion flames used in atomic flourescence spectrometry". Analytical Chemistry, 41, pp.946-952.

SPALDING, D.B. (1970):
"Mathematische modelle turbulenter flammen". VDI Berichte, 146, VDI Verlag, Dusseldorf, pp.25-30.

SPALDING, D.B. (1971-a):
"Concentration fluctuations in a round turbulent free jet". Chem. Eng. Sci., 26, pp.95-107.

SPALDING, D.B. (1971-b):
Private communication on wall functions.

TENNEKES, H. and LUMLEY, J.L. (1972):
"A first course in turbulence". MIT Press.

THRING, M.W. and NEWBY, M.P. (1953):
"Combustion length of enclosed turbulent jet flames". Fourth Symposium (International) on Combustion, Williams and Wilkins, pp.789-796.

TOOR, H.L. (1962):
"Mass transfer in dilute turbulent and non turbulent systems with rapid irreversible reactions and equal diffusivities". A.I.Ch.E., 8, pp.70-78.

TORREST, R.S. and RANZ, W.E. (1970):
"Concentration fluctuations and chemical conversion associated with mixing in some turbulent flows". A.I.Ch.E., 16, No.6, pp.930-942.

TRAVERS, B.E.L. and WILLIAMS, H. (1965):
"The use of electrical probes in flame plasmas". Tenth Symposium (International) on Combustion, pp.657-672.

TRIBUS, M. and DESOTO, S. (1961):
"Thermodynamics". D.Van Nostrand Co., Inc., Princeton, New Jersey.

VASILATOS, G. and TOOR, H.L. (1965):
"Second-order chemical reactions in a non-homogeneous turbulent fluid". A.I.Ch.E., 11, pp.666-673.

VLASOV, K.P. (1959):
"Experimental investigation of the combustion zone in a turbulent flame". Proceedings of the Moscow seminar on combustion held at the Energetics Institute of the USSR Academy of Sciences. Edited by L.N. Knitrin. Israel Program of Scientific Translations, pp.41-47.

VRANOS, A., FAUCHER, J.E. and CURTIS, W.E. (1969):
"Turbulent mass transport and rates of reaction in a confined hydrogen-air diffusion flame". Twelfth Symposium (International) on Combustion, the Combustion Insitute, pp.1051-1057.

WILLIAMS, F.A. (1965):
"Combustion Theory". Chapters 1,3, Addison-Wesley, Reading, Mass.

WOLFSHTEIN, M. (1967):
"Convection processes in turbulent impinging jets". Ph.D. Thesis, University of London.

ZELDOVICH, Y.B. (1949):
"On the theory of combustion of initially unmixed gases". Zhur. Tekhn. Fiz., 19, no.10. English Translation N.A.C.A. Tech. Mem. no. 1296 (1950).

NOMENCLATURE

		*Section or equation of first occurrence
c_p	specific heat	3.2-23
c_μ	constant in the turbulence model	3.2-5
Ct	Curtet number	4.3-1
E	activation energy	5.3.2
e	electronic charge = 1.6×10^{-19} Coulomb	2.4.1
F	mean of the unclipped Gaussian distribution	3.2-38
f	time-mean mixture fraction	3.2-12
g	time-mean square of fluctuations of mixture fraction	3.2-37
H	lower value of the heat of reaction of fuel	3.2-23
h	time-mean enthalpy	3.2-23
i	stoichiometric mass of oxidant	3.2-13
I_i	local positive-ion current	2.4.3
k	kinetic energy of turbulence	3.2-6
K	Boltzmann's constant = 1.38×10^{-23} J/^{o}K	2.4.1
ℓ	length scale of turbulence proportional to the size of the energy-containing eddies	3.2-8
M_j	molecular weight of species j	3.2-10
m_j	time-mean mass fraction of species j	3.2-10

*Hyphenated numbers denote equations.

n_+	concentration of positive ions	2.4-5
P	probability of chemical reaction	2.4-7
p	absolute pressure	3.2-11
$p(\tilde{f})$	probability density function of the mixture fraction $\tilde{f}$	3.2-38
$\mathcal{R}$	universal gas constant	3.2-11
R	radius of chamber	
R_c	converting resistance	2.4.3
r	distance in radial direction	
T	time-mean temperature	3.2-11
T_e	electron temperature	2.4.1
t	time or time scale	3.2-9
u	time-mean velocity in z-direction	
U	unit-step function	3.2-38
V	probe potential	2.4.1
V_c	comparator discrimination-level	2.4.3
V_H	comparator upper-limit output	2.4.3
V_L	comparator lower-limit output	2.4.3
v	time-mean velocity in radial direction	
w	time-mean square of vorticity fluctuation	Table 1.4.b
z	distance in axial direction	

Greek Symbols

δ	dirac delta function	3.2-38
ε	kinematic dissipation rate of turbulence energy	3.2-7

η	Kolmogorov's microscale of length, $\nu^{\frac{3}{4}} / \varepsilon^{\frac{1}{4}}$	5.3-13
λ	"reaction range" variable	5.3-2
μ	molecular viscosity	3.2-4
μ_t	turbulent viscosity	3.2-5
μ_{eff}	effective viscosity, $\equiv \mu + \mu_t$	3.2-5
ν	kinematic viscosity, $\equiv \mu/\rho$	
ρ	time-mean density	3.2-11
σ	standard derivation of the unclipped Gaussian distribution	3.2-38
$\sigma_k, \sigma_\varepsilon, \sigma_f, \sigma_g$	effective Schmidt number including both molecular and turbulent effects of subscripted entity	3.2.2
τ_i	fraction of time	2.4.3
τ_s	wall shear-stress	4.3
τ_t	total time	2.4.3
ψ	stream function	3.2-1
ω	vorticity	3.2-2

Subscripts

0	condition at the entering unpremixed oxidant stream
1	condition at the entering unpremixed fuel stream
$\mathfrak{C}$	condition at the axis of symmetry
fu	unburned fuel

ox	unburned oxidant
pr	products of combustion
st	stoichiometric

Superscript

$\sim$	instantaneous value
$'$	fluctuating component
*	dimensionless quantity

$\tilde{(\ )} \equiv (\ ) + (\ )'$

instantaneous time-mean fluctuating component

Special Notation

$\langle (\ )'^2 \rangle^{\frac{1}{2}}$	R.M.S.
$\langle\ \rangle$	time-mean of a fluctuating component or correlation

Appendix A

A.1 Introduction

The purpose of this appendix is to give more detailed survey of experimental and theoretical works currently available in the literature and summarized earlier in Tables 1.4.a and 1.4.b of chapter 1.

A.2 Experimental

(a) Time-mean concentration measurements

Hawthorne et al (1949) investigated the combustion of hydrogen in a vertical, cylindrical furnace having a diameter equal to twelve nozzle diameters. They used the quenched-sample technique to measure the time-mean concentration of the nozzle fluid (hydrogen) at many points in the flame. At some locations, the quenched sample withdrawn from the flame brush indicated the co-existence of fuel, oxidant and combustion products. These authors concluded that this sort of sample could only exist in an inhomogeneous mixture whose composition fluctuates locally between two states: fuel plus products and oxidant plus products. They introduced the concept of "unmixedness" to describe the fluctuations in the mixture concentrations. The flame length was obtained from the location along the furnace axis of the stoichiometric value of the time-mean concentration. A shorter flame was observed after removing the confining furnace walls, even though the enclosed flame was burning in 100% excess air. The authors attributed the decrease in flame length in part to the disappearance of the recirculating combustion products in the case of free flame, which resulted in lower nozzle fluid concentration along the axis. Furthermore, they deduced R.M.S. of concentration fluctuations from the time-mean data by assuming that the instantaneous concentration

follows a Gaussian distribution.

A more recent measurement of the time-mean concentration was carried out by Vranos et al (1969). They also employed the quenched-sample technique to obtain the time-mean mass fraction of both fuel (hydrogen) and oxidant (air) in a.3. in by 1.5 inch rectangular combustion chamber. Their measurements accorded with those of Hawthorne et al in that the profiles of the time-mean mass fractions of fuel and oxidant overlapped at some points in the flame. This finding confirms that the local composition fluctuates with time allowing the existence of either fuel and products or oxidant and products. The authors then deduced the local time-mean density and velocity from the measurement of total and static pressures. Turbulent exchange coefficients for the reactants, assumed to be the same for all the species, were determined by numerical solution of the time-mean conservation equation for inert species, and reaction rates were obtained by substituting these exchange coefficients into the conservation equation of a reacting species. They concluded that the reaction rate is proportional to the exchange coefficient and the square of the transverse concentration-gradient. This work provides quantitative data for the time-mean concentration, but all the other deduced quantities can only be regarded as qualitative, since no account for the fluctuations of concentration or of temperature was made in calculating the time-mean density.

Kent and Bilger (1972) measured the time-mean concentration of fuel (hydrogen) and oxygen in a free turbulent diffusion flame using

the quenched sample technique. Their equipment showed also the overlapping of the profiles of hydrogen and oxygen time-mean concentration. The authors stated that sampling errors can arise from the intermittent nature of the flow particularly in the outer regions of the flame, and that even isokinetic sampling cannot guarantee a correct time-mean value for the concentration.

El-Mahallawy et al (1973) mapped the time-mean mixture fraction. f, of a town gas turbulent diffusion flame in a horizontal cylindrical furnace. This was achieved by measuring the time-mean air/fuel ratio at many discrete points in the flow field. Instead of quenching the sample of the gas mixture withdrawn from the reaction zone, as in the experiments of Hawthorne et al and Vranos et al, the authors enriched the sample with oxygen to burn completely all traces of fuel. The burned sampled was then dried and analysed and the time-mean air/fuel ratio at a given point was considered proportional to the local ratio of concentrations of nitrogen to that of the sum of concentrations of carbon monoxide and carbon dioxide. Some results of these measurements will be presented later for comparisons with the present predictions.

(b) Measurements of the time-mean values and fluctuations of temperature

Smith et al (1969) obtained the contours of the time-mean temperature in free turbulent diffusion flames using a 0.13 mm dia. Iridium versus Iridium/Rhodium thermocouple. The errors in these measurements due to radiation losses were of the order of 5%.

Kent and Bilger (1972) measured the time-mean temperature in a free turbulent diffusion flame of a hydrogen jet surrounded by a

co-flowing air stream. They used a platinum versus platinum/Rhodium thermocouple coated with a special non-catalytic material. Even with great efforts spent to correct for radiation losses, they stated that other sources of error due to catalytic effects remained largely unquantifiable. Errors in time-mean temperature were reported to be $\pm$ 100°K.

Odidi (1974) measured the time-mean temperature in a turbulent town gas diffusion flame using a 0.1 mm dia. platinum/40% Rhodium versus platinum/20% Rhodium thermocouple coated with a non-catalytic ceramic mixture. He reported an estimated error of $\pm$ 2% that indicates a high degree of accuracy.

Temperature fluctuations in a turbulent diffusion flame were first measured by Kunugi and Jinno (1959) and later by Odidi (1974). Kunugi and Jinno used a base 0.06 mm dia. platinum versus platinum/Rhodium thermocouple. The accuracy of their data was limited because they compensated the thermal inertia of the wire up to a frequency of 1 KHZ only, whereas it should have been applied to at least 5KHZ to cover the spectrum of fluctuations in turbulent flames as reported by Günther and Simon (1969). Odidi (1974) employed a bare 0.04 mm dia. platinum/30% Rhodium versus platinum/6% Rhodium thermocouple and compensated the thermal inertia of the probe up to a frequency of 10 KHZ. The estimated error in these measurements was reported between + 15% and - 20%.

(c) Measurements of time-mean values and fluctuations of velocity

Kent and Bilger (1972) obtained the time-mean velocity profiles in a free turbulent hydrogen diffusion flame from a pitot-tube measurements of the dynamic head. The evaluation of the time-mean velocity was found extremely sensitive to small errors in the concentration measurements in the outer part of the flow where gradients

and fluctuations of the density are large. The authors reported that errors up to 25% in the time-mean density can result from errors of only 1% in the water concentration; this in turn will cause 25% error in the deduced time-mean velocity.

Velocity fluctuations in a free turbulent diffusion flame were measured by Ebrahimi (1967) who used a condensor microphone probe to detect the pressure fluctuations from which velocity fluctuations could be deduced. The evaluation of the velocity fluctuations, however, ignored the density fluctuations, rendering the data less reliable.

It is only recently that the laser doppler anemometer has been used to measure the time-mean values and R.M.S. of fluctuations of velocities in a confined turbulent diffusion flame (Baker et al 1974). Durst et al (1972) were the first to employ the laser-doppler anemometer to measure with a high degree of accuracy the R.M.S. fluctuations in a free turbulent premixed town gas flame. Baker et al (1973) used the same technique to measure velocity fluctuations in a free turbulent methane diffusion flame. They also obtained the time-mean velocity for the same flame.

(d) Measurements of positive-ion concentrations and chemi-luminescence:

The measurements of positive ion concentration are discussed in Chapter 2; it suffices to say here that no measurements of chemi-ionization or chemi-luminescence have so far been obtained for confined turbulent diffusion flames.

A.3 Theoretical

Pun and Spalding (1967) were the first to introduce a computational procedure for confined recirculating turbulent diffusion flames. The time-mean motion was governed by the equations of the stream functions and vorticity. The chemical reaction was represented by the equations of the species mass fractions and the enthalpy. The closure of these equations was achieved by assuming an effective viscosity which depended on the local mean density, the fluid mean kinetic energy entering the chamber and the dimensions of the chambers. The results of this procedure were plausible considering the simple turbulence model.

El-Mahallawy et al (1973) used the same procedure and the results agreed with their measurements of the mixture fraction distribution in an axisymmetric furnace. No account was taken for the turbulent fluctuations of scalar quantities.

Spalding (1970) introduced, and incorporated in a numerical procedure, his k-w-g turbulence model for predicting free turbulent diffusion flames. The three variables k, w and g respectively stand for the kinetic energy of turbulence, the mean square of vorticity fluctuations and the mean square of concentration fluctuations. The partial differential equations for these variables together with those for the mean motion and the time-mean mass fraction were closed by calculating the effective viscosity from the values of the two variables k and w. The effects of both temperature and density fluctuations on the time-mean density were neglected in that procedure. The predicted results accorded with

the experimental evidence in that a thick flame brush was obtained, although no quantitative assessment could be made through the lack of suitable measurements.

In their study of a free turbulent diffusion flame, Kent and Bilger (1972) extended Spalding's k-w-g model by including the effect of concentration fluctuations on the time-mean density. They reported that the predicted time-mean velocities agreed with the measurements, but the predicted flame length was some 44% shorter than the observed length. One may attribute this discrepancy to the unrealistic probability density distribution which was assumed by the authors for the time-variation of the concentration.

Chung (1972) postulated a simplified statistical theory of turbulence in his study of the equilibrium and near equilibrium diffusion flame in a turbulent shear flow. He replaced the Navier-Stokes equations by a statistically closed equation set by assuming a Maxwellian distribution function for the fluctuations of all the dependent variables. The flow was considered incompressible, and hence the effect of combustion on the flow structure was neglected. Nevertheless, the analysis indicated that the thickness of the reaction zone of an equilibrium turbulent diffusion flame is of the order of the integral scale of turbulence. The consideration of the near-equilibrium chemical reaction demonstrated that the flame thickness is the same as that of the equilibrium reaction situation except that the former flame boundaries are more diffuse, and its overall reaction rate increases with temperature fluctuations.

Bush and Fendell (1973) made use of the k-kl turbulence model

of Rodi and Spalding (1970) to formulate a closure for the Navier-Stokes equations in a thin, turbulent shear layer. They postulated that the distribution of the time-mean mixture fraction, f, is the same for both reacting and non-reacting turbulent shear flows under the same boundary and initial conditions. The assumption of self-similar velocity-profiles was introduced to transform the set of partial differential equations into a set of ordinary differential equations. The profiles for the time-mean fraction, f, could then be obtained from the knowledge of the probability density distribution of the instantaneous mixture fraction f.

Recently, Sala and Spalding (1973) used the k-w-g model in predicting the time-mean temperature distribution, thermal radiation and particle distribution for an axisymmetric turbulent diffusion flame in a liquid-fuel fired furnace. Again, the effect of concentration and temperature fluctuations was neglected in calculating the time-mean density. In that study the flow in the furnace was assumed to have one predominant direction, and recirculation was neglected.

Appendix B

B.1 Introduction

The purpose of this appendix is to provide more details about the method which was used to solve the two equations (3.2-41) and (3.2-42) for F and σ (sec. 3.2.5).

In section B.3 of the appendix, the integrals appearing in eqs. (3.2-41) to (3.2-50) are expanded in a form suitable for numerical computations.

B.2 The method of obtaining F and σ

The method of obatining F and σ is based on a suggestion by Naguib (1973) whereby certain values are tabulated for F and σ within a range suitable for the flow studies. The corresponding values of the mean f and the variance g of the clipped Gaussian distribution, $p(\tilde{f})$, are determined by substituting the values of F and σ into eqs. (3.2-41) and (3.2-42) respectively and storing the results. This is the first part of the method; it is carried out before starting the finite-difference solution-procedure of the equation set (3.2-3).

When the solution-procedure provides the values of f and g at each node in the flow field, we can extract from the initially stored values the corresponding F and σ. For example, consider a grid-node n in the flow field with the predicted values of f and g being equal to f_n and g_n respectively. To obtain F and σ, a search operation through the stored values (f, g vs. F, σ) is then performed to find the intersection point (e.g., point s in fig. B.2.a) of the two f

and g curves with values equal to f_n and g_n respectively. The values of the corresponding F and σ, i.e., F_s and σ_s, complete the specification of $p(\tilde{f})$ at the grid-node n.

Fig. B.2.a

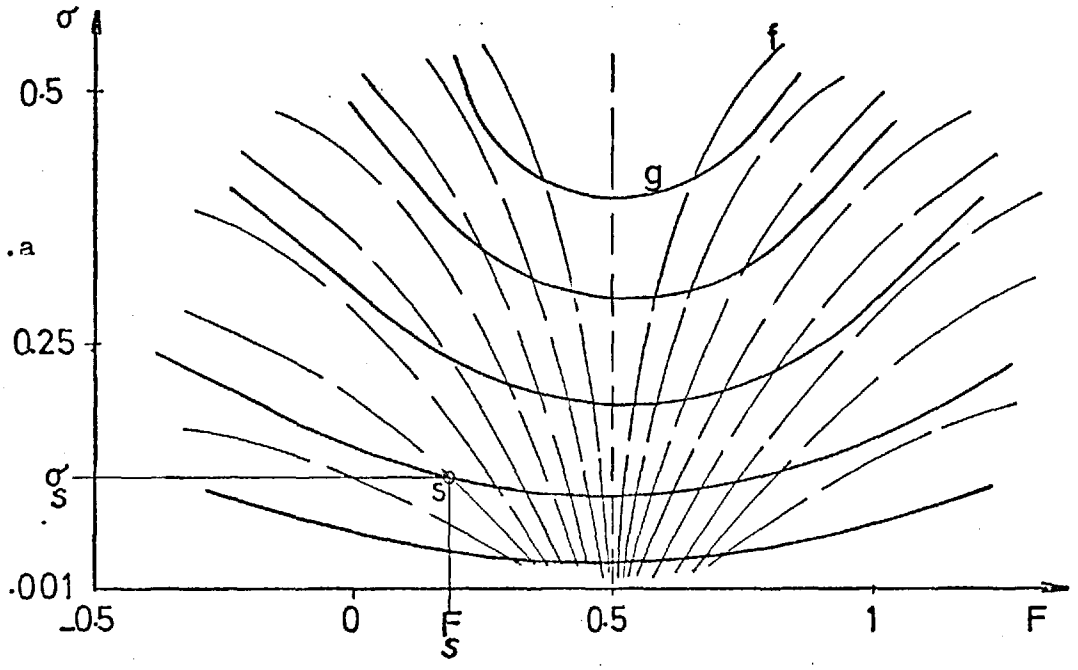

B.3 Expanding the integrals

The integrals appearing in eqs. (3.2-41) to (3.2-50) are expanded below by reference to the number of the equation.

Eq. (3.2-41)

$$\int_0^1 \tilde{f}\, e^{-(\tilde{f}-F)^2/2\sigma^2}\, d\tilde{f}/(\sigma\sqrt{2\pi})$$

$$= (F-1)\, P_1 - F_0 P_0 + (D_0 - D_1)\, \sigma \quad ,$$

where $$P_0 \equiv \int_{-\infty}^{Y_0} e^{-y^2/2}\, dy/(\sigma\sqrt{2\pi}) \quad ,$$

$$P_1 \equiv \int_{-\infty}^{Y_1} e^{-y^2/2}\, dy/(\sigma\sqrt{2\pi}) \quad ,$$

$$Y_0 \equiv -F/\sigma \quad ,$$

$$Y_1 \equiv (1-F)/\sigma \quad ,$$

$$D_0 \equiv e^{-y_0^2/2} / \sqrt{2\pi} \quad ,$$

$$D_1 \equiv e^{-y_1^2/2} / \sqrt{2\pi} \quad .$$

The above definitions apply to all integrals in the next equations.

Eq. (3.2-42)

$$\int_0^1 \tilde{f}^2 \, e^{-(\tilde{f}-F)^2/2\sigma^2} \, d\tilde{f}/(\sigma\sqrt{2\pi})$$

$$= (Y_0 D_0 - Y_1 D_1)\,\sigma^2 - (F^2 + \sigma^2)\,P_0$$

$$+ (F^2 + \sigma^2)\,P_1 + (D_0 - D_1)\,2\sigma F$$

Eq. (3.2-43)

$$\int_{f_{st}}^1 [(\tilde{f}-f_{st})/(1-f_{st})] \, e^{-(\tilde{f}-F)^2/2\sigma^2} \, d\tilde{f}/(\sigma\sqrt{2\pi})$$

$$= (D_{st} - D_1)\,\sigma/I\, f_{st} + (P_1 - P_{st})\,F/I\, f_{st}$$

$$+ (P_{st} - P_1)/I \quad ,$$

where $I \equiv i/m_{ox,0}$,

and i is the stoichiometric amount of oxygen required to burn completely one kg of fuel.

Eq. (3.2-44)

$$\int_0^{f_{st}} (1-\tilde{f}/f_{st})\, e^{-(\tilde{f}-F)^2/2\sigma^2}\, d\tilde{f}/(\sigma\sqrt{2\pi})$$

$$= P_{st}\,(1-F/f_{st}) + P_0\,(F/f_{st}) + (D_{st}-D_0)\,\sigma/f_{st} \quad ,$$

where $P_{st} \equiv \int_{-\infty}^{y_{st}} e^{-y_{st}^2/2}\, dy/(\sigma\sqrt{2\pi})$,

$$y_{st} \equiv (f_{st}-F)/\sigma \quad ,$$

$$D_{st} \equiv e^{-y_{st}^2/2}/\sqrt{2\pi} \quad .$$

Eq. (3.2-46)

$$\int_0^1 [(\tilde{h} - H.\ \tilde{m}_{fu})/\Sigma_j \tilde{m}_j c_{p_j}]\, e^{-(\tilde{f}-F)^2/2\sigma^2}\, d\tilde{f}/(\sigma\sqrt{2\pi})$$

$$= \frac{1}{\sqrt{2\pi}} \left\{ \alpha \int_{y_0}^{y_{st}} [e^{-y^2/2}/(\gamma_1 + y\delta_1)]\, dy \right.$$

$$+ \theta \int_{y_0}^{y_{st}} [y\, e^{-y^2/2}/(\gamma_1 + y\delta_1)]\, dy$$

$$+ \eta \int_{y_{st}}^{y_1} [e^{-y^2/2}/(\beta_1 + y\zeta_1)]\, dy$$

$$\left. + \phi \int_{y_{st}}^{y_1} [y\, e^{-y^2/2}/(\beta_1 + y\zeta_1)]\, dy \right\} ,$$

where $\alpha \equiv h_0 + F\,(h_1 - h_0)$,

$$\beta \equiv m_{fu,1}\,(F/f_{st} - 1)/I \quad ,$$

$$\gamma \equiv m_{ox,0}\,(1 - F/f_{st}) \quad ,$$

$$\delta \equiv -\sigma\, m_{ox,0}/f_{st} \quad ,$$

$$\zeta \equiv m_{fu,1}\, \sigma/I\, f_{st} \quad ,$$

$$\theta \equiv \sigma\,(h_1 - h_0) \quad ,$$

$$\eta \equiv (m_{fu,1}\, H/I)\,(1 - F/f_{st}) + \alpha \quad ,$$

$$\phi \equiv \theta - H\, m_{fu,1}\, \sigma/I\, f_{st} \quad ,$$

$$\gamma_1 \equiv c_{p,pr} + \gamma\,(c_{p,ox} - c_{p,pr}) \quad ,$$

$$\delta_1 \equiv \delta\,(c_{p,ox} - c_{p,pr}) \quad ,$$

$$\beta_1 \equiv c_{p,pr} + \beta\,(c_{p,fu} - c_{p,pr}) \quad ,$$

$$\zeta_1 \equiv \zeta\,(c_{p,fu} - c_{p,pr}) \quad .$$

The four integrals appearing above are then evaluated numerically using Bode's formula.

Eq. (3.2-47)

$$\int_0^1 \left[1/\tilde{T}\, \Sigma_j (\tilde{m}/M)_j\right] e^{-(\tilde{f}-F)^2/2\sigma^2}\, d\tilde{f}/(\sigma\sqrt{2\pi})$$

$$= \frac{1}{\sqrt{2\pi}} \left\{ \gamma_1 \int_{y_0}^{y_{st}} \left[e^{-y^2/2} / (\alpha + \theta y)(\gamma_2 + y\delta_2) \right] dy \right.$$

$$+ \delta_1 \int_{y_0}^{y_{st}} \left[y\, e^{-y^2/2} (\alpha + \theta y)(\gamma_2 + y\delta_2) \right] dy$$

$$+ \beta_1 \int_{y_{st}}^{y_1} \left[e^{-y^2/2} / (\eta + y\phi)(\beta_2 + y\zeta_2) \right] dy$$

$$\left. + \zeta_1 \int_{y_{st}}^{y_1} \left[y\, e^{-y^2/2} / (\eta + y\phi)(\beta_2 + y\zeta_2) \right] dy \right\}$$

where $\gamma_2 \equiv 1/W_{pr} + \gamma\,(1/W_{ox} - 1/W_{pr})$,

$\delta_2 \equiv \delta\,(1/W_{ox} - 1/W_{pr})$,

$\beta_2 \equiv 1/W_{pr} + \beta\,(1/W_{fu} - 1/W_{pr})$,

$\zeta_2 \equiv \zeta\,(1/W_{fu} - 1/W_{pr})$.

Again, the four integrals appearing above are integrated numerically using Bodes' rule.

Eq. (3.2-50)

$$\int_0^1 \tilde{T}^2\, e^{-(\tilde{f}-F)^2/2\sigma^2}\, d\tilde{f}/(\sigma\sqrt{2\pi})$$

$$= \frac{1}{\sqrt{2\pi}} \left\{ \alpha^2 \int_{y_0}^{y_{st}} \left[e^{-y^2/2} / (\gamma_1 + y\delta_1)^2 \right] dy \right.$$

$$\left. + \theta^2 \int_{y_0}^{y_{st}} \left[y^2\, e^{-y^2/2} / (\gamma_1 + y\delta_1)^2 \right] dy \right.$$

$$+ 2\alpha\theta \int_{y_0}^{y_{st}} [y\, e^{-y^2/2}/(\gamma_1 + y\delta_1)^2]\, dy$$

$$+ \eta^2 \int_{y_{st}}^{y_1} [e^{-y^2/2}/(\beta_1 + y\zeta_1)^2]\, dy$$

$$+ \phi^2 \int_{y_{st}}^{y_1} [y^2\, e^{-y^2/2}/(\beta_1 + y\zeta_1)^2]\, dy$$

$$+ 2\phi\eta \int_{y_{st}}^{y_1} [y\, e^{-y^2/2}/(\beta_1 + y\zeta_1)^2]\, dy \Bigg\} .$$

The six integrals in the above result are evaluated numerically using Bodes' rule.